Norwegian University of Life Sciences

Master's Thesis 2023   30 ECTS
Faculty of Chemistry, Biotechnology and Food Science

Exploration of the plastic-binding potential of lytic polysaccharide monooxygenases

Peer Stian Fredheim Gårviken
Chemistry and Biotechnology

Acknowledgments

Abstract

Lytic polysaccharide monooxygenases (LPMOs) are mono-copper enzymes that possess a unique ability to oxidize crystalline surfaces of recalcitrant polysaccharides that are inaccessible to canonical hydrolytic enzymes. The powerful nature of reactive oxygen species generated by LPMOs has led some researchers to believe that these enzymes may be relevant to oxidative degradation of other polymers resistant to hydrolysis, including plastics. This idea is partly based on the notion that the high crystallinity and hydrophobicity of materials such as polyethylene may to some extent resemble the surface properties of known LPMO substrates (e.g., cellulose or chitin).

This thesis was aimed at investigating whether the potential similarity between insoluble polysaccharides and industry relevant plastics results in ability of LPMOs to bind polyethylene (PE), polyethylene terephthalate (PET) and polypropylene (PP). To address this question, screening experiments featuring a variety of LPMOs were performed, and multiple screening techniques were evaluated, including binding competition assays with LPMOs, cellulose and plastics of interest.

The results obtained in this thesis project indicate that some but not all LPMOs indeed possess a noticeable degree of binding to LDPE, HDPE, and PP. This is particularly the case for CelS2 (also referred to as *Sc*LPMO10C), a model bacterial LPMO comprising a family 10 catalytic domain and an auxiliary family 2 carbohydrate-binding module (CBM). This LPMO was studied in detail by comparing its binding to plastics to the binding data obtained with two engineered variants of the enzyme: CelS2$_{TR}$, lacking CBM, and CelS2-CBM1, possessing a family 1 carbohydrate-binding module instead of the wild-type CBM. The later protein was designed and produced as the part of this project. The experiments indicated that it is the CBM and not the catalytic domain of CelS2 that contributes most to the observed binding to plastics. Importantly, the ability of family 2 CBM to guide the LPMO binding to plastics was shown to be much higher than of family 1 CBM. Therefore, the carbohydrate-binding module of the wild-type CelS2 represents a potential starting point for future protein engineering campaigns aimed at creating proteins that can strongly bind to crystalline hydrophobic polymers, such as PE.

2

Sammendrag

Lytiske polysakkaridmonooksygenaser (LPMO-er) er enkelt-kopper enzymer som besitter en unik egenskap til å oksidere krystallinske overflater av motstandsdyktige polysakkarider som er utilgjengelige for konvensjonelle hydrolytiske enzymer. Den kraftfulle naturen til reaktive oksygenarter som dannes av LPMO-er, har fått noen forskere til å tro at disse enzymene kan være relevante for oksidativ nedbrytning av andre polymerer som er motstandsdyktige mot hydrolyse, inkludert plastmaterialer. Denne ideen er delvis basert på tanken om at den høye krystalliniteten og hydrofobiteten til materialer som polyetylen, til en viss grad, kan ligne overflateegenskapene til de naturlige substratene som LPMO-er fra før kan oksidere (for eksempel cellulose eller kitin).

Denne avhandlingen hadde som mål å undersøke om den potensielle likheten mellom uløselige polysakkarider og plastmaterialer fører til at LPMO-er binder seg til polyetylen (PE), polyetylentereftalat (PET) og polypropylen (PP). For å svare på dette spørsmålet ble det utført screening-eksperimenter med LPMO-er fra ulike LPMO-familier, og flere screening-teknikker ble evaluert, inkludert konkurranseanalyser av binding med LPMO-er, cellulose og plastmaterialer av interesse.

Resultatene som ble oppnådd i dette prosjektet indikerer at noen, men ikke alle, LPMO-er faktisk har en merkbar grad av binding til LDPE, HDPE og PP. Dette gjelder spesielt for CelS2 (også referert til som ScLPMO10C), en modellbakteriell LPMO som består av en katalytisk domene tilhørende familie 10 og en tilleggsfamilie 2 karbohydratbindingsmodul (CBM). Denne LPMO-en ble grundig undersøkt ved å sammenligne bindingen til plastmaterialer med bindingdataene som ble oppnådd med to konstruerte varianter av enzymet: CelS2$_{TR}$, som mangler CBM, og CelS2-CBM1, som har en familie 1 karbohydratbindingsmodul i stedet for familie 2 CBM til den naturlige typen. CelS2-CBM1 ble designet og produsert som en del av dette prosjektet. Eksperimentene indikerte at det er CBM og ikke den katalytiske domenen til CelS2 som bidrar mest til den observerte bindingen til plastmaterialer. Viktigst er det at evnen til familie 2 CBM til å veilede LPMO-ens binding til plastmaterialer viste seg å være mye høyere enn familie 1 CBM. Derfor representerer karbohydratbindingsmodulen til den ville typen CelS2 et potensielt startpunkt for fremtidige protein-ingeniørkampanjer med mål om å skape proteiner som sterkt kan binde seg til krystallinske hydrofobe polymerer, som for eksempel PE.

Table of Contents

Abbreviations

A_{280}	absorbance of ultraviolet light at 280 nanometers
AA	auxiliary activities
Ao	*Aspergillus oryzae*
BHET	bis-(2-hydroxyethyl) terephthalate
CAZy	Carbohydrate-active enzyme database
CBM	carbohydrate-binding module
CBM1	family 1 carbohydrate-binding module
CBM2	family 2 carbohydrate-binding module
DTT	Dithiothreitol
DSI	Dermaseptin SI
E. coli	*Escherichia coli*
EDTA	Ethylenediaminetetraacetic acid
His-tag	Hexahistidine purification tag
HPAEC	high-performance anion-exchange chromatography
HDPE	High-density polyethylen
IEX	ion-exchange chromatography
LPMO	Lytic polysaccharide monooxygenase
NaOAc	Sodium acetate, CH_3COONa
PAD	Pulsed amperometric detection
pI	Isoelectric point
ROS	Reactive oxygen species
Sc	*Streptomyces coelicolor*
LDS-PAGE	Lithium Dodecyl Sulfate - Polyacrylamide Gel Electrophoresis
LDPE	Low-density polyethylene
LCC	leaf-compost cutinase
MHET	Mono-2-hydroxyethylterephthalic acid
Nc	*Neurospora crassa*
RPM	Revolutions Per Minute
SD	Standard Deviation
PBM	polyhydroxyalkanoate binding modules

PP	Polypropylene
PET	Polyethylene terephthalate
SEC	Size-Exclusion Chromatography
Tf	*Thermobifida fusca*
TGS	Tris-Glycine-SDS
TA	terephthalic acid

1. Introduction

1.1. Plastic pollution and the approaches to plastic recycling
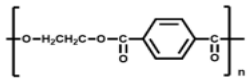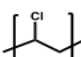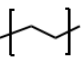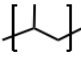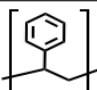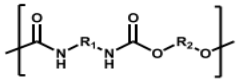
The introduction of the first fully synthetic plastic, Bakelite, can be traced back to 1907 and was invented by Leo Hendrick Baekeland (Hirano and Asami 2013). Since then, plastics have exhibited remarkable versatility and success, offering advantages such as cost-effectiveness, ease of molding and sterilization, and robust mechanical properties (Millet, et al. 2019). These inherent qualities make plastics exceptionally well-suited for a diverse array of applications, including efficient food preservation, the production of clothing and footwear, aseptic medical packaging, plastic-based medical devices, and numerous other uses (Sivaram, Roy and Ray 2021, Andrady and Neal 2009). However, their very highly durable properties also make them resistant to degradation which make it accumulate in nature (Ishigaki, et al. 2004). The accumulation of plastic waste is a major societal problem (Brandon and Criddle 2019). Plastic waste is accumulating in ecosystems, and food chains, posing a threat to wildlife and humans (Pandey, et al. 2023). It is predicted to be 12000 Mt (million metric tonnes) of plastic waste by 2050 (Geyer, Jamebeck and Law 2017, Tiller and Nyman 2018). By 2050, it is estimated that there will be more plastic by weight than fish in the ocean, 99 % of seabirds will have ingested plastics, and the average consumer of seafood is predicted to ingest 11,000 pieces of microplastic every year (Cauwenberghe and Janssen 2014, Dutta and Choudhury 2018). Microplastics are considered particles with a size lower than 5 mm (Betts 2008), these very small granules of plastic can easily be absorbed by a variety of organisms such as marine organisms which can further transfer the microplastics to organisms higher up in the food chain (Betts 2008). One of the reasons microplastics are easily absorbed by animals is due to their very long durability and their highly hydrophobic nature which make them resistant to being dissolved in water (Mato, et al. 2001). In humans, microplastics can cause alternation in the human chromosomes which may lead to infertility, obesity, and cancer (Çobanoğlu, et al. 2021). Plankton, which is important for the photosynthesis and the fixation of inorganic CO_2, is exposed to non-recycled microplastics. The small fragments of plastics can penetrate cell walls and the membranes of plankton, leading to a decrease in chlorophyll concentration in the algae and compromising its ability to absorb solar energy (Besseling, et al. 2014).

Plastics are organic polymers that are formed by a long chain of polymers of carbon atoms, with or without the inclusion of oxygen, nitrogen, or sulfur atoms. Polymer chains of plastics typically consist of several thousand repeating units. Some of the vastly used plastics are polypropylene (PP), polyethylene terephthalate (PET), polyethylene (PE), polystyrene (PS), and polyvinyl chloride (PVC) (**Table 1.1.1**). Plastics are very recalcitrant materials that are robust and hard to recycle. Most plastics produced worldwide are not recycled but rather incinerated or landfilled (Madara, Namango and Wetaka 2016). There are two common types of recycling techniques: mechanical recycling and chemical recycling. Mechanical recycling is the most straightforward process, where plastics are, for

instance, shredded, washed, and dried. The resulting products are granules and flakes that can be used to make a new product (Kim, Laurens and Kevin 2017). The downside of mechanical recycling is that this method cannot be repeated for many cycles since the properties of materials will dramatically decrease (Garcia and Robertson 2017). The more difficult but much more flexible alternative is chemical recycling, that involves depolymerization of plastics and recovery of the products (Garcia and Robertson 2017, Kim, Laurens and Kevin 2017). These products can be used as precursors in chemical synthesis. In ideal situation, the products of polymer degradation can be repolymerized to recreate the original polymer. Most of commonly used plastics are based on "carbon-carbon" backbones. The "C-C" bonds are extremely hard to break, synthetic plastics such as PE, PP, PS, and PVC have a bond dissociation energy falling within the ranges of 330-370 kj/mol (Cheremisinoff 1989, Dick 2009, Knyazev 2007, Luo 2007). This high activation energy makes polymers like PE and PP difficult to depolymerize (Miskolczi, et al. 2009). Therefore, extreme procedures like pyrolysis are commonly used to break PE into shorter fragments (Kim, Laurens and Kevin 2017). Pyrolysis, also termed thermolysis, uses high temperatures between 300 and 700 °C in the absence of oxygen to degrade organic materials, such as different types of plastics (Qureshi, et al. 2020). The plastic polymers are depolymerized by heat induced generation of free radicals along the polymer backbone, leading to the subsequent scission of the molecule (Serrano, et al. 2005, González-Pérez, et al. 2015). The typical product yield after the pyrolysis of plastics, such as PP and PE, could include waxes, oils, benzoic acids, benzene, gases, light oils, and toluene (Qureshi, et al. 2020). On the other hand, some plastics (e.g., PET) contain ester bonds in their backbones. Unlike carbon-carbon bonds, ester bonds are prone to hydrolysis. The chemical hydrolysis of PET requires harsh conditions that can led to pitting corrosion on the PET surface and further compromise the structural strength (Brueckner, et al. 2008). Importantly, ester bonds in PET can also be cleaved by a recently discovered class of hydrolytic enzymes frequently referred to as PETases, under much milder conditions (Brueckner, et al. 2008). Traditional recycling methods, such as chemical recycling, often require harsh conditions and the use of toxic solvents to break down plastic polymers, making them less eco-friendly solutions (Patel, et al. 2000). Therefore, biochemical degradation by enzymes could provide an eco-friendly alternative. Enzymes serve as biological catalysts in numerous biological processes within all living organisms. Their efficiency is remarkable; for instance, they can enhance reactions by up to 17 orders of magnitude (Radzicka and Wolfenden 1995). Enzymes such as PETases are capable of degrading PET without the need for toxic solvents or high-energy-demanding approaches, making them a sustainable solution (Liu, et al. 2018).

Table 1.1.1. Plastic polymers, their chemical structure, and major applications. The table is adapted from (Tournier, et al. 2023)

Polymer	Abbreviation and code	Chemical Structure	Major uses; common commercial products
Poly(ethylene terephthalate)	PET 1		Packaging food and beverages; drink bottles, cups, food containers, textile fibers
High-density polyethylene	HDPE 2		Packaging; grocery bags; containers for shampoo, motor oil, detergent bleach
Poly(vinyl chloride)	PVC 3		Building; pipeline tubes, cables, garden furniture, fencing and carpet backing
Low-density polyethylene	LDPE 4		Packaging; bags, wrapping films, trays, computer components
Polypropylene	PP 5		Packaging; bottle caps, luggage, dishware, furniture, appliances, car parts
Polystyrene	PS 6		Packaging and building; carryout containers, trays, cups, foam packaging
Polyurethanes Polycarbonates, Polyesters, …	Others 7		Diverse applications; Multilayer packaging, some food containers, CD's, DVD's, safety glasses

1.1.1. PET degrading enzymes: tools for the green recycling of plastics

In 2016, Yoshida et al (Yoshida, Tanasupawat, et al. 2016) discovered the bacterium *Ideonella sakaiensis* that was able to grow on the amorphous surface of PET and use it as a sole carbon source. The strains were found on a plastic bottle made of PET at a recycling plant in Sakai City, Osaka, Japan (Yoshida, Tanasupawat, et al. 2016). *Ideonella sakaiensis* is a gram negative, aeorobic, mesophilic, rod-shape bacterium and grows in mild temperatures between 15-42°C but optimally at 30-37°C and

pH are between 5.5-9.0. The specific strain found in 2016 The genus *Ideonella* are chemo-organotrophs that utilize organic acids, carbohydrates, and amino acids as a sole carbon source (Yoshida, Tanasupawat, et al. 2016). Other strains of *Ideonella* such as *Ideonella azotifigens* use cellulose as a sole carbon source and are to be found in the grass rhizosphere which is in the root of the grass (Noar and Buckley 2009). Subsequently, they identified the bacterial enzyme responsible for PET degradation as PETase, specifically known as *Is*PETase (Ideonella sakaiensis PETase), categorized as a mesophilic catalyst for the efficient degradation of PET (Son, Joo, et al. 2020). PETase has evolved from the cutinase family of serine hydrolases, but the exact process of its evolution is not fully understood (Joho, et al. 2023). Following the discovery of PETase in 2016, another key enzyme involved in the degradation of PET was found in the same soil and bacteria as PETase in 2016, and it was identified as MHETase (Yoshida, Hiraga, et al. 2016). MHETase collaborates with PETase and is involved in the final degradation step of PET in a two-step process, producing the initial degradation product, Mono-(2-hydroxyethyl)terephthalic acid (MHET), which is further converted into terephthalic acid (TA) and ethylene glycol (Sagong, et al. 2020, Yoshida, Hiraga, et al. 2016). Other PET-degrading enzymes have also been found, including leaf-compost cutinase (LCC) (Guebitz and Cavaco-Paulo 2008, Donelli, et al. 2009, Vertommen, et al. 2005). LCC cutinase is known as a thermostable enzyme that can act on PET surfaces at temperatures ranging between 72-74°C. (Wei, et al. 2022). It is worth noting that many PET-degrading enzymes are evolved to act on other substrates, rather than PET, such as cutinases and lipases. Cutinase hydrolyze ester bonds of the plant polymer cutin, which is like the ester bond in PET structure (Chen, et al. 2013). Lipase which also can hydrolyze PET originally hydrolyses esters in oils and fat (Tokiwa and Suzuki 1977). The enzymatic hydrolysis mechanism of PET involves breaking ester bonds through the nucleophilic attack of the oxygen atom in the catalytic serine residue on the carbonyl carbon atom of the scissile ester bond. Subsequently, a water molecule performs a nucleophilic attack on the acyl-enzyme intermediate, leading to the release of reaction products. A simplified mechanism for enzymetic PET degradation (**Fig. 1.1.2.1**) (Han, Liu, et al. 2017, Berselli, Ramos and Menziani 2021, Jerves, et al. 2021). Recently, PETases has been engineered to improve their catalytic properties. For example, Tournier et al (Tournier, Topham and Gilles, et al. 2020) introduced 4 mutations into leaf-branch compost cutinase (LCC), improving thermostability of the enzyme and PET depolymerization rate 98 times compared to wild-type enzyme (Tournier, Topham and A. Gilles, et al. 2020). Machine learning-aided engineering has paved the way to improve PETases for breaking down PET plastics. FAST-PETase, a genetically engineered enzyme, differs in five mutations compared to the wild-type PETase and has demonstrated superior hydrolytic activity. It exhibits improved thermostability, showing 2.4 to 38-fold higher activity at 40 and 50°C, compared to the wild-type variant (Lu, Daniel J. Diaz, et al.

2022). Furthermore, FAST-PETase has been shown to efficiently break down both untreated, amorphous sections, and the entire thermally pretreated water bottle at 50°C. (Lu, Diaz, et al. 2022, Son, Cho, et al. 2019, Austin, et al. 2018, Han, Liu, et al. 2017). Another modified variant capable of degrading PET at very high temperatures is identified as HotPETase, and it has shown a nearly twofold increase in thermal stability compared to the wild-type variant, with a temperature of 82.5°C compared to 48.8°C for IsPETase (Ding, et al. 2023).

1.1.2. Oxidative enzymes as the potential solution for depolymerization of non-hydrolysable plastics

While hydrolysable plastics, such as PET, can be degraded by hydrolytic enzymes, the enzyme technology to depolymerize unhydrolyzable plastics (such as PE and PP) does not exist so far. Nevertheless, laccase, a multi-copper enzyme that plays a central role in the oxidation reactions it catalyzes, is recognized for its ability to degrade aromatic compounds (Mayer and Staples 2002). Interestingly, laccase has demonstrated the capability to degrade non-aromatic PE. (Santo, Weitsman and Sivan 2013). A study by Santo et al (Santo, Weitsman and Sivan 2013) highlighted the potential of extracellular copper-induced laccase to degrade PE, resulting in an approximate 20% reduction in molecular weight (Santo, Weitsman and Sivan 2013). However, the authors note that despite the promising results, many reports on oxidative enzymes involved in the depolymerization of plastics are often not followed up in the literature, potentially indicating challenges with reproducibility. Some researchers believe that oxidative enzymes involved in degradation of plant biomass (which is mainly composed of cellulose) may be relevant to the degradation of plastics (Zhao, et al. 2004). There is some similarity between these polymers: cellulose is a crystalline and rather hydrophobic substance. The same is the case with plastics. Among the oxidative enzymes capable of depolymerizing plant biomass, Lytic polysaccharide monooxygenases (LPMOs) are promising proteins considering their potential use in degradation of plastics (Forsberg, Stepnov, et al. 2020). LPMOs are recently discovered copper enzymes that possess a unique ability to directly attack crystalline and otherwise inaccessible surfaces of their substrates by generating reactive oxygen species. Because of this powerful redox chemistry, LPMOs are capable of degrading substrates that are very recalcitrant.
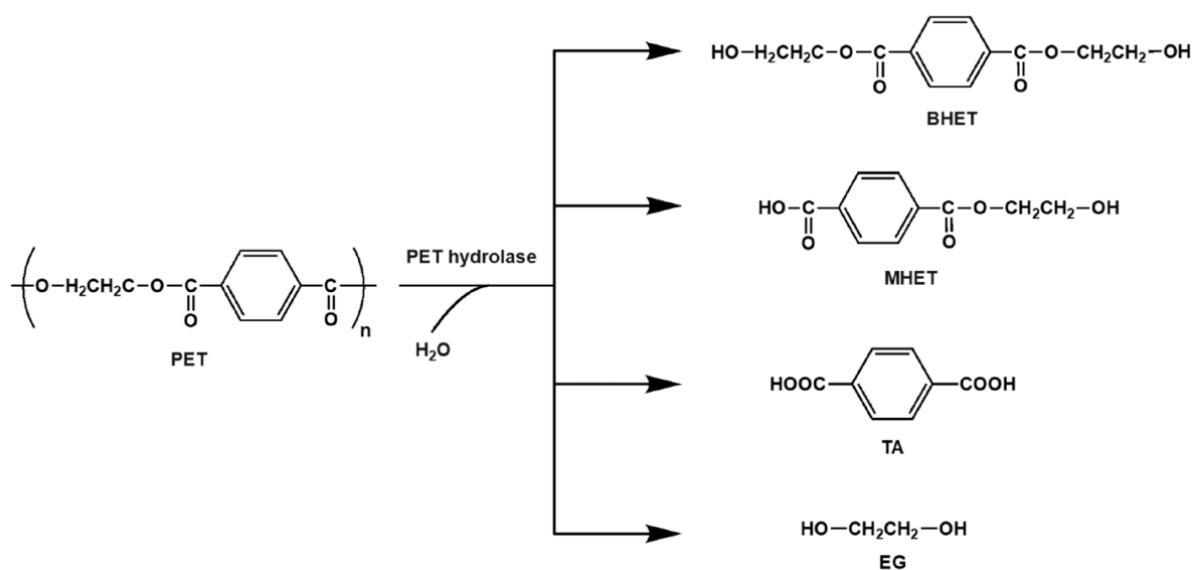
Fig. 1.1.2.1 Products of enzymatic PET degradation. The figure shows the chemical structure of PET and the products of enzymatic PET hydrolysis. This figure is an adapted version of a figure appearing in (Tournier, et al. 2023). BHET, bis-(2-hydroxyethyl) terephthalate; MHET, mono(2-hydroxyethyl) terephthalate; terephthalic acid (TA), and ethylene glycol (EG) are formed after hydrolysation of PET.

1.2. Lytic polysaccharide monooxygenases

1.2.1. What are LPMOs?

Lytic polysaccharide monooxygenases (LPMOs) are enzymes that contain a single copper atom and catalyse the oxidative cleavage of glycosidic bonds in recalcitrant polysaccharides, which cannot be efficiently depolymerized using classical hydrolytic enzymes (Borisova, Isaksen, et al., Structural and Functional Characterization of a Lytic Polysaccharide Monooxygenase with Broad Substrate Specificity 2015). The copper is coordinated by two histidine residues, forming a structural motif referred to as the "histidine brace" (Quinlan, et al. 2011, Ciano, et al. 2018). The first LPMO (Cbp21, acting on chitin) was discovered by Vaaje-Kolstad et al. in 2010 (Vaaje-Kolstad, Westereng, et al. 2010). Since then, many other LPMOs have been described. These enzymes are found in all kingdoms of living organisms and are currently organized in 8 families: AA9, AA10, AA11, AA13, AA14, AA15, AA16, AA17 (**Table 1.2.1.1**) (Levasseur, et al. 2013) (Couturier, et al. 2018, Sabbadin, et al. 2018).

Table 1.2.1.1. Summary of the various families of LPMOs, along with their substrate preferences and their occurrence. The table is adapted from (Tamilvendan Manavalan 2021).

Family	Occurrence	Known substrates
AA9	Fungi	cellulose, hemicelluloses
AA10	Bacteria, plants, viruses	cellulose, chitin
AA11	Fungi	chitin
AA13	Fungi	starch
AA14	Fungi	xylan
AA15	Metazoa, Oomycota, Alveolata, Rhodophyta, Chlorophyta, Haptophyta, Ichthyosporea, Phaeophyceae, Bacillariophyceae, viruses	cellulose, chitin
AA16	Fungi, Oomycota	cellulose
AA17	Oomycota	pectin

In hydrolytic enzymes involved in biomass degradation in Nature, the active sites are located in pockets, grooves or clefts (Lee, et al. 2011). However, in LPMOs the active sites are flat **(Fig. 1.2.1.1)**, which emphasizes the fact that these enzymes can directly attack crystalline surfaces of their substrates, rather than individual polymer chains (Vaaje-Kolstad, Forsberg, et al., Structural diversity of lytic polysaccharide monooxygenases 2017). It has been shown that aromatic residues that surround the active site in LPMOs bind to substrate. The arrangement of these aromatic residues is believed to determine the specificity and regioselectivity of LPMOs toward their substrates (Bennati-Granier, et al. 2015).
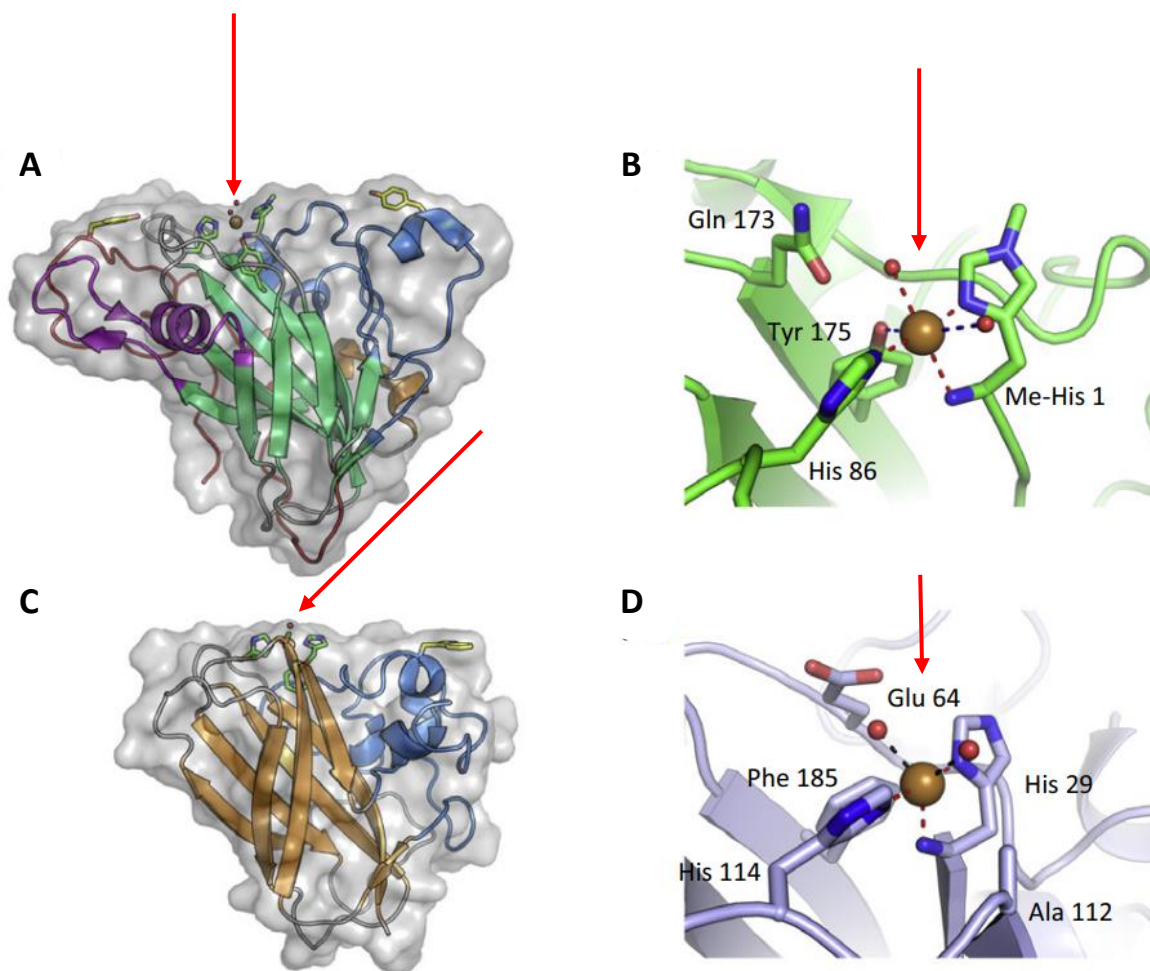
Fig. 1.2.1.1. Topology and the active site configuration of AA10 and AA9 LPMOs. The figure shows overall folds and active sites of TaAA9 (AA9; panels A and B) and EfAA10A (AA10; panels C and D). The copper atom is rendered as a brown sphere. The binding surfaces of LPMOs are highlighted by the red arrows. The figure is adapted from (Hemsworth, et al. 2015).

Before LPMO can oxidize a substrate, it requires the reduction of its bound copper from the resting Cu(II) state to the active Cu(I) state by an electron donor, such as gallic acid (**Fig. 1.2.1.2**). The reduced Cu(I) atom will then further interact with either O_2 or H_2O_2 to generate a highly reactive state capable of hydroxylating a C1- or C4-carbon of the targeted bond (Bissaro, Várnai, et al. 2018), resulting in cleavage of the glycosidic bond and release of oxidized and native products as shown in **Fig. 1.2.1.3**.
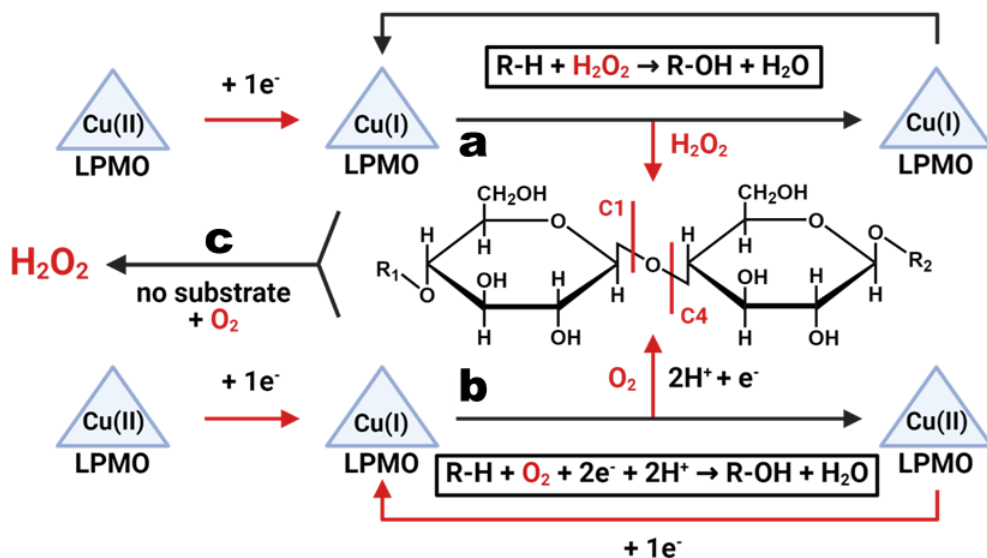
Fig. 1.2.1.2. Simplified mechanism of LPMO catalysis. After active site copper is reduced from the resting Cu(II) state to the active Cu(I) state, the enzyme-bound metal becomes capable of interacting with either H_2O_2 (a) or O_2 (b) to generate a highly reactive state capable of hydroxylating a C1- or C4-carbon of the targeted bond, resulting in bond cleavage. In the absence of substrate, reduced LPMO will react with O_2, leading to H_2O_2 formation (c). The figure was adapted from (Manavalan, et al. 2021).
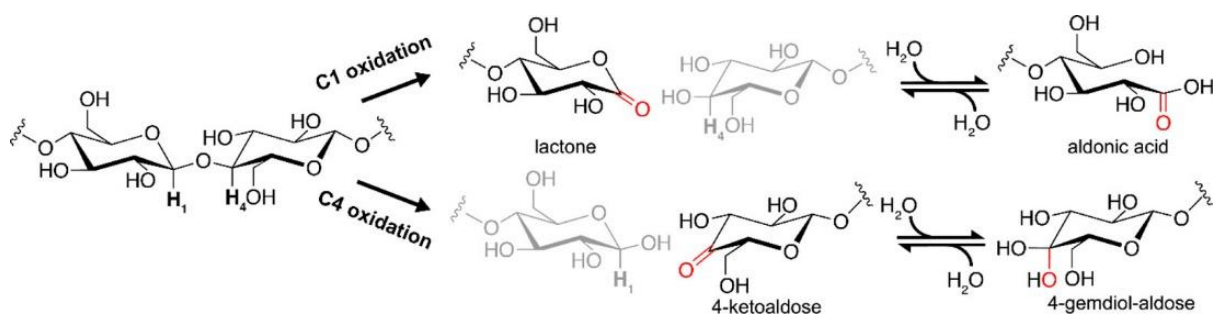
Fig. 1.2.1.3. Depolymerisation of cellulose by LPMOs. The figure shows a formation of oxidized products from cellulose as the result of C1 or C4 oxidation. Note that some LPMOs produce a mixture of both C1- and C4-oxidized sugars. The figure is taken from (Manavalan, et al. 2021).

1.3. Carbohydrate binding modules (CBMs) in LPMOs

Carbohydrate binding modules (CBMs) are small auxiliary domains that improve LPMO binding to their substrates. Historically, CBMs have received significant attention due to their role in augmenting the efficiency of polysaccharide degradation by canonical glycoside hydrolases (GHs) (Guillén, Sánchez and Rodríguez-Sanoja 2010). Within biomass-degrading enzymes, CBMs primarily function is

to guide the enzyme to its respective polysaccharide substrate, consequently increasing the enzyme's concentration on the target surface. As it is the case with many other carbohydrate-active enzymes, LPMOs are often multi-modular. Most of the CBMs associated with LPMOs are classified as Type A CBMs, which have evolved to bind crystalline surfaces (**Fig. 1.3.1**) (Wu, et al. 2013). However, Type B CBMs bind to glycan chains and are the most abundant form of CBM to date. Type B CBM bind individual glycan chains and accommodates longer sugar chains with four or more monosaccharides. This type has been identified in fungal starch oxidizing AA13 enzymes. On the other hand, Type C CBMs recognize short sugar ligands containing one to three monosaccharide units. Type C CBMs, such as the 'chitin/Chito-oligosaccharide-binding' CBM14 and CBM18, have been found in family AA15 enzymes. (**Fig. 1.3.1**) (Sabbadin, et al. 2018, Sabbadin, et al. 2021).
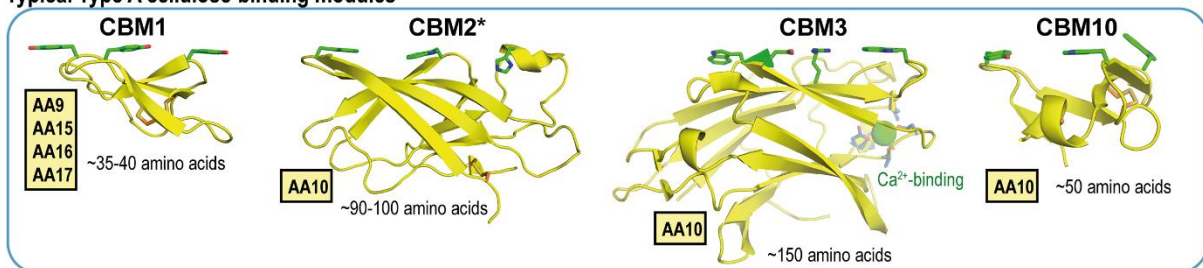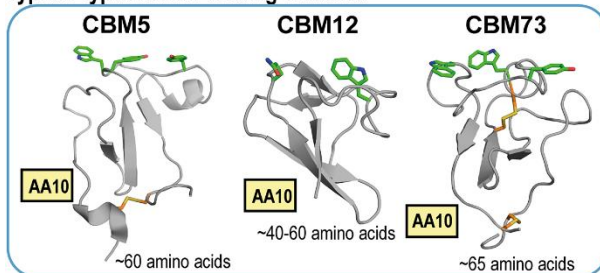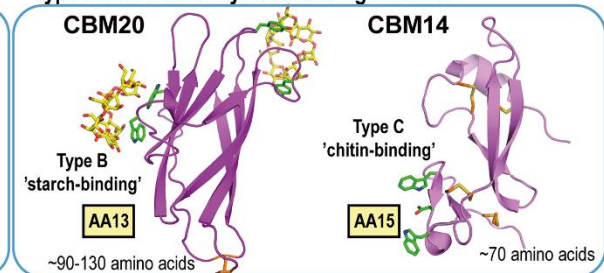
Fig. 1.3.1. CBM types and families are commonly found in LPMOs. The figure shows overall folds of typical CBM modules found across LPMO families. The figure is an adapted from (Forsberg and Courtade 2023).

CBMs rely on hydrophobic residues to bind their hydrophobic substrates. Type A CBMs such as CBM from family 1 and family 2 bind to insoluble carbohydrates via a planar hydrophobic binding face, where the conserved aromatic residues, mainly tryptophans and tyrosines on the binding surface align with cellulose or chitin polymer chains (Pell, et al. 2003, Graham, et al. 2022). Numerous studies have provided compelling evidence that the stacking interactions between aromatic residues and the sugar rings of polysaccharides and oligosaccharides play a pivotal role in determining the overall affinity of Type A CBMs which leads to the carbohydrate-protein interaction (Pell, et al. 2003). CBMs such as CBM2 in CelS2, a two-domain cellulose-active LPMO from *Streptomyces coelicolor* are tethered to the LPMO catalytical domain by a flexible linker, which makes it possible for the

catalytical part of the enzyme to oxidize relatively large surface around the anchoring point as shown in **Fig. 1.3.2.**
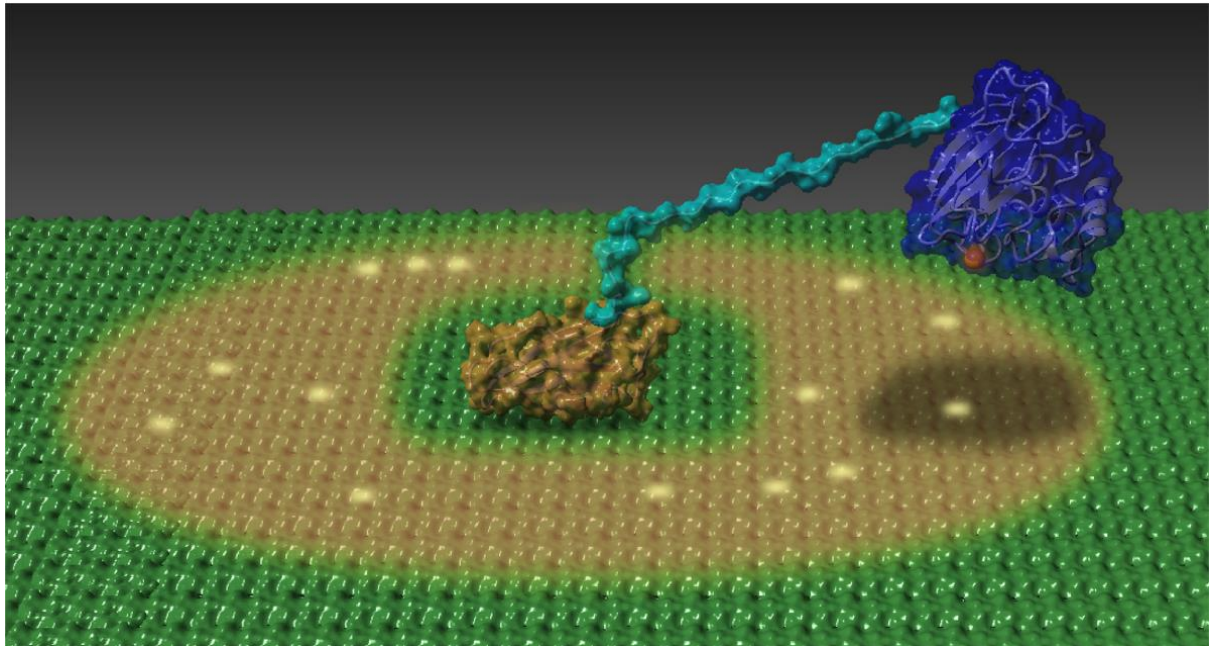
Fig. 1.3.2. Oxidation of cellulose by CelS2, a two-domain enzyme comprising AA10 catalytic core and a family 2 CBM. The figure shows CBM2 (orange) docked to the surface of cellulose (green), which is tethered by a flexible linker (cyan) to the copper loaded catalytical domain (blue). The brown shadowed area represents a theoretical area which the LPMO can oxidize. The figure is taken from (G. Courtade, Z. Forsberg, et al. 2018).

1.3.1. The role of CBMs in LPMO activity

As it was alluded to above, the CBMs have been shown to be very important in binding to substrates. It has been demonstrated that removal of CBM2 from CelS2 led to a significant decrease in binding to cellulose (Forsberg, Røhr, et al. 2014), indicating that CBM plays a dominating role in binding, compared to catalytic domain. It has been observed that the truncation of CBM2 from CelS2 not only reduced the release of oxidized sugars over time, but also resulted in a shorter lifespan of the catalytic domain (**Fig. 1.3.1.1**) (Forsberg, Bissaro, et al. 2018, Loose, et al. 2018, Stepnov, Eijsink and Forsberg 2022). This decrease in lifespan was attributed to inadequate or insufficient binding of the substrate, leading to enzyme auto-catalytic oxidative inactivation (Loose, et al. 2018). The roles of carbohydrate-binding modules (CBMs) in modular lytic polysaccharide monooxygenases (LPMOs) have been investigated by Courtade et al (G. Courtade, Z. Forsberg, et al. 2018). This study has revealed that CBMs play a more intricate role beyond their conventional function of promoting substrate binding. It was demonstrated that the full-length CelS2, compared to the isolated catalytic domain, exhibited different product profile, leading to release of shorter oligosaccharides. This was explained by the idea that the CBM-mediated strong binding of LPMO to the substrate surface

promotes multiple localized cleavages of the same cellulose chain, resulting in overall lower degree of polymerization of the solubilized products, compared to the truncated enzyme lacking CBM.
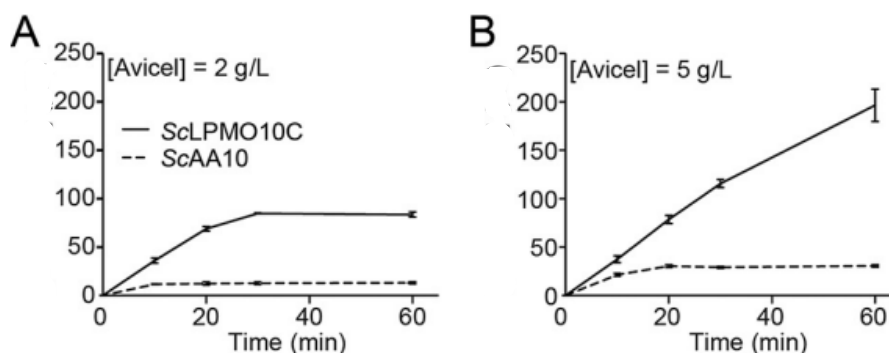
Fig. 1.3.1.1. The release of oxidized products from Avicel by the full-length CelS2 and its truncated catalytic domain, lacking CBM. CelS2 (also referred to as *Sc*LPMO10C) has higher cellulose oxidation rate (solid lines) compared to its truncated catalytical domain, lacking CBM (dotted lines). Note that reaction catalyzed by the truncated LPMO ceases early on, indicating enzyme inactivation. The figure is adapted from (G. Courtade, Z. Forsberg, et al. 2018).

1.3.2. CBM binding to PET

There is indication that some CBMs, evolved to bind to cellulose or chitin, can also bind to PET. Engineered variants of leaf-compost cutinases (LCC) have demonstrated efficient PET degradation. Among these variants, LCC^{YCCG} stands out due to its exceptional thermostability, with a melting point of 97.5°C, and improved PET hydrolysis activity compared to other engineered versions like LCC^{WCCG} and LCC^{ICCG} (Graham, et al. 2022). As a result, there is keen interest in exploring the incorporation of CBMs into LCC^{YCCG} to investigate potential enhancements in binding to PET surfaces. Graham et al. (Graham, et al. 2022) was investigating the fusion of binding domains with PET hydrolases, they observed that LCC^{YCCG}: TrCBM1 and LCC^{YCCG}: TtCBM10 showed significantly higher product yields compared to the LCC^{YCCG} catalytic domain alone at low substrate loadings (<3 weight percent % PET). However, as they increased wt % PET loading with the same enzyme the advantage of the fusion enzymes diminished. By 20 wt % PET loading, the advantage of the synthetic fusion constructs was completely lost. Another study was done with cutinase (Thc_Cut1) by Ribitsch et al. They fused Thc_Cut1 with CBM1 or polyhydroxyalkanoate depolymerase-binding module (PBM). They found out that the new enzymes adsorbed in a much higher extent to PET films compare to the wild-type enzyme as they measured a higher number of hydrolysed products (Ribitsch, et al. 2013).

1.4. Aim of the study

Lytic polysaccharide monooxygenases (LPMOs) are mono-copper enzymes that possess a unique ability to oxidize crystalline surfaces of recalcitrant insoluble polysaccharides. As alluded to above, the powerful nature of reactive oxygen species generated by LPMOs has led some researchers to believe that these enzymes may be relevant to oxidative degradation of other polymers, including plastics. This idea is partly based on the notion that the high crystallinity and hydrophobicity of materials such as PE or PET may to some extent resemble the surface properties of common LPMO substrates (e.g., cellulose or chitin).

The main aim of this study was to assess whether the potential similarity between insoluble polysaccharides and industry relevant plastics results in ability of LPMOs to bind PE, PET, or PP. To answer this question, screening experiments involving multiple LPMOs from various enzyme families were performed and various screening techniques were evaluated as discussed below.

Additionally, **this project aimed to investigate** the prospects of improving LPMO binding to PE, PET or PP by substituting the original carbohydrate-binding module with other types of binding domains, previously reported to have some affinity to plastics. Three new engineered variants of CelS2, a model bacterial LPMO, were designed and studied as part of the thesis.

2. Materials

2.1. Laboratory equipment

Table 2.1.1. Overview of laboratory equipment used in this project.

Equipment	Supplier
1.5 and 2 ml microcentrifuge tubes	Sigma-Aldrich
15- and 50-ml conical centrifuge tubes	Greiner bio one
96-well filter plates with 0.45 µm filter	Millipore
Analytical balance Secura®, Sartorius	VWR
Ultrafiltration tubes: Amicon® Ultra-15 Centrifugal Filters, molecular mass cut-off of 10 kDa	Sigma-Aldrich
ÄKTA Pure protein purification system with an F9-R fraction collector	GE healthcare
Automatic pipettes	Thermo scientific
Beckman Coulter centrifuge	
UV-VIS Spectrophotometers: BioPhotometer® D30 Cary 60	Eppendorf Agilent Technologies
Fast protein liquid chromatography (FPLC) equipment:	
Bio-Rad NGC medium-pressure chromatography	Bio-Rad

system with an NGC-FC fraction collector	
HiTRAP 5ml, Q-Sepharose	Cytiva
Disposable bottle top filters with 0.22 μm membranes	VWR
Gel electrophoresis equipment: Mini-Protean® Tetra cell Mini-Protean® Tetra electrode assembly PowerPac 3000 power supply Gel Doc™ EZ imager Stain-free sample tray Mini-Protean® TGX Stain Free™ precast gels	Bio-Rad Bio-Rad Bio-Rad Bio-Rad Bio-Rad
HPAEC-PAD equipment: Dionex™ ICS-5000 HPLC system with PAD detection Dionex™ CarboPac™ PAμanalytical column Dionex™ disposable gold electrodes	Thermo Fisher Scientific Thermo scientific
Heraeus™ Pico™ 21 Microcentrifuge Heraeus™ Multifuge™ X1 Centrifuge Avanti™ J-25 high performance centrifuge with a JA-10 rotor	Thermo scientific Thermo scientific Beckman Coulter

Fume hood: Telstar AV-100	Telstar
Incubator 37°C	Termax
Magnetic stirrer	IKA
Microtiter plates: 96-well	VWR
Pipette tips	VWR
pH meter: 913 Metrohm	Metrohm
Syringes: 2 & 5 ml 20 & 50 ml	BD Emerald BD Plastipak
Thermomixer	Eppendorf
Uvettes: 1x1 cm	Eppendorf
Vortex mixer	IKA
Water bath	VWR
Vacuum Pump	Millipore
Vacuum Manifold: MultiScreenHTS	Millipore
Syringe filters: 0.22 µm	Sarstedt
Sonicator bath: Branson 3510DTH	Branson
Serological pipettes: 10 ml	Sarstedt
Heating Block	Thermo Scientific
Milli-Q$^{®}$ IQ 7003/05/10/15 Ultrapure & Pure Lab Water Purification System	Sigm-Aldrich
Water bath	Julaba
Q-POD$^{®}$ Ultrapure Water Remote Dispenser	Merck Millipore

2.2. Chemicals

Table 2.2.1. Overview of commercially available reagents used in this project.

Chemical	Formula	Supplier
Bacto™ tryptone		Thermo Scientific
Bacto™ yeast extract		Thermo Scientific
BenchMark™ Protein Ladder		Thermo scientific
Copper sulfate	$Cu(II)SO_4$	VWR
Disodium phosphate	Na_2HPO_4	Sigma-Aldrich
Ethanol	EtOH	VWR
Ethylenediaminetetraacetic acid (EDTA)	$C_{10}H_{16}N_2O_8$	Sigma-Aldrich
Gallic acid	$C_7H_6O_5$	Sigma-Aldrich
Glycerol		
Hydrogen peroxide, 30% (w/w) in water	H_2O_2	Sigma-Aldrich
Kanamycin	$C_{18}H_{36}N_4O_{11}$	gibco
NuPAGE™ LDS sample buffer (4X)		Thermo Scientific
NuPAGE™ sample reducing agent (10X)		Thermo Scientific
Sodium acetate (NaOAc)	CH_3COONa	Sigma-Aldrich
Sodium chloride	NaCl	VWR
Sodium hydroxide, 50% (w/w) in water	NaOH	Sigma-Aldrich
Sodium phosphate	NaH_2PO_4	Sigma-Aldrich
Sucrose	$C_{12}H_{22}O_{11}$	VWR
Tris	$NH_2C(CH_2OH)_3$	Sigma-Aldrich
Tris-Glycine-SDS buffer (10X)		Sigma-Aldrich

2.3. Enzymes

Table 2.3.1. Overview of enzymes used in this project.

Enzyme name	Enzyme type	Expression vector	Source
*Ao*LPMO13A	family 13 LPMO	pBSY_GCW14	produced in-house
CbpD	family 10 LPMO	pNIC-CH	produced in-house
CelS2*	family 10 LPMO	pRSET-B	produced in-house
CelS2-CBM1	family 10 LPMO	pET-26(b)+	produced in-house **as a part of this project**
CelS2$_{TR}$**	family 10 LPMO	pRSET-B	produced in-house
LCC_ICCG	cutinase (PETase)	pET-21(b)+	produced in-house

*Nc*LPMO9C	family 9 LPMO	pBSY_GCW14	produced in-house
*Tf*Cel6A	family GH6 cellulase	pNIC-CH	produced in-house

* - CelS2 is also known as *Sc*LPMO10C** - a truncated form of CelS2 lacking the carbohydrate binding module and the linker (see Table 2.3.2 for details)

Table 2.3.2. Amino acid sequences and predicted molecular weights of CelS2 variants used in this study. Green colour: The catalytical domain**; Black colour:** The interdomain linker; **Red colour:** Auxilary binding module. The sequences shown in the table correspond to mature proteins lacking the signal peptide.

LPMO and predicted molecular weight (kDa)	Amino acid sequence
CelS2* (35 kDa)	HGVAMMPGSRTYLCQLDAKTGTGALDPTNPACQAALDQSGATALYNWFAVL DSNAGGRGAGYVPDGTLCSAGDRSPYDFSAYNAARSDWPRTHLTSGATIPVE YSNWAAHPGDFRVYLTKPGWSPTSELGWDDLELIQTVTNPPQQGSPGTDGG HYYWDLALPSGRSGDALIFMQWVRSDSQENFFSCSDVVFDGGNGEVTGIRG SGSTPDPDPTPTPTDPTTPPTHTGSCMAVYSVENSWSGGFQGSVEVMNHGT EPLNGWAVQWQPGGGTTLGGVWNGSLTSGSDGTVTVRNVDHNRVVPPDG SVTFGFTATSTGNDFPVDSIGCVAP
CelS2$_{TR}$** (21 kDa)	HGVAMMPGSRTYLCQLDAKTGTGALDPTNPACQAALDQSGATALYNWFAVL DSNAGGRGAGYVPDGTLCSAGDRSPYDFSAYNAARSDWPRTHLTSGATIPVE YSNWAAHPGDFRVYLTKPGWSPTSELGWDDLELIQTVTNPPQQGSPGTDGG HYYWDLALPSGRSGDALIFMQWVRSDSQENFFSCSDVVFD
CelS2-CBM1 (30 kDa)	HGVAMMPGSRTYLCQLDAKTGTGALDPTNPACQAALDQSGATALYNWFAVL DSNAGGRGAGYVPDGTLCSAGDRSPYDFSAYNAARSDWPRTHLTSGATIPVE YSNWAAHPGDFRVYLTKPGWSPTSELGWDDLELIQTVTNPPQQGSPGTDGG HYYWDLALPSGRSGDALIFMQWVRSDSQENFFSCSDVVFDGGNGEVTGIRG SGSTPDPDPTPTPTDPTTPPTHTPTQSHYGQCGGIGYSGPTVCASGTTCQVLN PYYSQCL
Cels2-PBM (30 kDa)	HGVAMMPGSRTYLCQLDAKTGTGALDPTNPACQAALDQSGATALYNWFAVL DSNAGGRGAGYVPDGTLCSAGDRSPYDFSAYNAARSDWPRTHLTSGATIPVE YSNWAAHPGDFRVYLTKPGWSPTSELGWDDLELIQTVTNPPQQGSPGTDGG HYYWDLALPSGRSGDALIFMQWVRSDSQENFFSCSDVVFDGGNGEVTGIRG SGSTPDPDPTPTPTDPTTPPTHTAFTCTATTASNYAHVQAGRAHDSGGIAYAN GSNQSMGLDNLFYTSTLAQTAAGYYIVGNCP
Cels2-DSI (27 kDa)	HGVAMMPGSRTYLCQLDAKTGTGALDPTNPACQAALDQSGATALYNWFAVL DSNAGGRGAGYVPDGTLCSAGDRSPYDFSAYNAARSDWPRTHLTSGATIPVE YSNWAAHPGDFRVYLTKPGWSPTSELGWDDLELIQTVTNPPQQGSPGTDGG HYYWDLALPSGRSGDALIFMQWVRSDSQENFFSCSDVVFD GGNGEVTGIRGSGSTPDPDPTPTPTDPTTPPTHTGLWSTIKQKGKEAAIAAAK AAGQAALGAL

2.4. Bacterial strains

Table 2.4.1. Bacterial strains.

Bacterial strain	Supplier
E. coli One Shot® BL21 Star™ (DE3)	Invitrogen

2.5. Plastics and insoluble polysaccharides used in binding experiments

Table 2.5.1. Overview of plastics and insoluble polysaccharides.

Type of polymer	Supplier	Particle size
Polypropylene (PP)	Borealis AG	≤ 300 µm
Low-density polyethylene (LDPE)	Borealis AG	200-300 µm
High-density polyethylene (HDPE)	Braskem	200-300 µm
Polyethylene terephthalate (PET)	DuFor	≈ 100 µm
Avicel PH-101 (microcrystalline cellulose)	Sigma	≈ 50 µm
β-chitin	Orange	75-200 µm

2.6. Buffers and other solutions

2.6.1. 500 mM sodium phosphate buffer, pH 6.0

The buffer was prepared using the following protocol: 500 ml of 500 mM NaH2PO4 and 500 ml of 500 mM Na2HPO4 stock solutions were made by diluting 59.99 g and 134 g, respectively, in Milli-Q H2O. The compounds were each dissolved in approximately 300 ml of Milli-Q water. Next, the volumes were adjusted to 500 ml using a volumetric cylinder. Next, both solutions were mixed by gradually adding Na_2HPO_4 to NaH_2PO_4, until reaching pH 6.0, as indicated by a pH meter. Finally, the resulting solution is filtered through a 0.22 um filter and stored at room temperature.

2.6.2. 1 M Tris-HCl, pH 8.0

121.4 g of Tris was dissolved in approximately 700 ml of Milli-Q H_2O. 37 % HCl was used to adjust the pH to 8.0, and the final volume was adjusted with Milli-Q H_2O to 1 L in a volumetric cylinder. The buffer solution was filtered through a bottle top filter (0.2 μm) using a vacuum filtration system and stored at room temperature.

2.6.3. Buffers for protein anion-exchange chromatography

Binding buffer (buffer A): 20 mM Tris-HCl, pH 8.0.

1 M Tris-HCl, pH 8.0	10 ml
Milli-Q H_2O	490 ml

The buffer solution was stored at room temperature.

Elution buffer (buffer B): 20 mM Tris-HCl, pH 8.0 supplied with 1 M NaCl.

1 M Tris-HCl, pH 8.0	10 ml
NaCl	29.2 g
Milli-Q H_2O	to 500 ml final volume

The buffer solution was filtered through a bottle top filter (0.2 μm) using a vacuum filtration system and stored at room temperature.

2.6.4. Buffer for protein size-exclusion chromatography

Running buffer: 20 mM Tris-HCl, pH 8.0 supplied with 300 mM NaCl.

1 M Tris-HCl, pH 8.0	10 ml
NaCl	17.54 g
Milli-Q H_2O	to 500 ml final volume

The buffer solution was filtered through a bottle top filter (0.22 μm) using a vacuum filtration system and stored at room temperature.

2.6.5. Buffer for periplasmic extraction

Spheroplast Buffer

Sucrose	171 g

1 M Tris-HCl with pH 8.0	100 ml
0.5 M EDTA	1 ml
Milli-Q H$_2$O	to 1000 ml final volume

The spheroplast buffer was filtered through a bottle top filter (0.22 µm) using a vacuum filtration system and thereafter stored at 4°C.

2.6.6. Eluents for high-performance anion-exchange chromatography with pulsed amperometric detection

Eluent A	0.1 M NaOH
Eluent B	0.1 M NaOH with 1 M NaOAc
Eluent C	Milli-Q H$_2$O

To make eluents A and C, 2 L of Milli-Q H$_2$O was measured with a volumetric flask and transferred into respective eluent tanks. To make eluent B, 82.03 g of NaOAc was dissolved in Milli-Q H$_2$O in a 1 L volumetric flask and filtered through a bottle top filter (0.2 µm) into the eluent tank. All eluents were degassed for 20 minutes using sonicator bath. Finally, 10.4 ml or 5.2 ml of 50 % (w/v) NaOH was added to eluents A or B, respectively, using a serological pipette. The solutions were mixed well before placing under N$_2$.

2.7. Cultivation medium

LB – medium

Bacto™ Tryptone	10 g
Bacto™ Yeast Extract	5 g
NaCl	10 g
Milli-Q H$_2$O	to 500 ml final volume

All the powders listed in the table above were added to a glassware beaker and dissolved in approximately 300 ml of Milli-Q-H$_2$O using a magnetic stirrer. After all the powder was completely dissolved, the volume was adjusted to 500 ml using a volumetric cylinder. The medium was then transferred to a blue cap bottle and autoclaved at 121 °C for 20 min before being stored at room temperature.

2.8. Kanamycin stock solution

Preparation of 1000X stock at 50 mg/ml

Kanamycin sulfate	0.5 g
MilliQ H$_2$O	10 ml

0.5 g of Kanamycin sulphate was dissolved in approximately 7 ml of distilled water. The volume was adjusted to 10 ml with a volumetric cylinder. After filtration, it was filtered through a 0.2 µm filter and stored at -20 ^{0}C.

2.9. LPMO reductant solution

100 mM gallic acid

Gallic acid	85.06 mg
Dimethyl sulfoxide (DMSO)	5 ml

85.06 mg of gallic acid was dissolved in approximately 4 ml DMSO. The volume was adjusted to 5 ml using a volumetric cylinder and was filtered through a 0.2 µm syringe filter. Stored in 50 µL aliquots at -20°C covered in aluminium foil.

3. Methods

3.1. Synthesis and cloning of LPMO genes

The CelS2-CBM1, CelS2-PBM and CelS2-DSI genes were codon optimized for expression in *Escherichia coli* and synthesized by GenScript (Piscataway, NJ, USA). The resulting synthetic DNA constructs contained a 66 bp leader sequence, encoding for the pelB signal peptide ("MKYLLPTAAAGLLLLAAQPAMA"), followed by the LPMO genes. The genes were cloned into the pET-26(b)+ expression vector (Merck, Darmstadt, Germany) using NdeI/XhoI restriction sites and sequenced (Sanger sequencing) by GenScript. The vector is designed with a T7lac promoter, which interacts with T7 RNA polymerase. This promoter is regulated by a lac repressor and requires an inducer, such as IPTG, to bind to the lac repressor and relieve its inhibitory effect on gene expression. In this project, the activity of this RNA polymerase is controlled by the inducible lacUV5 promoter within Escherichia coli BL21(DE3). Upon induction using β-D-1-thiogalactopyranoside (IPTG), the

30

expression of T7 RNA polymerase is initiated, resulting in a rapid and enhanced production of LPMO (Dubendorf and Studier 1991)

3.2. Heat-shock transformation

Heat-shock transformation is a common and simple method for introducing exogenous DNA into *Escherichia coli* cells. This technique involves subjecting the cells to a brief and rapid increase in temperature, commonly referred to as heat shock. The heat shock results in a formation of pores in the cell membrane. These pores facilitate the entry of supercoiled plasmid DNA into the cytoplasm. Importantly, heat-shock transformation depends on a pre-treatment of *E. coli* cells with an ice-cold $CaCl_2$ solution. The cells subjected to $CaCl_2$ gain the ability to uptake DNA upon a heat-shock and are referred to as "competent cells". The exact mechanism of heat-shock transformation is still unknown. It is thought that calcium ions play a crucial role in transformation by acting as a cation bridge between the negatively charged phosphorylated lipid A in lipopolysaccharide and the phosphate backbone of DNA. The addition of ice-cold $CaCl_2$ solution facilitates the binding of DNA to the cell surface. Subsequently, a short period of heat-shock enables the entry of DNA into the cell. (Chang 2017)

Method

E. coli BL21 (DE3) competent cells suspension was retrieved from the -80°C freezer and allowed to thaw on ice for 10 minutes. Next, 50 µL of cell suspension were combined with 1 µl of plasmid solution (introducing approximately 10 ng of pDNA) in a 10 ml round-bottom polypropylene tube and incubated on ice for 30 minutes. After the incubation period, the tube was subjected to a 45-second heat shock in a 42°C water bath. Immediately following the heat shock, 250 µL of pre-warmed LB media was added to the 10 ml tube containing the cells. The tube was then placed in a shaking incubator for 1 hour (37 °C, 200 RPM) to allow for expression of the antibiotic resistance gene. Finally, 100 µL of the transformation mixture was carefully spread onto a surface of LB agar plate containing 50 µg/ml kanamycin. The plates were incubated overnight at 37 °C.

3.2.1. Generation of-80 stocks

The stock was generated by inoculating 2 ml of LB medium supplied with 50 mg/ml kanamycin with a colony of the transformed *E. coli* cells. The cells were incubated overnight. Next, 500 uL of the overnight culture was mixed with 500 uL of 50% glycerol and stored at -80 C until further use.

3.3. Expression of LPMOs

3.3.1. Small-scale induction experiments

2 ml of LB medium supplied with 50 µg/ml kanamycin was inoculated with a -80 stock of *E. coli* BL21 (DE3) cells transformed with pET-26(b)+ expression vectors encoding for CelS2-CBM1, CelS2-PBM or CelS-DSI LPMOs. The cells were cultivated overnight in 15 ml conical centrifuge tubes (37 °C, 200 RPM), and then 1 ml (one half) of the resulting cultures was transferred to a new tube and supplied with 10 µl of 100 mM IPTG solution, resulting in 1 mM final concentration of the inducer. All tubes were incubated for 3 more hours (37 °C, 200 RPM). Finally, 20 µl aliquots were taken, mixed with 20 µl of LDS-PAGE sample buffer and analyzed by LDS-PAGE to assess the levels of LPMO expression in the presence or absence of IPTG (see section 3.6 below).

3.3.2 LPMO expression in 1L culture of *E. coli* BL21 (DE3) using induction with IPTG

50 ml of autoclaved LB medium was transferred to a 500 ml sterile Erlenmeyer flask. The medium was supplied with kanamycin (50 µg/ml) and inoculated with -80 stocks of *E. coli* BL21 (DE3) cells transformed with pET-26(b)+ expression vector encoding for CelS2-CBM1 or CelS2-PBM LPMOs. The Erlenmeyer flask was incubated at 37 °C, 200 RPM overnight. The overnight culture was used to inoculate 2x500 ml LB medium supplied with 50 µg/ml kanamycin (5 ml of the overnight culture was added per 500 ml of a fresh medium). The resulting new cultures were incubated in 1L glass bottles (500 ml of culture per bottle) at 37°C in a LEX-24 bioreactor using compressed air for mixing and aeration until reaching the optical density of 0.6 units at 600 nm. Next, ITPG was added to both of 500 ml cultures to a final concentration of 1 mM to induce the expression of LPMO genes. Finally, the cultures were cooled down to room temperature and further incubated for 24 hours to be used for periplasmatic extraction (see below, section 3.4).

3.3.3. LPMO expression in 1L culture of *E. coli* BL21 (DE3 in the absence of IPTG

2x500 ml of LB medium supplied with 50 µg/ml kanamycin were inoculated with -80 stocks of *E. coli* BL21 (DE3) cells transformed with pET-26(b)+ expression vector encoding for CelS2-CBM1 or CelS2-PBM LPMO. The cultures were incubated in 1 L glass bottles (500 ml of culture per bottle) for 24 hours in a LEX-24 bioreactor using compressed air for mixing and aeration and were used for periplasmatic extraction.

3.4. Periplasmatic extraction by osmotic shock

The periplasmic space is located between the cell wall and the inner membrane. In Nature, bacterial LPMOs often contain N-terminal signal peptides that will guide them to the periplasm. During the translocation between the cytoplasm and the periplasm, these signal peptides are removed. The removal of the signal peptide is essential for the correct folding of the LPMO active site. In this project, CelS2-CBM1 was recombinantly produced in *E. coli*, and the transport to periplasm was ensured by substituting the native signal peptide of CelS2 with PelB signal peptide ("MKYLLPTAAAGLLLLAAQPAMA"). PelB is a signal peptide often used in recombinant protein expression in *E. coli* (Shi, et al. 2021). After being transported into periplasm, bacterial LPMOs are typically secreted through the outer membrane outside of the cell. *E. coli* is not capable of such secretion, hence periplasmatic extraction was needed to liberate the target LPMO. To access the periplasmic space and release the trapped proteins, a cold osmotic shock method was utilized. During this procedure, cells containing the target protein are first resuspended in a spheroplast buffer containing a high concentration of sucrose resulting in high osmotic strength. This high osmotic strength leads to water diffusing out of the cells, causing them to shrink. Next, the deformed cells are resuspended in ice-cold Milli-Q water. The rapid diffusion of water into the cells upon resuspension causes them to rapidly expand, causing a disruption of the outer membrane and a release of the periplasmatic proteins into the solution.

Method

E. coli cells were harvested by centrifugation of 1 L overnight culture for 10 minutes at 6000 RPM (6370 g force) (4°C) using an Avanti™ J-25 high-performance centrifuge equipped with a JA-10 rotor. The supernatant was discarded, and the cells were resuspended in 200 ml of cold spheroplast buffer (see section 2.5.3) while keeping the suspension on ice all the time. The suspension was subjected to centrifugation for 10 minutes at 8000 RPM (11330 g force) (4°C). The supernatant was removed, and the pellet was incubated at room temperature for 15 minutes followed by resuspension in 200 ml of ice-cold Milli-Q H_2O. The suspension was subjected to centrifugation again for 10 minutes at 8000 RPM (4°C). The supernatant, containing periplasmic proteins, was collected, filtered through a 0.22 μm filter and stored at 4°C prior to further purification.

3.5. Purification of CelS2-CBM1 by ion-exchange chromatography

In this project, CelS2-CBM1 was purified from periplasmic extracts using ion-exchange chromatography (IEX). This purification technique relies on the variation in affinity of different proteins towards the column resin, composed of polymer beads containing positively charged (anion-exchange sorbents) or negatively charged (cation-exchange sorbents) functional groups. Proteins are zwitterionic compounds since they possess both positively and negatively charged amino acid residues. The overall charge will depend on the protein sequence and the pH of solution. The pH at which the protein carries no net charge is referred to as its isoelectric point (pI). The protein will exhibit a negative overall charge in case the pH of the solution is higher than the pI, or a positive overall charge in case pH of the solution is lower than the pI. Therefore, same proteins can potentially bind to both anion-exchange and cation-exchange resins. The proteins retained by ion-exchange columns are eluted by introducing competing ions into the mobile phase (e.g., by supplying the running buffer with NaCl). As different proteins will exhibit different overall charges, they will display varying retention times upon the elution. In this project, the pI value of CelS2-CBM1 was predicted using ExPASy ProtParam (Gasteiger E. 2005) ([Expasy - ProtParam tool](#)) tool and amounted to 4.46. Q Sepharose is an anion-exchange resin composed of crosslinked agarose beads with quaternary ammonium (Q) strong anion exchange groups. These groups were deliberately chosen to ensure strong binding of LPMO at mildly alkaline conditions (pH 8.0).

 Method

The purification of Cels2-CBM1 from the periplasmic extract was performed using a HiTrap® Q Sepharose Fast Flow 5 mL column installed on an ÄKTA™ Pure chromatography system. The column was equilibrated with five volumes of buffer A (20 mM Tris-HCl, pH 8.0) and 200 ml of periplasmic extract was applied to the resin with a flow rate of 2.50 ml/min. The column was then washed with five volumes of buffer A. Proteins were eluted using a linear gradient of buffer B (0% - 50 % B), which was 20 mM Tris-HCl, pH 8.0 supplied with 1 M NaCl with a flow rate of 2.50 ml/min over 100 minutes. The eluted fractions were monitored using UV detector (λ = 280 nm). To confirm the presence of the target enzyme in the collected fractions, LDS-PAGE gel electrophoresis was performed. Fractions containing the enzyme was analyzed by using LDS-page, and were pooled together and concentrated to approximately 500 μl volume using Amicon® Ultra-15 centrifugal filters with a molecular weight cut-off of 10 kDa. The resulting protein sample was further purified by size exclusion chromatography (see section 3.6).

3.6. Purification of CelS2-CBM1 by size exclusion chromatography

Size exclusion chromatography is widely employed as a final step of protein purification. This technique facilitates the isolation of individual proteins based on their size. The SEC resin is composed of spherical beads containing pores of different sizes. Smaller proteins are retained within the pores for a longer duration compared to the larger proteins that elute earlier. NaCl is often added to SEC buffers to suppress potential binding to the resin.

<u>Method</u>

The further purification of the Cels2-CBM1 sample was performed using ProteoSEC Dynamic 3-70 kDa HR column installed on the BioRad NGC chromatography system. The column was equilibrated with one column volume of 20 mM Tris-HCl, pH 8.0 supplied with 300 mM NaCl with a flow rate of 1 ml/min. 500 µL of concentrated IEX eluate was applied to the resin. Proteins were eluted using one column volume of the same buffer used to equilibrate the column. The eluted proteins were monitored using UV detector (λ = 280 nm). To confirm the presence of the target enzyme in the collected fractions, LDS-PAGE gel electrophoresis was performed. Fractions containing the enzyme were pooled together and concentrated to 1 ml using Amicon® Ultra-15 centrifugal filters with a molecular weight cut-off of 10 kDa prior to copper saturation.

3.7. Copper saturation

Lytic polysaccharide monooxygenases (LPMOs) are mono-copper enzymes that rely on metal binding for their catalytic activity. Once LPMO is purified in the lab, copper saturation is often used to ensure that all protein species are active. To do so, LPMOs are typically incubated with 2-fold or 3-fold molar excess of Cu(II) followed by desalting to remove the unbound metal.

<u>Method</u>

Copper-saturated LPMO was prepared by co-incubating the purified enzyme with $Cu(II)SO_4$ at a 1:3 molar ratio for 30 min, at room temperature in 20 mM Tris-HCl, pH 8.0, containing 300 mM NaCl. Excess copper was removed from the preparation using a PD MidiTrap G-25 desalting column (GE Healthcare, Chicago, USA) equilibrated with 15 ml (3 column volumes) of 50 mM sodium phosphate buffer, pH 6.0. 110 µl of LPMO $Cu(II)SO_4$ solution was loaded into the column, followed by 1890 µl of 50 mM sodium phosphate buffer, pH 6 to elute the desalted protein. The resulting 2 ml desalted protein sample was stored at 4 °C until further use.

3.8. Lithium dodecyl sulphate-polyacrylamide gel electrophoresis (LDS-PAGE)

LDS-PAGE is a powerful tool for assessing composition and purity of protein samples. LDS-PAGE allows to separate charged proteins based on their mobility in porous polyacrylamide gels by applying an electric filed. Before separation, proteins are subjected to denaturation by boiling the samples in the presence of lithium dodecyl sulphate (LDS, an anionic detergent) and dithiothreitol (DTT, a reducing agent). LDS binds to protein surface, promoting the denaturation and introducing negative charge. DTT reduces and breaks the disulphide bonds, further disrupting protein structure. LDS is also present in gels and gel electrophoresis buffer, so the proteins remain unfolded all the time during the experiment. Under such conditions, proteins will migrate towards the anode when electric field is applied. Importantly, the rate of migration through a gel will depend on the protein molecular weight (the smaller proteins will move faster), allowing to separate polypeptides based on their mass.

<u>Method</u>

The protein samples were prepared by mixing them with an equal volume of LDS-PAGE sample buffer and subsequently subjected to boiling at 100 °C for 5 minutes using a Grant QBD2 Block heater. A Mini-Protean® TGX Stain-Free™ precast gel cassette was inserted into the Mini-Protean® Tetra electrode assembly, which was placed inside a Mini-Protean® Tetra electrophoretic cell. The internal chamber of the assembled cell was filled with Tris-Glycine-SDS buffer. Next, 10 µL protein samples were carefully deposited into the respective wells in the gel using an automatic pipette. The cell was connected to the PowerPac 3000 power supply, and the potential difference of 250 volts was applied to the system for approximately 20 minutes. Finally, the gel was carefully removed from the cassette and placed in a stain-free sample tray for analysis. Gel imaging and densitometry were performed using the Gel Doc™ EZ Imager and Image Lab 6.1 software. The stain-free gels used in this project contained trihalo compounds. These compounds have the capability to react with the tryptophan residues present in proteins when the gel is imaged using UV-light. The reaction products are fluorescent allowing for a detection of protein bands without using any staining solutions.

3.9. Measuring protein concentration using UV spectroscopy

One of the easiest and fastest tools for measuring protein concentration is UV spectroscopy. Most proteins contain tryptophan and tyrosine residues that can be detected by recording the optical absorbance of solutions at 280 nm. Therefore, protein concentration can be determined using the Beer-Lambert law:

$$A = \varepsilon * L * c$$

According to the equation, the absorbance (A) of a protein sample is directly proportional to its molar concentration (c) and the optical path (L) of the spectrophotometric cell. The molar extinction coefficient (ε) is a protein-specific parameter which depends on the amino acid composition and can be predicted using computational tools.

Method:

The optical absorbance of protein solutions was measured with a BioPhotometer® D30 spectrophotometer at 280 nm wavelength using UV-transparent disposable micro cuvettes with 1 cm optical path. Samples containing buffer, but lacking proteins were used as blanks. The theoretical extinction coefficients for the proteins of interest (see table 3.9.1) were calculated using ProtParam tool (Gasteiger E. 2005) (Expasy - ProtParam tool) and were used to convert the absorbance values into the molar concentration of protein samples.

Table. 3.9.1 Extinction coefficient of LPMOs in this project. The extinction coefficients were retrieved from Bioexpasy ProtParam (Gasteiger E. 2005) (Expasy - ProtParam tool).

Type of LPMO	Extinction coefficient $M^{-1} cm^{-1}$
CelS2$_{TR}$	52160
CelS2**	75775
CelS2-CBM1	58370
CelS2-PBM	59735
CelS2-DSI	57660
CbpD	82320
NcLPMO9C	46910
AoLPMO13A	51775

3.10. Assessing LPMO binding to insoluble polymers using UV spectroscopy and LDS-PAGE

To investigate binding of LPMOs to insoluble polymers, 2 µM enzymes were incubated with 50 mg of Avicel, β-chitin, PET, LDPE, HDPE, PP or in the absence of these compounds in 500 µl of 50 mM sodium phosphate buffer, pH 6.0. The experiments were carried out in 2 ml microcentrifuge tubes at 25 °C using a thermomixer set to 1000 RPM to ensure a uniform distribution of polymer particles in suspension. After 40 minutes of incubation, 200 µl aliquots were collected and filtered using a 96-well filter plate and a vacuum pump. The concentration of free (i.e., unbound) LPMOs in these samples was determined by UV-spectroscopy as described above (see chapter 2.9) and assessed by LDS-PAGE in a qualitative fashion. To assess the potential UV absorbance signal of soluble contaminants released from polymer samples, a set of control experiments were carried out using 50 mg of Avicel, β-chitin, PET, LDPE, HDPE, or PP in the absence of any LPMO in the same way as described above.

3.11. Comparing CelS2 and CelS2-CBM1 oxidative activity on cellulose

Beyond evaluating the binding of LPMO upon substituting the family 2 CBM on CelS2 with family 1 CBM, it is also a great interest to compare the oxidative activities on its native substrate, cellulose, between CelS2 and CelS2-CBM1. This exploration aims to discern whether the oxidative activity on cellulose is either altered, enhanced, or remains unchanged.

Method:

1 µM Cels2 or Cels2-CBM1 was incubated with 1% (w/v) Avicel followed by 50 µM sodium phosphate buffer, pH 6.0, Milli-Q H_2O, and 1 µM gallic acid to start the reaction. The final volume was 600 µL. The experiment was carried out in 2 ml microcentrifuge tubes at 30 °C using a thermomixer set to 1000 RPM. 100 µL aliquots were collected at different timepoints and filtered using a 96-well filter plate and a vacuum pump to stop the reaction (separate the substrate form the enzyme). The concentration of soluble oxidized product of cellulose was determined by High-performance anion exchange chromatography (HPAEC) as described below (see chapter 3.13).

3.12. Assessing the reduction in activity of LPMO on cellulose in the presence of plastics.

In this project, it was proposed that the degree of reduction of LPMO activity towards its natural substrate (e.g., cellulose) in the presence of PET, LDPE, HDPE, or PP can be used as an indirect indicator for binding to these plastics. The stronger the LPMO affinity towards the substance of interest, the less oxidation of cellulose is expected due to the competition between cellulose and the other polymer for protein binding.

<u>Method</u>

50 mg of PET, LDPE, HDPE, or PP was weighted in 2 ml microcentrifuge tubes by using an analytical balance weight, followed by addition of 250 µl of Milli-Q water, 30 µl of 500 mM sodium phosphate buffer, pH 6.0, and 20 µl of 25 µM LPMO solution (total volume of 300 µl). The enzyme-substrate suspensions were incubated at 25°C for 40 minutes in a thermomixer set to 1000 RPM. The resulting concentration of LPMO and sodium phosphate buffer during the pre-incubation step was $\approx$ 1.6 µM and 50 mM, respectively. After pre-incubation, 75 µl of Milli-Q water, 20 µL of 500 mM sodium phosphate buffer, pH 6.0, 50 µl of 10% (w/v) Avicel, 5 µL of 100 mM gallic acid and 50 µl of 1 mM H_2O_2 were added to each tube to start the LPMO reaction for determination of the amount of LPMO not bound to the plastic. The final reaction volume amounted to 500 µl. The final concentrations of LPMO, reductant, cellulose, and H_2O_2 during the reaction phase were 1 µM, 1 mM, 1% (w/v), and 100 µM, respectively. The tubes were incubated for 3 minutes at 25°C in the thermomixer set to 1000 RPM. Next, 250 µL aliquots were sampled from the mixtures and filtered through a 0.45 µm membrane using a filter plate to stop the LPMO reactions. The soluble oxidized products released by LPMOs from Avicel were analyzed by HPAEC-PAD as described below. To assess the effects of PET, LDPE, HDPE and PP on cellulose oxidation, the areas of peaks of oxidized LPMO products were compared to the product peaks obtained in a reference reaction containing LPMO substrate but lacking polymers of interest. This reference reaction was carried out for 3 minutes at 25°C in the thermomixer set to 1000 RPM, using 1 µM LPMOs, 1 mM gallic acid, 1% (w/v) Avicel, and 100 µM H_2O_2. An additional set of reference reactions were set up under the same conditions with decreasing amount of LPMO (1 µM, 0.5 µM, and 0.1 µM enzyme) to simulate a decrease in free enzyme concentration due to binding, and to show that such a decrease will result in a detectible drop in Avicel degradation.

3.13. The detection and analysis of LPMO products by high-performance anion-exchange chromatography with pulsed amperometric detection (HPAEC-PAD)

High-performance anion exchange chromatography (HPAEC) is a commonly used method for detection and quantification of oligosaccharides of various nature. Due to the presence of hydroxyl groups, carbohydrates can behave as very weak acids. At alkaline pH (> 12), these groups undergo

deprotonation, resulting in a negative charge on oligosaccharide molecules and allowing them to interact with positively charged resins. The elution of the analytes is achieved by introducing competing negatively charged ions (usually by introducing NaOAc into the running buffer). HPAEC systems are typically equipped with amperometric detectors. The amperometric detection is performed using solid anodes, commonly made of gold, platinum, or glassy carbon, under a constant applied potential (or under potential, applied in short pulses in case of so-called pulsed amperometric detection or PAD) (Corradini, Cavazza, & Bignardi, 2012). The electro-oxidation of oligosaccharides results in a current within the amperometric cell which is proportional to the concentration of the analyte in the solution.

Method

The analysis of oxidized cellulose products was performed using a Dionex ICS5000 system coupled to a pulsed amperometric detector and equipped with a CarboPac PA200 analytical column. A stepwise gradient with an increasing amount of eluent B (eluent B: 0.1 M NaOH and 1 M NaOAc; eluent A: 0.1 M NaOH) was applied according to the following program: 0–5.5% B over 3 min, 5.5–15% B over 6 min, 15–100% B over 11 min, 100–0% B over 6 s, 0% B over 6 min. The flow rate was 0.5 ml/min. Chromeleon 7.0 software was used for data analysis and processing. C1-oxidized cello-oligosaccharide standards with a degree of polymerization of two and three (DP2, DP3) were prepared in-house according to previously described method. (Stepnov, Forsberg, et al. 2021)

3.14. inhibition of PETase activity on PET in the presence of Cels2 or Cels2$_{TR}$ LPMO

PETase (LCC^{ICCG}) is a widely recognized enzyme for PET degradation. To evaluate the binding affinity of CelS2 or CelS2$_{TR}$ to PET, a strategy involves investigating the repression of PETase activity in the presence of one of these LPMOs. It is hypothesized that the higher the inhibition of PETase's ability to hydrolyze PET, the stronger the binding of CelS2 or CelS2$_{TR}$ to PET surfaces.

Method:

2 µM Cels2 or Cels2$_{TR}$ were pre-incubated in 2 ml microcentrifuge tubes with 50 mg of PET in 50 µM sodium phosphate buffer, pH 6.0, and Milli-Q H$_2$O for 30 minutes at 40 °C in a thermomixer set to 1000 RPM to ensure uniform distribution of polymer particles. Next, 0.2 µM LC_ICCG PETase was added to the microcentrifuge tubes to start the reaction, and the final volume was 500 µl. Subsequently, the tubes were placed back into the thermomixer set to 1000 RPM at 40°C. Next, the aliquots were collected at different timepoints, and 500 µL EtOH was added to stop the reaction, and the samples

were centrifuged at 12.000 g for 5 minutes to precipitate the PET particles. Finally, 500 µl aliquots were taken from the supernatants and loaded into UV-transparent quartz cuvette, and the concentration of soluble hydrolyzed products of PET was determined by UV spectroscopy (λ = 240 nm; K_{ext} = 13800 $M^{-1} \cdot cm^{-1}$) (Pirillo, Pollegioni and Molla 2021).

4. Results

4.1. Binding of CelS2 to plastics and insoluble polysaccharides

To set up methods allowing for rapid screening of LPMO binding to various types of plastics, CelS2 (also known as *Sc*LPMO10C) was selected as a model enzyme. This bacterial LPMO was among the first lytic polysaccharide monooxygenases to be discovered. CelS2 comprises a family 10 (AA10) catalytic domain connected to a C-terminal family 2 carbohydrate-binding module (CBM2) through a linker (Zarah Forsberg 1 2011), (Gaston Courtade 2018). CelS2 is capable of oxidative depolymerization of cellulose, resulting in the formation of C1-oxidized products. The main reason behind choosing CelS2 as the model in this thesis is the fact that the binding of this enzyme to microcrystalline cellulose (Avicel) is very well-studied. Furthermore, this LPMO is easy to produce on 50-100 mg scale in *E. coli*, hence the large amount of protein was readily available in the lab at the start of the project.

To assess the binding potential of CelS2 towards insoluble polysaccharides (Avicel and β-chitin) and industry relevant plastics (PET, LDPE, HDPE, and PP), 50 mg of these compounds were incubated with 2 µm LPMO in 500 µl of 50 mM sodium-phosphate buffer, pH 6.0 for 40 minutes at 25 °C and 1000 RPM. After incubation, the bound protein was removed by filtration of the substrate (containing the bound protein fraction) and the residual concentration of free LPMO was measured using UV spectroscopy (**Fig. 4.1.1**). The free protein concentration determined in a filtrate obtained after incubation of CelS2 in buffer in the absence of any polymers was used as a reference value (i.e., was set as 100% free protein).
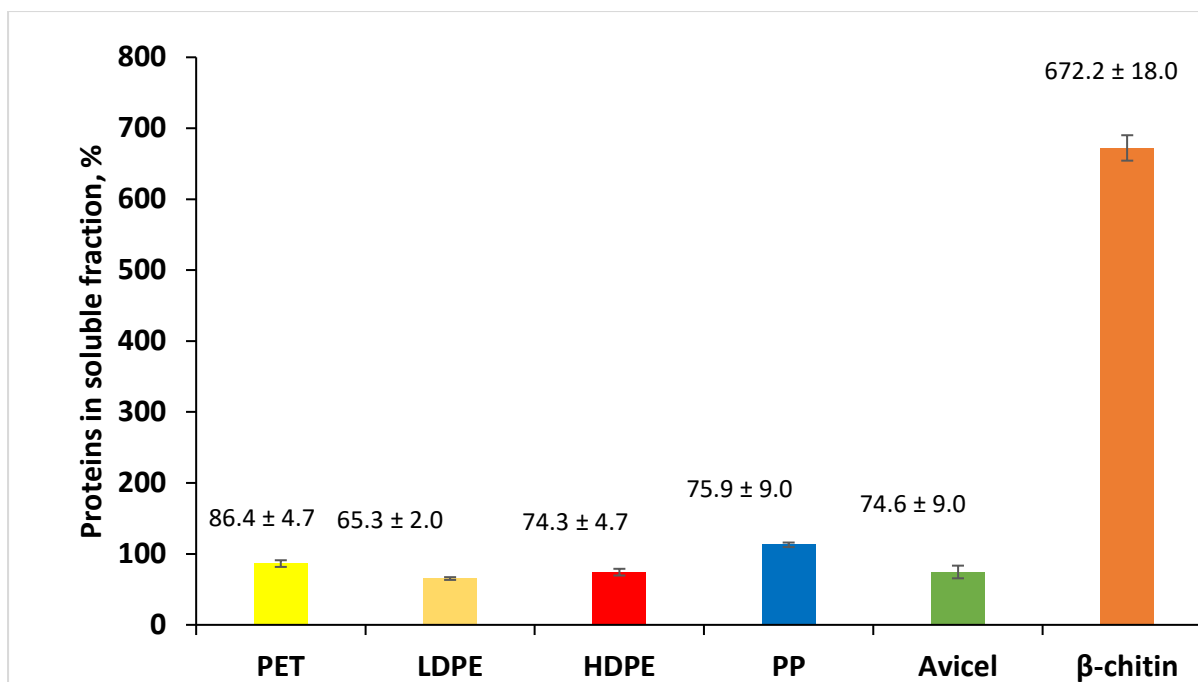
Fig. 4.1.1. Binding of CelS2 to polysaccharides and plastics. The figure shows the relative amount of free protein detected in solution by UV spectroscopy (λ = 280 nm) after 40 minutes of pre-incubation of 2 μM LPMO with 50 mg of polymers in 500 μl of 50 mM sodium-phosphate buffer, pH 6.0. The insoluble fraction containing bound enzyme species was removed by filtering through a 0.4 μm membrane prior to measuring the absorbance. The protein concentration determined in the control experiment featuring LPMO, but lacking polysaccharides or plastics was set as 100%. All experiments were carried out in a thermomixer (25 °C, 1000 RPM). Error bars indicate standard deviations between replicates (n = 3). Note that the impossibly high (>> 100%) signal observed in the experiment with β-chitin indicates contamination with UV-absorbing soluble compounds which are present in this polymer sample.

The results of the initial experiment indicated that CelS2 is able to bind to LDPE and HDPE to a significant extent as 65.3 ± 1.9 and 74.3 ± 4.7 % protein remained in solution after LDPE- or HDPE-bound LPMO species were removed, respectively (meaning that 34.7 ± 1.9 % of LDPE and 25.7 ± 4.7 % of HDPE was bound to the plastic). Note that according to spectroscopy data, 74.6 ± 9.0 % of CelS2 remained in solution after incubation with Avicel, which is comparable to the results obtained with LDPE and HDPE. Strikingly, the residual protein concentration measured after incubation with β-chitin amounted to 672 % (**Fig. 4.1.1**), pointing out an possible unknown UV-absorbing sub-micron particles that may pass through the filter and contaminating polymer sample and interfering with the protein concentration assay.

The LDS-PAGE analysis of residual protein in samples previously used in UV-spectroscopy experiments (**Fig. 4.1.2**) revealed a very strong binding of CelS2 to both β-chitin and Avicel compared to other types of polymers tested. CelS2 bands were completely undetectable in the samples incubated with Avicel, indicating ≈100% binding to cellulose. Taken together, the data in **Fig. 4.1.1** and **Fig. 4.1.2** show that

UV spectroscopy data obtained with β-chitin and Avicel is not reliable. To check whether any of polymers used in the project contained UV-absorbing contaminants that interfered with the protein concentration assay, the incubation experiments were carried out again, this time substituting LPMO with the same volume of Milli-Q H_2O. Indeed, a strong UV signal was observed in solutions in the absence of LPMO in the case of both Avicel and β-chitin, after insoluble fractions were filtered out (**Fig. 4.1.3**). These background signals were then used to correct the previously obtained CelS2 binding data. Note that the adjusted UV spectroscopy data (**Fig. 4.1.4**) indicate strong binding of CelS2 to both cellulose and β-chitin, which is in line with previous observations (Forsberg, Røhr, et al., Comparative Study of Two Chitin-Active and Two Cellulose-Active AA10-Type Lytic Polysaccharide Monooxygenases 2014).

Next, LDS-PAGE gel densitometry was evaluated as an alternative tool to study CelS2 binding. The relative areas of LPMO bands shown in **Fig. 4.1.2** were determined using image analysis software provided with a gel imaging system. These values were then used as indirect indicators of the residual protein concentration in experimental samples. The results retrieved from LDS-PAGE gel densitometry for LDPE, HDPE, PP, and PET indicated 75.1 ± 5.6, 83.7 ± 5.1, 98.5 ± 4.6, and 94.7 ± 1.7 free protein, respectively. Comparing this new dataset to the binding data previously obtained by UV spectroscopy revealed a noticeable correlation as shown in **Fig. 4.1.5**. Using gel densitometry resulted in much lower standard deviation when studying binding to Avicel and β-chitin. However, gel densitometry is much more time demanding and since both methods performed well when studying plastics, the UV spectroscopy-based approach was used in all the experiments described below.
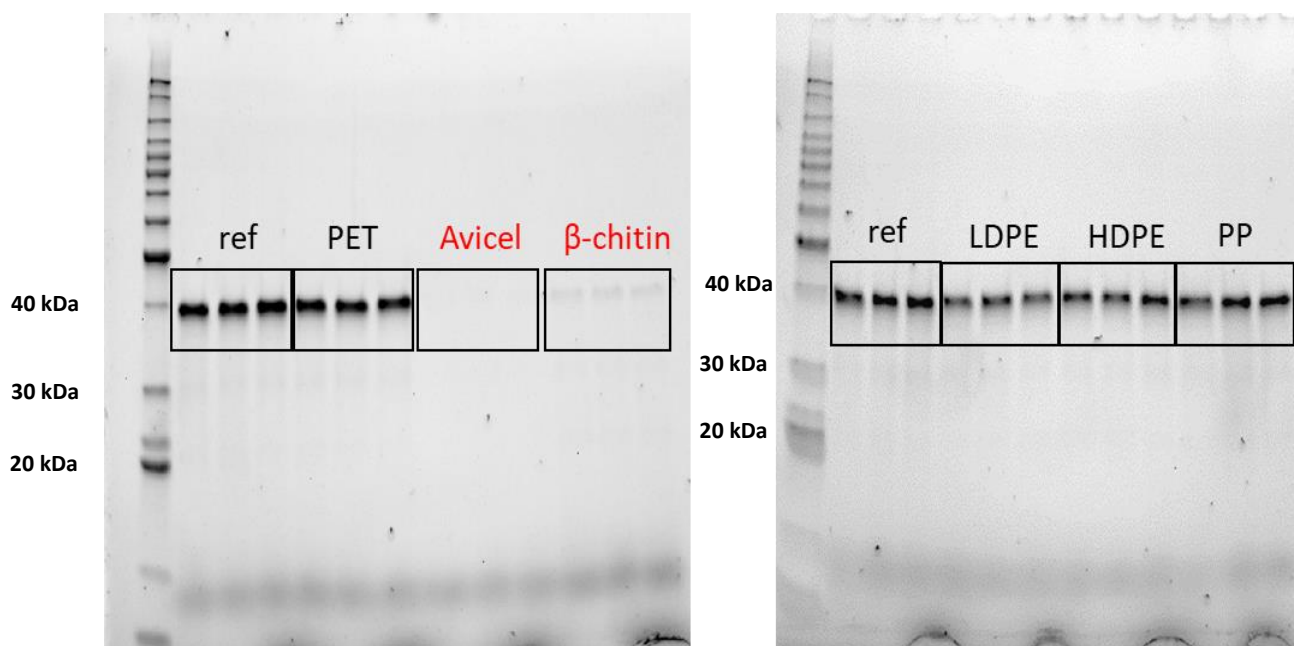
Figure 4.1.2: LDS-PAGE analysis of CelS2 samples obtained in binding experiments after incubation with various plastics or carbohydrates followed by filtration. The lanes are labelled with the names of polymers that were present during the incubation. See Fig. 4.1.1 for the experimental conditions. The lanes marked with "ref" correspond to the control LPMO samples incubated in the absence of any insoluble polymers. Note that LDS-PAGE data obtained in the presence of Avicel, and β-chitin indicates strong binding of Cels2 to these polymers.
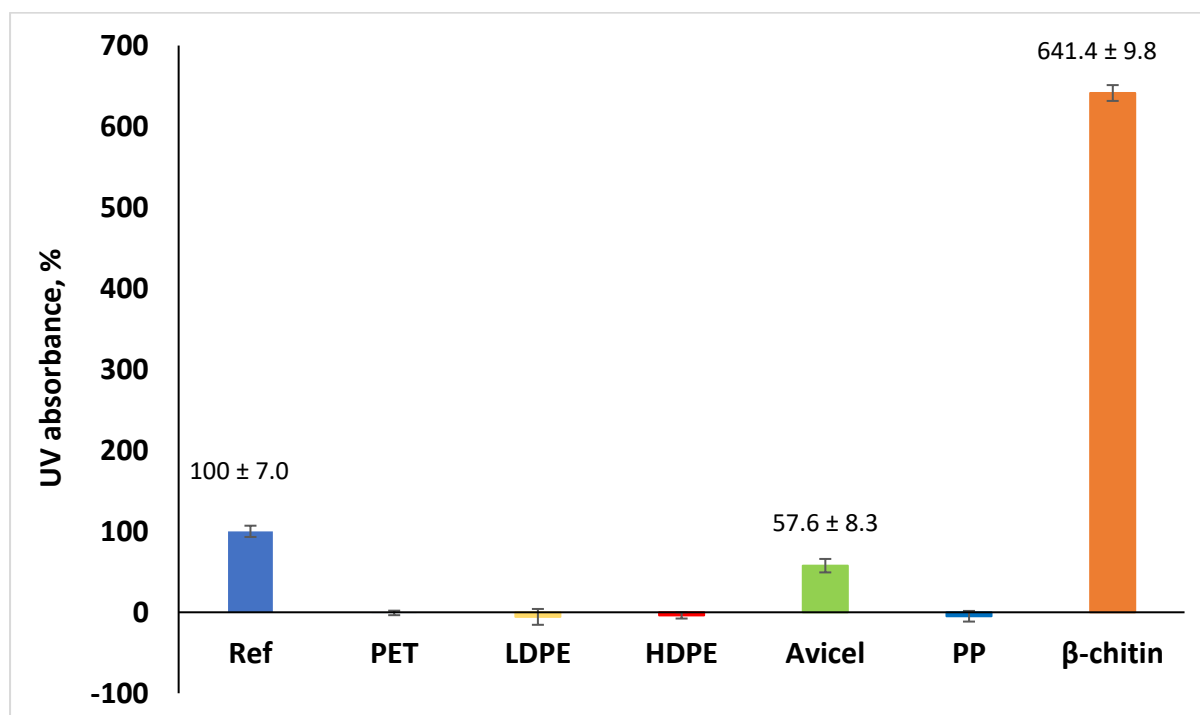
Fig. 4.1.3. Screening for UV absorbing contaminants. The figure shows the UV absorbance of control samples (λ = 280 nm) obtained by pre-incubating 50 mg of various polymers in 500 µl of 50 mM sodium-phosphate buffer, pH 6.0. All experiments were carried out in a thermomixer (25 °C, 1000 RPM). The insoluble fraction was removed by filtering through a 0.4 µm membrane prior to

measurement. The UV absorbance is given as a relative value compared to a signal obtained with 2 µM CelS2. Note that the results obtained with Avicel and β-chitin in the absence of LPMO clearly indicate contamination of polymer samples. Error bars indicate standard deviations between replicates (n = 3).

Figure 4.1.4: Binding of CelS2 to polysaccharides and plastics after background correction. The figure shows the results of the binding experiment (Fig. 1) corrected for the background signal observed in Avicel and β-chitin.

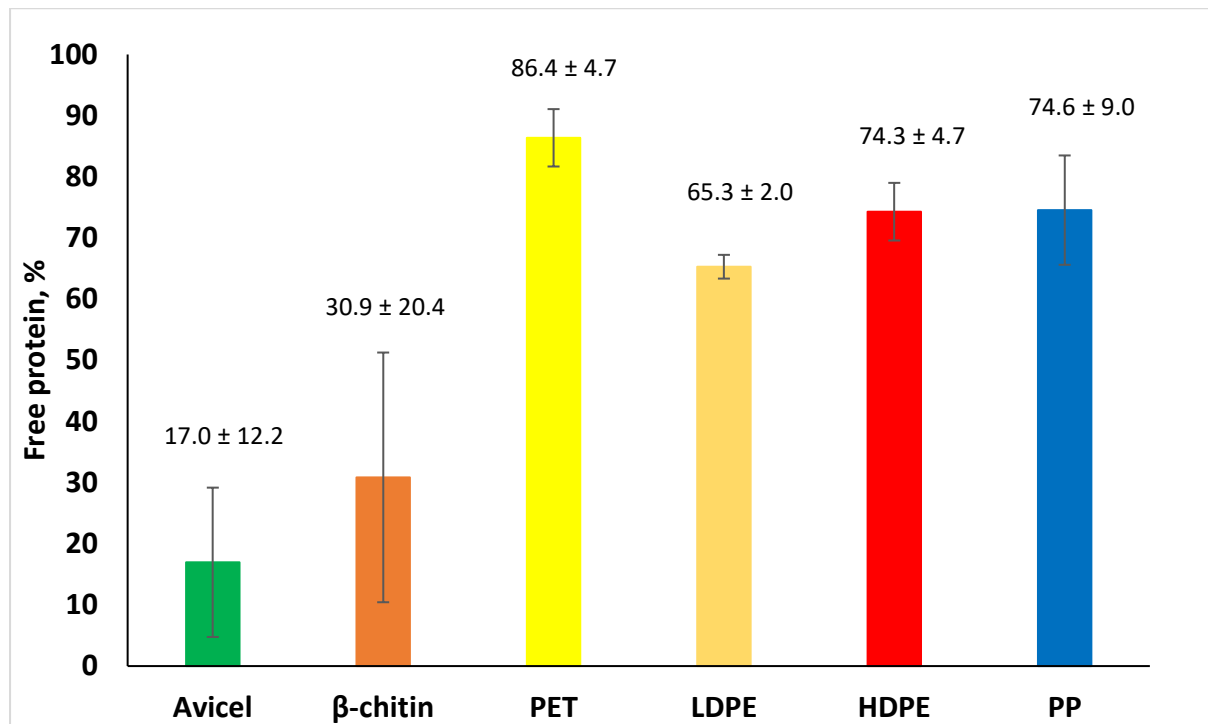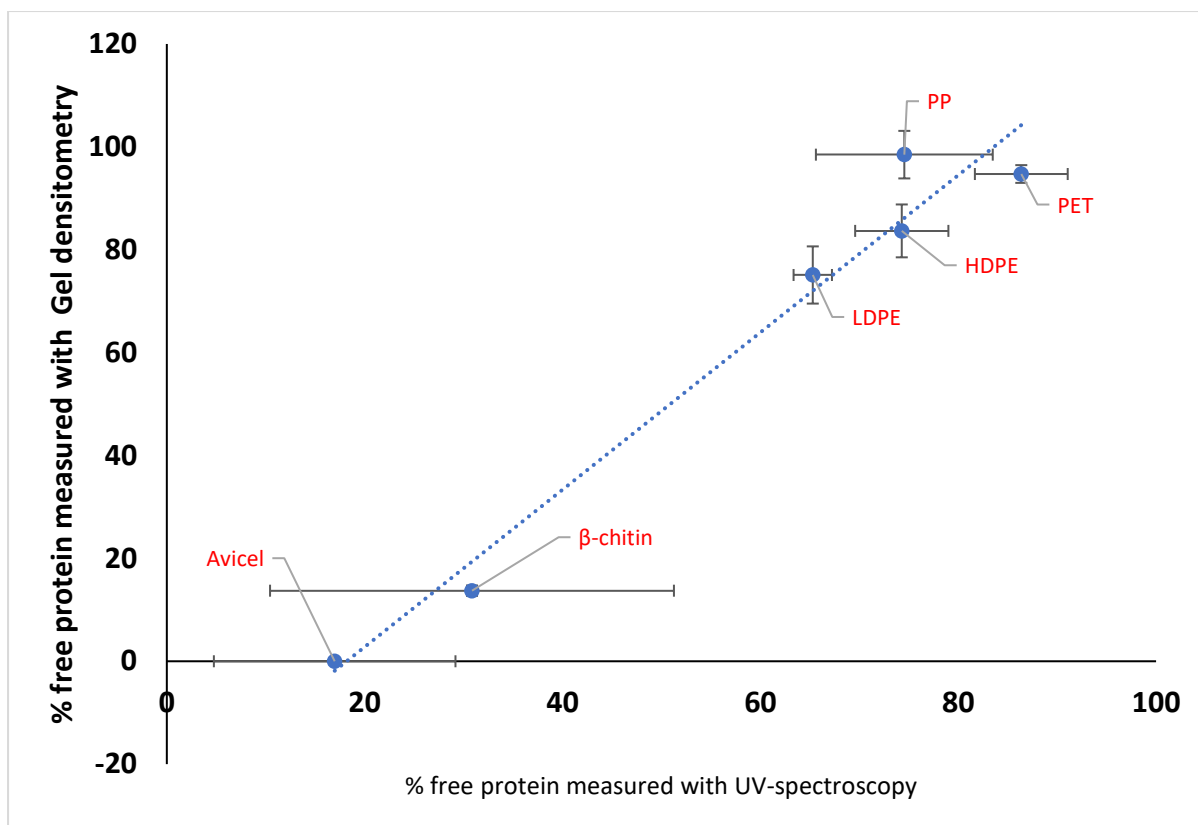**Fig. 4.1.5. The relationship between the concentration of free CelS2 measured in binding experiments using UV spectroscopy or LDS-PAGE gel densitometry.** The x-axis represents the free protein concentration assessed by UV spectroscopy shown in Fig. 4.1.4. The data plotted in the y-axis represents the free protein concentration assessed by measuring the area of CelS2 bands on LDS-PAGE gels shown in Fig. 4.1.2. Error bars indicate standard deviations between replicates (n = 3). Note that the figure shows a noticeable correlation between the data obtained using two different methods.

4.2. Investigating the role of CBM in Cels2 binding to plastics and insoluble polysaccharides

Previous studies have shown that the CBM of CelS2 binds much stronger to cellulose than the catalytic domain (G. Courtade, Z. Forsberg, et al. 2018). To investigate whether CBM plays a similar major role in LPMO interaction with plastics, a truncated variant of CelS2 lacking carbohydrate binding module (called CelS2$_{TR}$) was used as a model (**Table 2.3.2**). Avicel, LDPE, and β-chitin were selected for this analysis due to their previously observed high binding to CelS2. The binding of CelS2$_{TR}$ to LDPE, β-chitin, and Avicel was assessed by UV spectroscopy, as described above. Compared to previous results obtained with Cels2 (**Fig. 4.1.4**), CelS2$_{TR}$ displayed a decreased binding to β-chitin: 134.0 ± 34.9 % free protein was detected in soluble fraction after incubation with this polysaccharide as opposed to just 30.9 ± 20.4 % free protein observed in the experiment with wild-type CelS2. The binding of CelS2$_{TR}$ to LDPE was somewhat decreased compared to the wild-type LPMO. 86.2 ± 14.9 % free protein was detected in the experiment with the truncated enzyme in contrast to 65.3 ± 2.0 % free protein

observed in the experiment with wild-type CelS2. Note that due to the high standard deviation observed in the experiment with CelS2$_{TR}$ involving LDPE, the contribution of CBM to binding cannot be determined with precision. However, this data provides at least some indication that CBM may indeed play some role in the binding of CelS2 to LDPE. The standard deviations between data obtained in experiments with Avicel are very high to make any claims regarding this polymer.
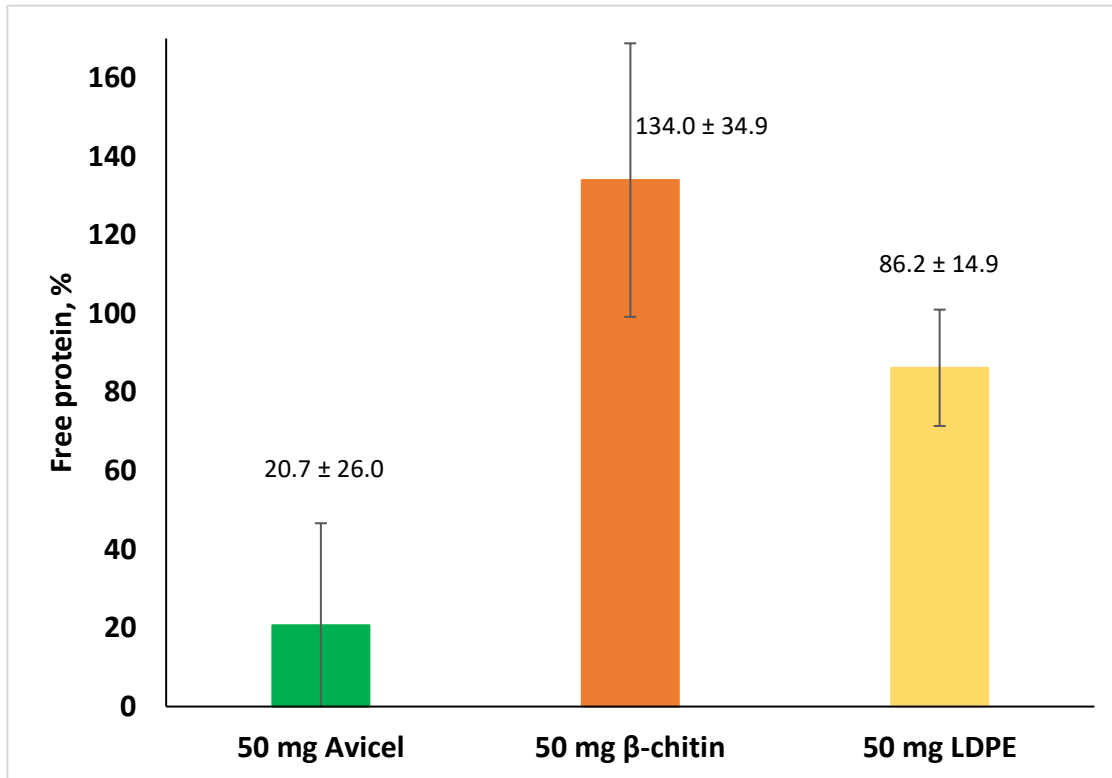

Fig 4.2.1. Binding of CelS2-$_{TR}$ to Avicel, β-chitin, and LDPE. The figure shows the relative amount of free protein detected in solution by UV spectroscopy (λ = 280 nm) after 40 minutes of pre-incubation of 2 μM LPMO with 50 mg of polymers in 500 μl of 50 mM sodium-phosphate buffer, pH 6.0. The insoluble fraction containing bound enzyme species was removed by filtering through a 0.4 μm membrane prior to measuring the absorbance. The protein concentration determined in the control experiment featuring LPMO, but lacking polysaccharides or plastics was set as 100%. Note that the high signal observed in the experiment with β-chitin suggests a lower binding affinity of Cels2 when the CBM domain is removed, and what can be observed in the experiment with LDPE see Fig 3.

4.3.   Design and expression of Cels2-CBM1, Cels2-DSI, and Cels2-PBM

In an attempt to improve CelS2 binding to plastics, three novel chimeric forms of this LPMO were designed by substituting the family 2 CBM with 1) a family 1 CBM from *Tr*Cel7A cellulase; 2) the hydrophobic peptide Dermaseptin SI (DSI); 3) a polyhydroxyalkanoate binding module (PBM) from cutinase (LCC_ICCG) found in *Alcaligenes faecalis* (**See table 2.3.1**)*.* Family 1 CBM from TrCel7A has previously shown to improve the activity and PET binding of PETase (LCC[YCCG]), after being fused with the enzyme. (Rosie Graham 1 2 2022). DSI has previously been used as an anchor to immobilize

enzymes on PET surfaces (Niclas Büscher 2019). PBM from PBM from Thc_Cut1 binds to polyhydroxyalkanoates, which are hydrophobic molecules resembling plastics (Doris Ribitsch 2013). The corresponding genes were synthesized by GenScript and cloned into pET-26(b) + expression vector. The *E. coli* expression strains were established by transformation of BL21 (DE3) *E. coli* cells with the corresponding plasmids. The initial expression of Cels2-CBM1, Cels2-DSI and Cels2-PBM was carried out by inoculating 2 ml of LB medium with a single colony from a petri dish with the respective expression strain. The cell cultures were incubated overnight at 37°C and 200 RPM. After overnight incubation of the cells, the cultures were split in two parts and the experiment was conducted for 3 more hours in the presence or in absence of 1 mM IPTG. To verify the expression of the LPMOs, aliquots of the cultures were taken and analyzed using LDS-PAGE. The results shown in **Fig. 4.3.1** indicate the expression of CelS2-CBM and CelS2-PBM both in the presence or absence of the IPTG. There were no clear signs of expression of CelS2-DSI.
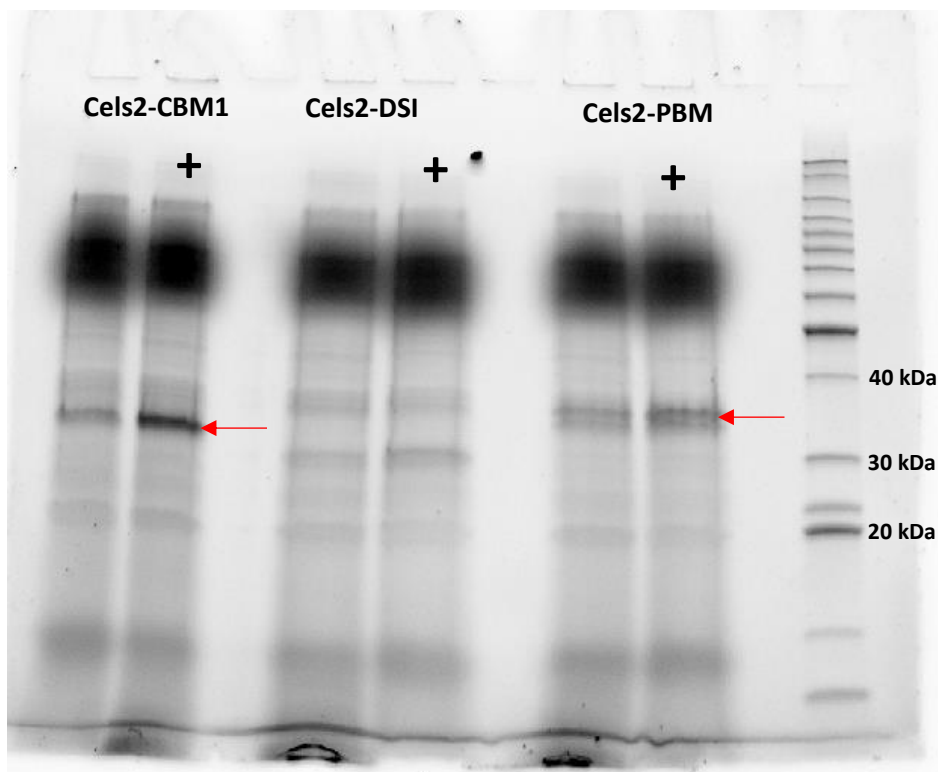

Fig 4.3.1. Small-scale LPMO expression experiment. The lanes are labelled with the respective LPMO names, with a "+" sign indicating the addition of IPTG as an inducer. Arrows indicate bands corresponding to CelS2-CBM1 and CelS2-PBM. No clear sign of CelS2-DSI expression was observed both in the presence or absence of IPTG.

To produce CelS2-CBM1, the corresponding *E. coli* expression strain was cultivated in 2 x 500 ml of LB medium at 37° C until OD_{600} of 0.6 units was reached followed by 24 hours of induction with 1 mM ITPG at room temperature. The cells were harvested by centrifugation and subjected to periplasmic extraction. The LDS-PAGE analysis of periplasmic extract (**Fig. 4.3.2**) revealed that only a negligible fraction of target LPMO was present in the periplasm, potentially indicating that most of the enzyme was misfolded and insoluble. To increase the yield of soluble LPMO, another expression experiment was carried out. This time, *E. coli* cells were cultivated at 37 °C for 24 hours in the absence of IPTG, which resulted in a significant decrease in total amount of target LPMO (**Fig. 4.3.3**). At the same time, the amount of CelS2-CBM1 in periplasm has increased, indicating a potential trade-off between the overall level of LPMO expression and its solubility. The obtained periplasmic extract was subjected to purification using anion-exchange and size-exclusion chromatography as described in section 4.5.

Fig. 4.3.2. Expression and periplasmic extraction of CelS2-CBM1 after induction with IPTG. The figure shows an LDS-PAGE electropherogram of samples obtained during CelS2-CBM1 expression experiment. "wc", a whole-cell sample taken from *E. coli* BL21 (DE3) culture after 24h of induction with 1 mM IPTG at room temperature; "suc", a sample of culture supernatant obtained by treating cells with spheroplast buffer containing sucrose; "per", a sample of culture supernatant (i.e., periplasmic extract) obtained by treating cells with ice-cold water. Note that the periplasmic extract exhibits a thin band (marked with the red arrow), likely corresponding to CelS2-CBM1. The red box indicates the position of the LPMO band in the electropherogram of the whole-cell sample.
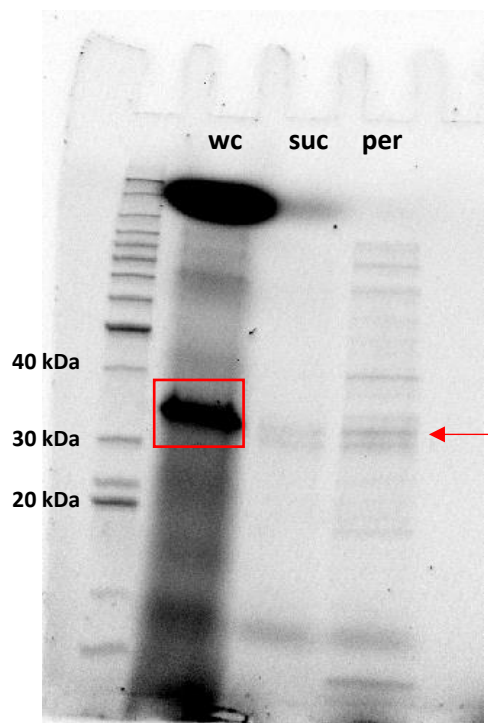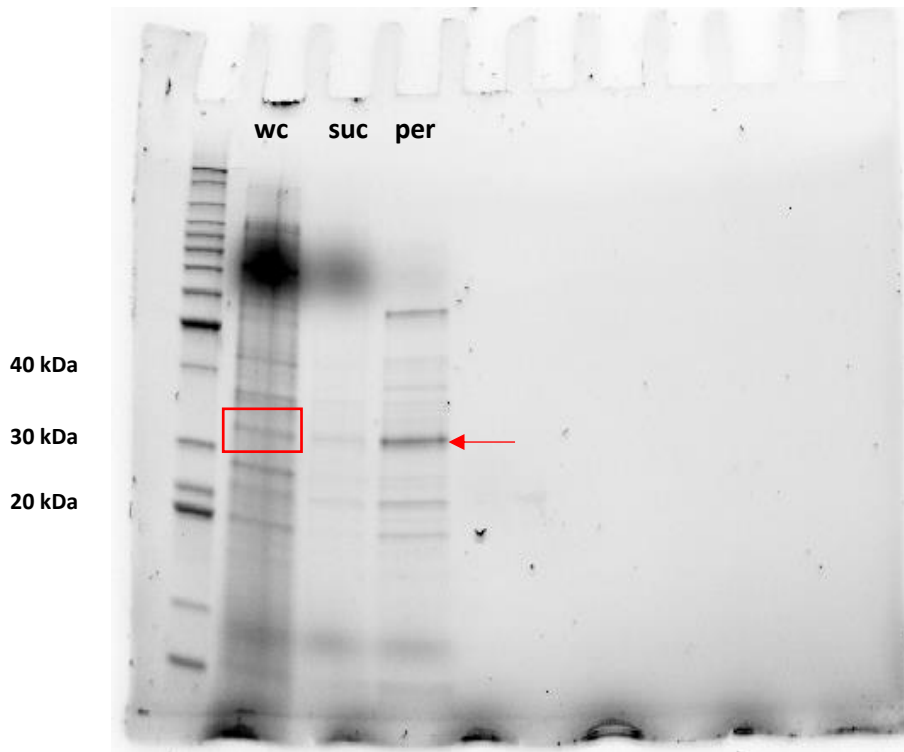
Fig 4.3.3. Expression and periplasmic extraction of CelS2-CBM1 in the absence of IPTG. The figure shows an LDS-PAGE electropherogram of samples obtained during the CelS2-CBM1 expression experiment. "wc", a whole-cell sample taken from *E. coli* BL21 (DE3) culture after incubation overnight at 37°C; "suc", a sample of culture supernatant obtained by treating cells with spheroplast buffer containing sucrose; "per", a sample of culture supernatant (i.e., periplasmic extract) obtained by treating cells with ice-cold water. Note that the periplasmic extract exhibits a clear band (marked with the red arrow), corresponding to CelS2-CBM1. The red box indicates the position of the LPMO band in the electropherogram of the whole-cell sample.

The production of CelS2-PBM was attempted using the same two strategies as described above. In both cases, soluble LPMO was not detected in the periplasmic extract as shown in **Fig.4.3.4**.
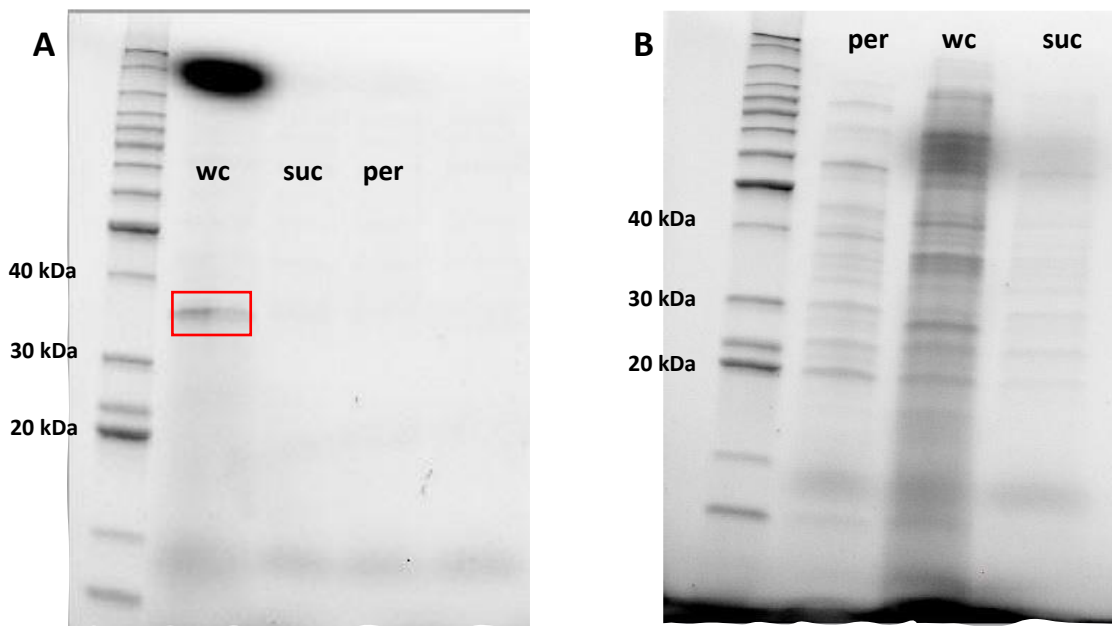
Fig 4.3.4. Expression and periplasmic extraction of c after induction with IPTG or in the absence of IPTG. The figure shows an LDS-PAGE electropherogram of samples obtained during the CelS2-PBM expression experiment after the addition of 1 mM IPTG (panel A) or in the absence of IPTG (panel B). "wc", a whole-cell sample taken from *E. coli* BL21 (DE3) culture after incubation overnight at 37°C, highlighted by the red square in panel A; "suc", a sample of culture supernatant obtained by treating cells with spheroplast buffer containing sucrose; "per", a sample of culture supernatant (i.e., periplasmic extract) obtained by treating cells with ice-cold water. protein was not detected in the periplasmic fraction in the both experiments (panel A and B).

4.4.   Purification of Cels2-CBM1 with Anion-exchange Chromatography

Cels2-CBM1 was purified from the periplasmic extract by anion-exchange chromatography. After the application of the periplasmic extract to the column, the bound proteins were eluted using a linear NaCl gradient, resulting in three peaks (**Fig. 4.4.1**). The fractions corresponding to elution peaks were collected and analyzed by LDS-PAGE (**Fig. 4.4.2**). LDS-PAGE results indicated that the target LPMO was contained in fractions 15-18. The samples containing target LPMO were pooled, concentrated, and further purified by size-exclusion chromatography.
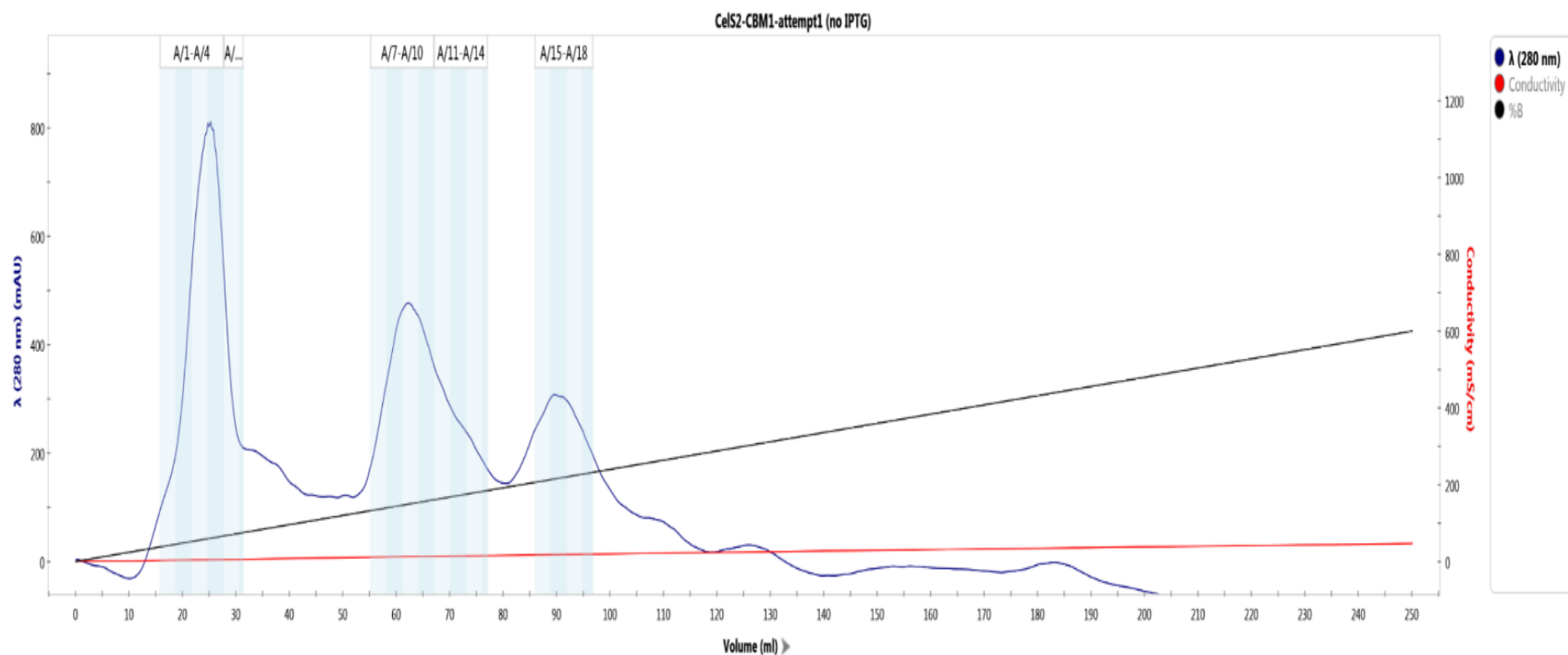
Figure 4.4.1. Purification of ScAA10C by anion-exchange chromatography. The figure shows elution profile obtained during the purification of Cels2-CBM1 by anion-Exchange Chromatography. Protein elution from the column was detected by monitoring A_{280} of the column flow-through, represented by the dark-blue curve. The black curve shows the NaCl gradient (0 - 0.5 M) applied to elute proteins bound to the column. The conductivity of the solution within the column is represented by the light red curve. Fraction numbers are shown above the peaks. The chromatogram was generated by using the ChromLab software.
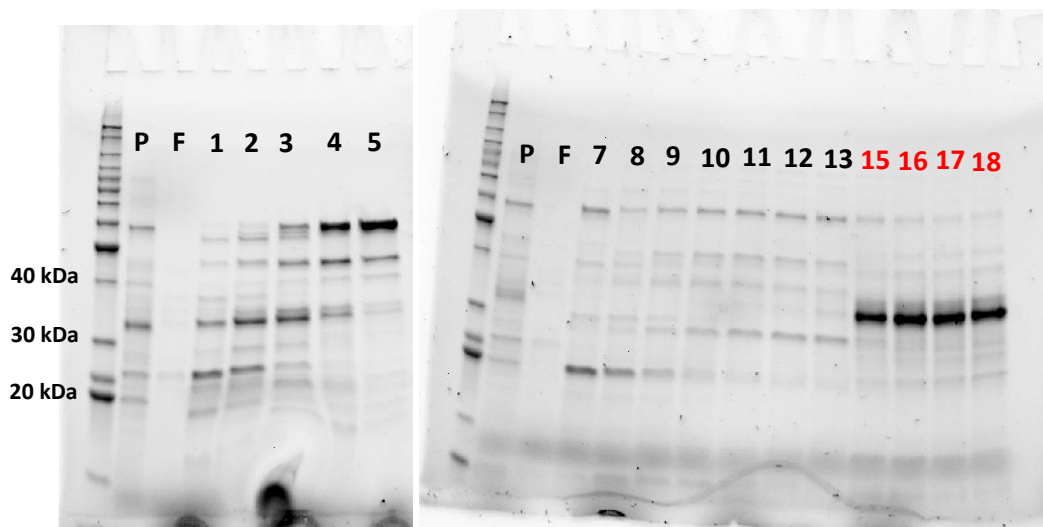
Figure 4.4.2. LDS-PAGE analysis of the fractions obtained during purification of CelS2-CBM1 by anion-exchange chromatography. The lanes are labeled with fraction numbers. The P and F labels indicate samples taken from the periplasmic extract applied to a column before the elution (P) or from the flow-through fraction (F), containing proteins that were not bound to the resin. Fractions marked with a red color exhibit distinct bands at ≈31 kDa, corresponding to Cels2-CBM1.

4.5. Size-exclusion chromatography

Cels2-CBM1 was further purified after anion-exchange chromatography with size-exclusion chromatography (SEC). After the application of the protein sample to the column, the bound proteins were eluted using one column volume of running buffer. Fractions 9-13 containing CelS2-CBM1 were collected and pooled together, highlighted by the red arrow on the peak shown in **Fig 4.5.1**. The pooled fractions were then concentrated to a final volume of 1 ml using ultrafiltration. To assess the purity of the protein, the concentrated sample was analyzed by LDS-page gel electrophoresis, as shown in **Figure 4.5.2**. The total LPMO yield amounted to approximately 1 mg of protein per 1 L of *E. coli* culture. The purified LPMO was copper-saturated and stored at 4°C until further use.
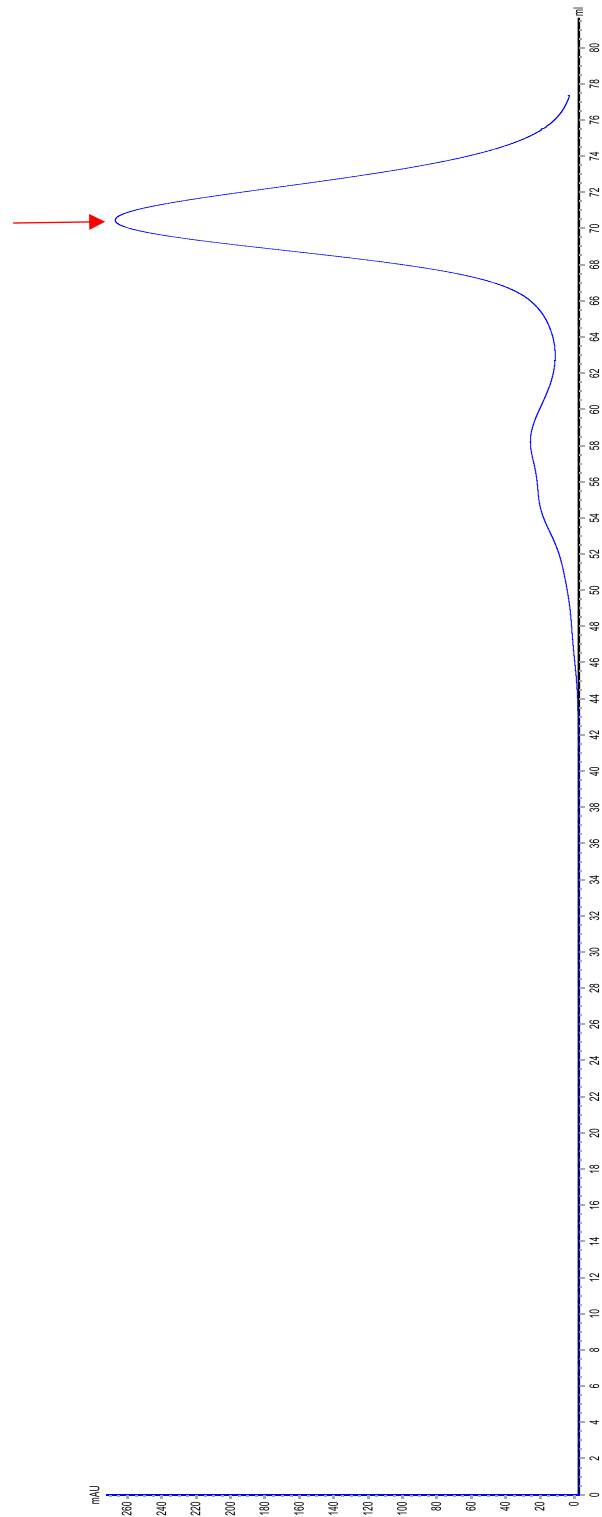
Figure 4.5.1. Chromatogram from purification of Cels2-CBM1 by SEC. The figure shows the elution profile obtained during the purification of Cels2-CBM1 by ProteoSEC Dynamic 3-70 kDa HR resin column. Protein elution from the column was detected by monitoring A280 of the column flow-through, represented by the dark blue curve. The bound proteins were eluted from the column with one column volume running buffer. The figure displays a major peak representing the elution of the target protein Cels2-CBM1 highlighted by the red arrow.
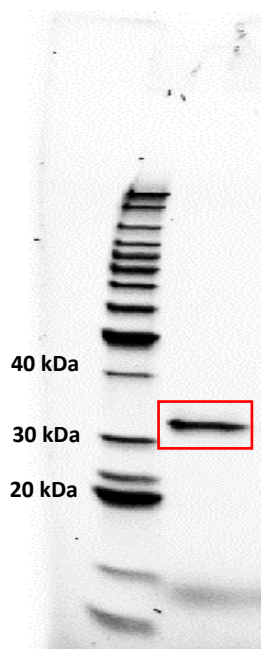
Figure 4.5.2. LDS-PAGE analysis of fractions obtained during SEC. The lane marked with a red square are the pooled fractions obtained from Size-Exclusion Chromatography and contain purified Cels2-CBM1, highlighted by the red square. The distinct band suggests a pure protein after purification with SEC.

4.6.   Cellulose oxidation by CelS2-CBM1

After copper saturation of Cels2-CBM1, its cellulose oxidation capability was compared to wild-type Cels2 to determine the effect of the CBM1 on CelS2 catalysis. Reactions with 1 µM LPMOs and 1 % (w/v) Avicel were carried out in 50 mM sodium phosphate buffer, pH 6.0 supplied with 1 mM gallic acid at 30 °C. The results presented in **Fig. 4.6.1** show that the ability of Cels2-CBM to oxidize cellulose is not compromised. This observation indicates that the substitution of the wild-type family 2 CBM with a family 1 CBM did not impair the enzyme capacity to bind cellulose.
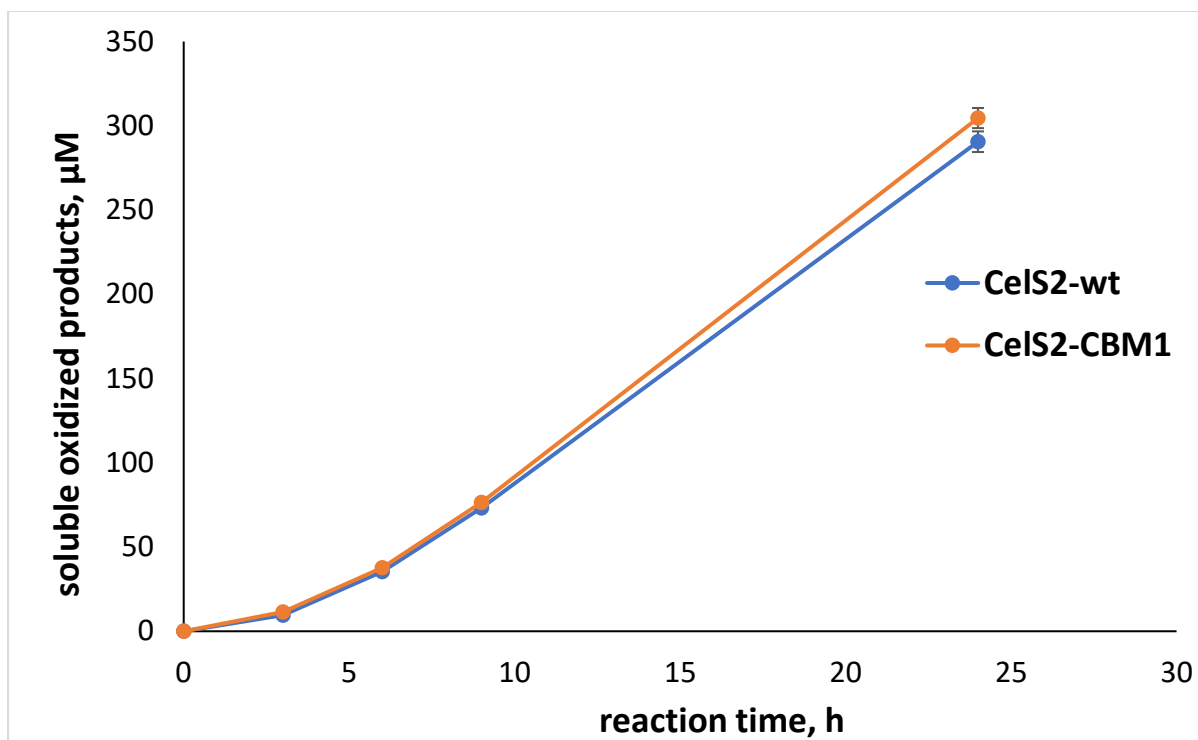
Fig. 4.6.1. Cellulose oxidation by CelS2 and CelS2-CBM1. The figure shows the release of oxidised products in LPMO reactions (1 µM LPMOs in 50 mM sodium phosphate buffer, pH 6.0, 30°C) with 1% (w/v) Avicel that was carried out using 1 mM gallic acid as the reductant. Error bars indicate standard deviations between triplicates and are in most cases hidden by the markers. Note that the experiment indicates that the main function of oxidizing cellulose is retained when substituting the original family 2 CBM domain with the family 1 CBM domain, as both variants show similar levels of activity towards cellulose.

4.7.   Binding of CelS2-CBM1 to plastics and insoluble carbohydrates

To evaluate the binding of CelS2-CBM1 to insoluble polymers of interest, a set of experiments were carried out according to the previously established method, based on UV spectroscopy. The results showed a general decrease in binding on all the plastic polymer tested, but most significant with LDPE: 97.5 ± 10.5 % free protein was detected in soluble fraction after incubation with LDPE as opposed to 65.3 ± 2.0 % free protein observed in the experiment with wild-type CelS2 (**Fig. 4.7.1**). The results indicate that the introduction of family 1 CBM results in reduced binding to plastic polymers. At the same time, the binding of CelS2-CBM1 to cellulose was significant, which is not surprising, given the fact that CelS2-CBM1 shows the same Avicel oxidation rate compared to wild-type CelS2 (**Fig. 4.6.1**).
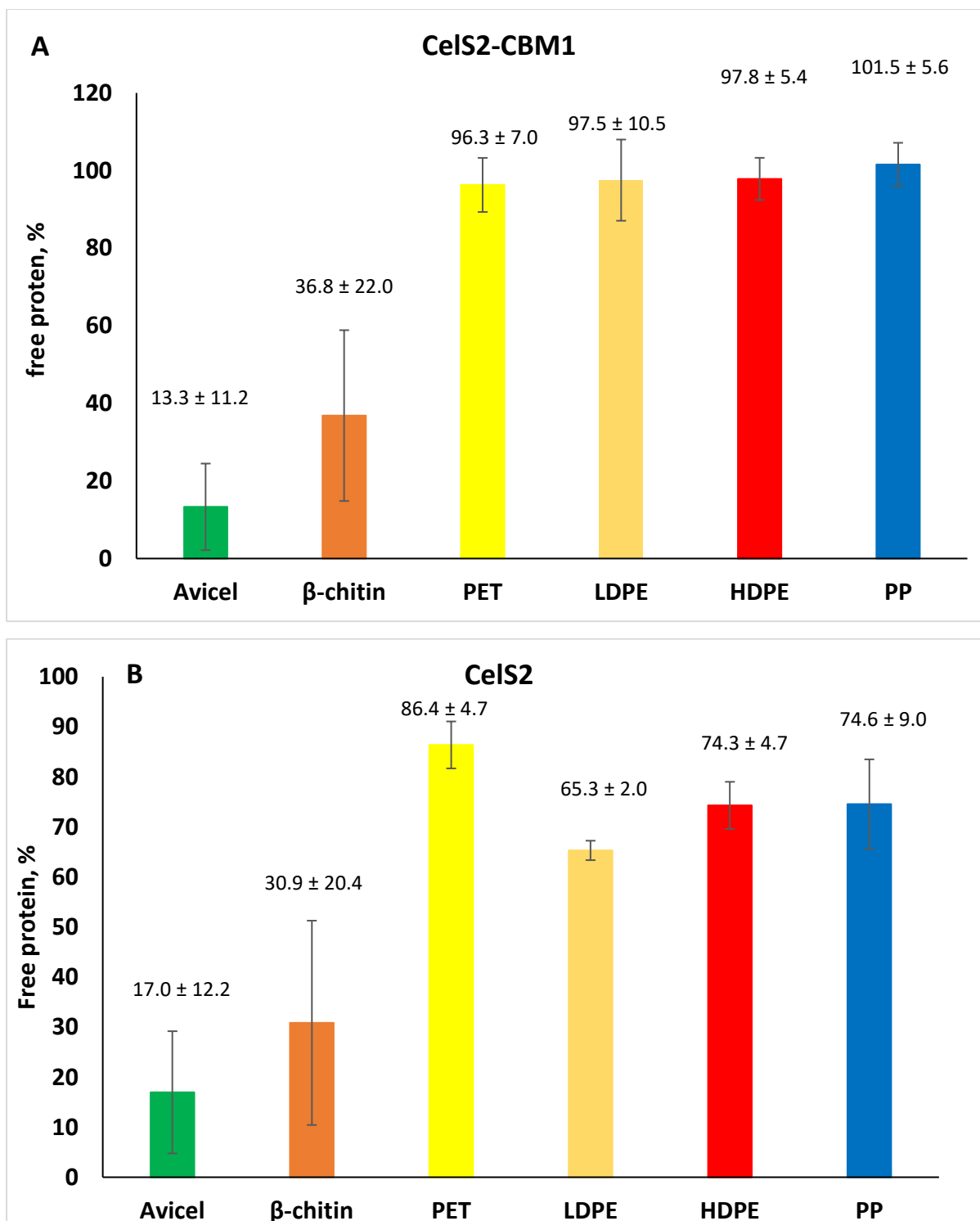
Fig. 4.7.1. Binding of CelS2-CBM1 and CelS2 to polysaccharides and plastics. The figure shows the relative amount of free protein detected in solution by UV spectroscopy (λ = 280 nm) after 40 minutes of pre-incubation of 2 µM CelS2-CBM1 (Panel A), and CelS2 (Panel B) with 50 mg of polymers in 500 µl of 50 mM sodium-phosphate buffer, pH 6.0. The insoluble fraction containing bound enzyme species was removed by filtering through a 0.4 µm membrane prior to measuring the absorbance. The protein concentration determined in the control experiment featuring LPMO, but lacking polysaccharides or plastics was set as 100%. All experiments were carried out in a thermomixer (25 °C, 1000 RPM). Error bars indicate standard deviations between replicates (n = 3).

4.8. Binding to plastics by CbpD, *Nc*LPMO9C, and *Ao*LPMO13A

To take a deeper look at how the LPMO binding to various types of plastics may depend on the domain architecture of the enzyme, more LPMOs were tested using a spectroscopy-based method. CbpD is the LPMO of the opportunistic pathogen *Pseudomonas aeruginosa,* which has recently been shown to be a lytic polysaccharide monooxygenase active on chitin and an important virulence factor for the bacterium (Askarian, et al. 2021). CbpD is composed of three domains, a AA10 catalytical domain, a GbpA2 domain with unknown function, and a carbohydrate-binding module 73 (CBM73) (Dade, Douzi, et al. 2022). *Ao*LPMO13A is an LPMO from *Aspergillus oryzae* lacks any CBMs and has only an AA13 domain that was shown to have oxidative activity on starch substrates. (Meier, et al. 2018). *Nc*LPMO9C is an LPMO from *Neurospora crassa* and is composed of a AA9 catalytical domain and a family 1 carbohydrate binding module (CBM1) and acts on cellulose and hemicellulose (Borisova, Isaksen, et al. 2015).
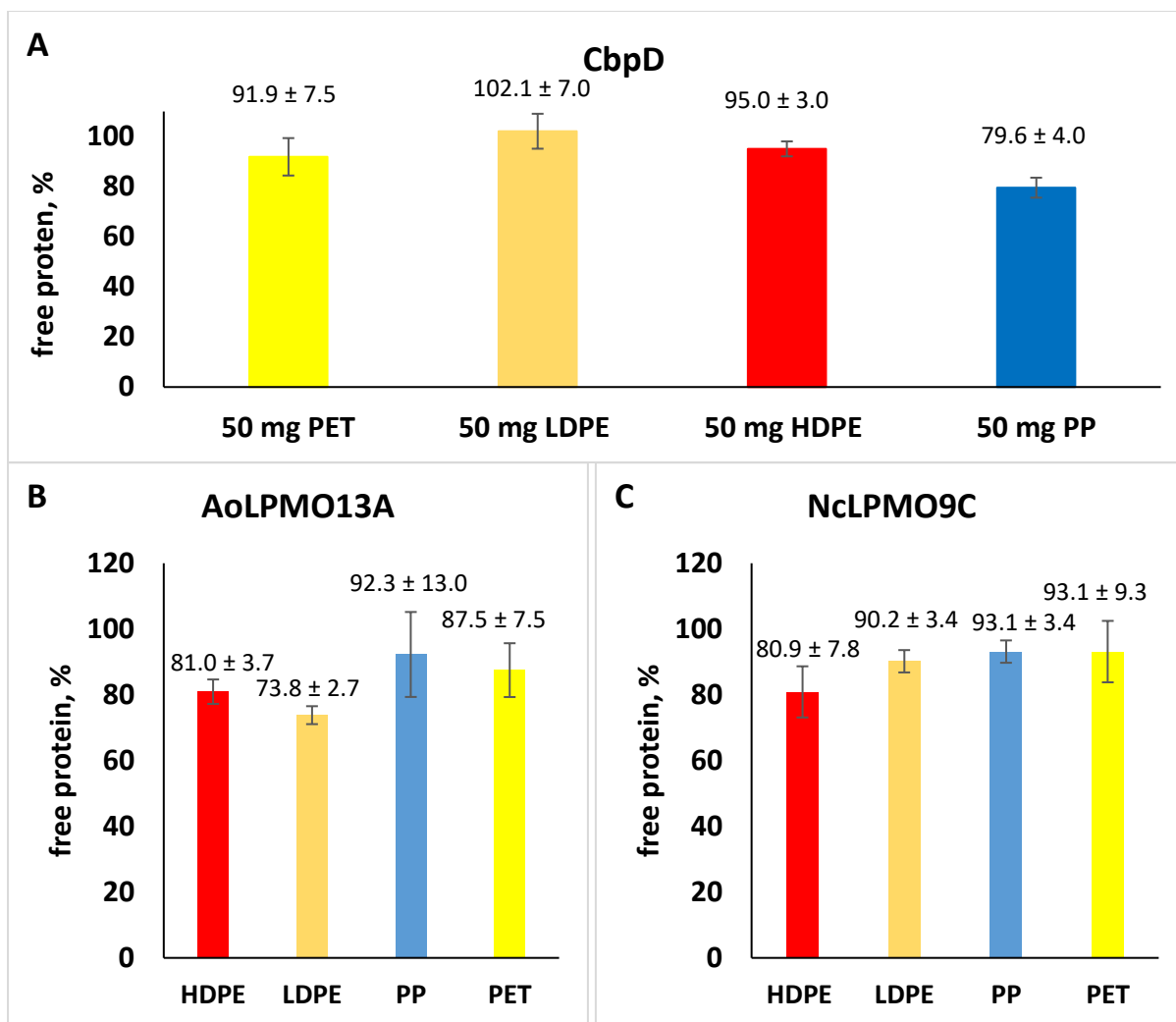
Fig. 4.8.1. Binding of CbpD, AoLPMO13A and NcLPMO9C to plastics. The figure shows the relative amount of free protein detected in solution by UV spectroscopy (λ = 280 nm) after 40 minutes of pre-incubation of 2 μM of CbpD (panel A), *Ao*LPMO13A (panel B) and *Nc*LPMO9C (panel C) with 50 mg of polymers in 500 μl of 50 mM sodium-phosphate buffer, pH 6.0. The insoluble fraction containing bound enzyme species was removed by filtering through a 0.4 μm membrane prior to measuring the absorbance. The protein concentration determined in the control experiment featuring LPMO, but lacking polysaccharides or plastics was set as 100%. All experiments were carried out in a thermomixer (25 °C, 1000 RPM). Error bars indicate standard deviations between replicates (n = 3 for AoLPMO 13A and NcLPMO9C and n = 2 for CbpD).

It was observed that CbpD had a relatively strong binding on PP, NcLPMO9C showed a very weak binding toward HDPE, and AoLPMO13A had a relatively strong binding toward HDPE (**Fig. 4.8.1**). Taken together, the results of binding experiments obtained with all 6 LPMOs studied in the project (**Table 2.3.1**), show a notable variation which is further addressed below (see Discussion). Note that the same experimental conditions were applied for all the LPMO variants tested. The binding data reveal Cels2-wt has the strongest overall binding affinity toward plastic polymers.

4.9. Oxidation of cellulose by CelS2 and CelS2-CBM1 in the presence of plastics

One of the disadvantages of the spectroscopy-based method used to study LPMO binding to plastics in this thesis is that a relatively high amount of protein is required to achieve an adequate level of the absorbance signal and measure the free protein concentration in solution. Furthermore, the UV absorbance signal will vary from protein to protein depending on the extinction coefficient, which may complicate the comparison of results. To further complicate things, the UV spectroscopy-based method is sensitive to interfering compounds that may be present in polymer samples, as illustrated previously (**Fig. 4.1.1**). To address these issues, an alternative approach to detect LPMO binding to plastics was proposed and evaluated. This new approach is based on monitoring the inhibition of LPMO activity on cellulose in the presence of another polymer that will compete for the enzyme binding. It is reasonable to expect that a high degree of LPMO binding to plastics present in the reaction will result in a low cellulose oxidation rate.

It is well-known that the addition of hydrogen peroxide will speed-up LPMO reactions by several orders of magnitude (Bissaro, Røhr, et al. 2017) potentially allowing for detection of CelS2 products within first minutes of experiment. To confirm this point, the LPMO reactions were conducted at 25 °C using 1% (w/v) Avicel and varying concentrations of CelS2 in 50 mM sodium phosphate buffer, pH 6.0 supplied with 100 µM H_2O_2. The experiments were stopped after 3 minutes, and the oxidized reaction products were analyzed using HPAEC-PAD (**Fig. 4.9.1**). The results indicated that such a short incubation time was enough to produce the detectible amounts of oxidized cello-oligosaccharides using ≥0.5 µM CelS2. Note that under these conditions, the LPMO reaction rate displayed a strong dependency on the enzyme concentration.

Next, a new set of LPMO reactions were carried out under the same conditions using 1 µM CelS2 or CelS2-CBM1. However, this time LPMOs were first pre-incubated with 50 mg of PET, LDPE, HDPE, or PP for 40 minutes at 25 °C prior to the addition of Avicel, reductant, and H_2O_2. The control reaction carried out in the absence of plastics was used as a reference, to determine the maximum amount of products released when the competition between cellulose and other polymers for LPMO binding is not taking place. Cels2 activity was indeed repressed in the presence of LDPE (**Fig. 4.9.2**), the polymer that has resulted in pronounced LPMO binding according to previous UV spectroscopy experiments (**Fig. 4.1.3**). The amount of oxidized soluble products released from cellulose by LPMO is indicated by the area of corresponding chromatographic peaks (DP2$_{OX}$, DP3$_{OX}$, DP4$_{OX}$, DP5$_{OX}$, DP 6$_{OX}$, DP7$_{OX}$). The reduction in CelS2 activity in the presence of LDPE is evidenced by smaller peak areas shown in **Table 4.9.1.** The total area of peaks corresponding to oxidized LPMO products generated by CelS2 in the presence of

LDPE is approximately 0.74 nC*min and is 7-fold lower compared to the area of 4.93 nC*min observed in the reference experiment involving only cellulose and CelS2 (**Table. 4.9.1**). However, the activity of LPMO was not affected by the presence of HDPE: the total area of product peaks amounted to 4.85 nC*min compared to the reference value of 4.93 nC*minutes. This is surprising given that CelS2 binding to this polymer was observed using UV spectroscopy. At the same time, CelS2-CBM1 activity was not affected by the presence of any types of plastics involved in the experiment, including LDPE. The areas below the peaks obtained in every experiment were very close to the reference value of 3.04 nC*min (**Table 4.9.1**). This is in line with previous observations (**Fig. 4.7.1)** showing that CelS2-CBM1 capacity to bind to plastics is decreased compared to wild-type CelS2. The relationship between the UV spectroscopy data and the data derived from the competition experiments is further addressed below (see Discussion).
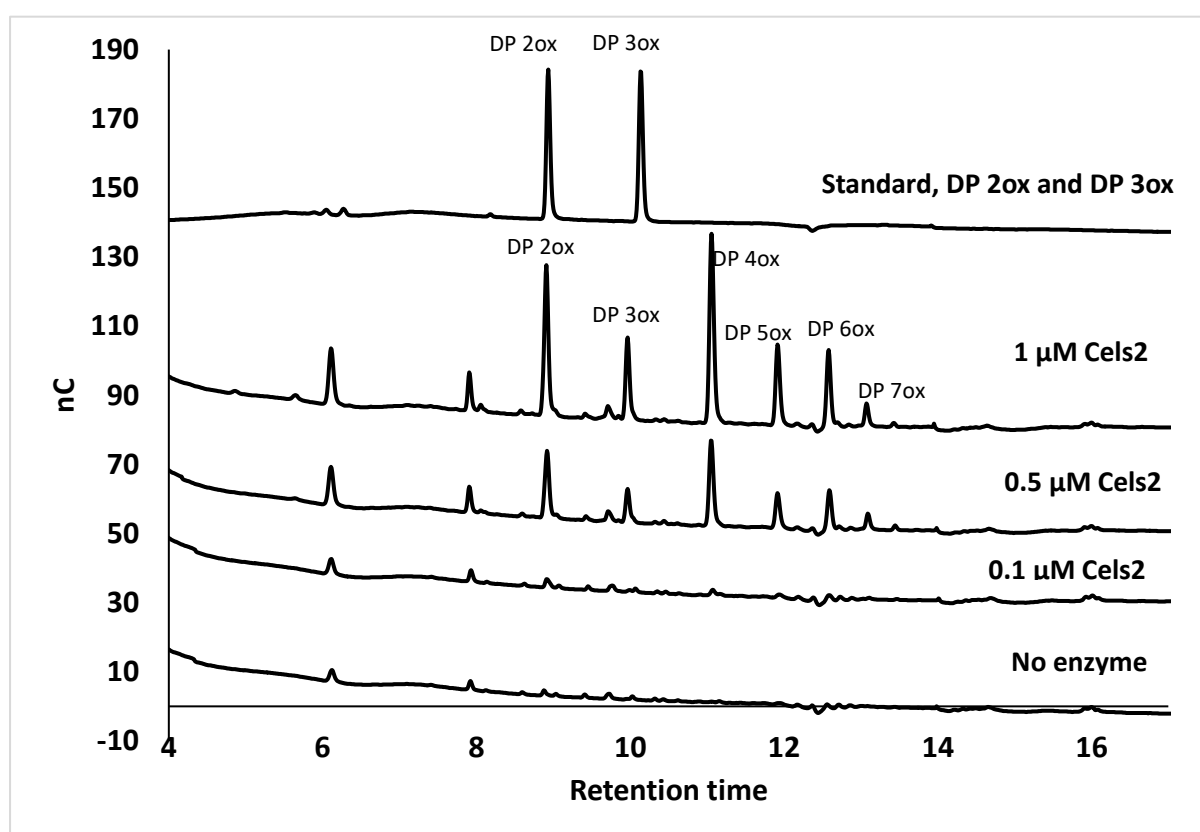
Figure 4.9.1. Oxidation of cellulose by CelS2 in the presence of H_2O_2. The figure shows HPAEC-PAD chromatograms of oxidized soluble products released by 0.1 µM – 1 µM CelS2 from 1% (w/w) Avicel after 3 minutes of incubation at 25 °C and 1000 RPM in 50 mM sodium phosphate buffer, pH 6.0, supplied with 100 µM H_2O_2 and 1 mM gallic acid. C1-oxidised cello-oligosaccharides with various degrees of polymerisation (2-7) are designated as dp2ox-dp7ox. Oxidized products formation was not observed in control reaction lacking the enzyme.
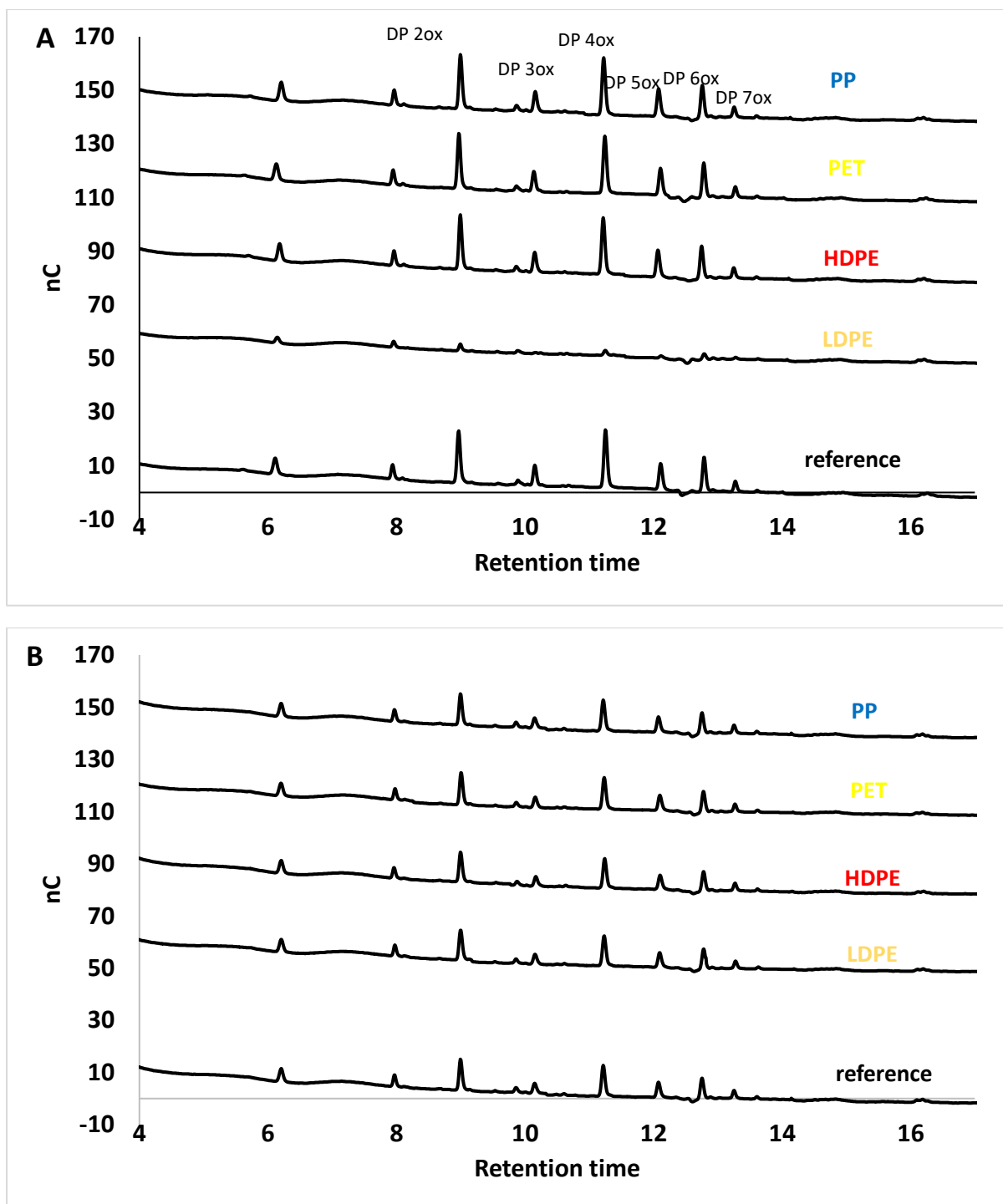
Figure 4.9.2. Oxidation of cellulose by CelS2 or CelS2-CBM1 in the presence of H₂O₂ and various plastics. The figure shows HPAEC-PAD chromatograms of oxidized soluble products released by 1 μM CelS2 (panel A) or CelS2-CBM1 (panel B) from 1% (w/w) Avicel after 3 minutes of incubation at 25 °C and 1000 RPM in 50 mM sodium phosphate buffer, pH 6.0, supplied with 100 μM H₂O₂ and 1 mM gallic acid. These 500 μl reaction mixtures contained 50 mg of PET, LDPE, HDPE, PP, or no plastics (a reference reaction). Product formation was not observed in control reaction lacking the enzyme. C1-oxidised cello-oligosaccharides with various degrees of polymerisation (2-7) are designated as dp2ox-dp7ox. The peaks were assigned according to the retention times observed in previous experiment (**Fig. 4.9.1**) involving dp2ox and dp3ox standard samples. Note that the low areas of CelS2 product peaks (panel A) observed in the presence of LDPE compared to a reference reaction indicate strong binding of CelS2 to these two polymers.

Table 4.9.1. Summed peak areas (DP2$_{ox}$-DP7$_{ox}$) of oxidized cellulose products generated by CelS2 or CelS2-CBM1 in the presence of various plastics. The values were derived from the chromatograms shown in Fig. 4.9.2.

Compound	Enzyme	Soluble oxidized products (DP2$_{ox}$-DP7$_{ox}$ total peak area, nC*min)
PET	CelS2	5.2925
LDPE	CelS2	0.7355
HDPE	CelS2	4.8508
PP	CelS2	4.9456
Reference (no plastics)	**CelS2**	**4.9306**
PET	CelS2-CBM1	2.8483
LDPE	CelS2-CBM1	2.9232
HDPE	CelS2-CBM1	2.9747
PP	CelS2-CBM1	3.0281
Reference (no plastics)	**CelS2-CBM1**	**3.0415**

4.10. Assessing the inhibition of PETase activity on PET in the presence of Cels2 or Cels2$_{TR}$ LPMO

UV-spectroscopy experiments with wild-type CelS2 indicated that the LPMO is capable of weak, but detectible binding to PET (**Fig. 4.1.4**). In this project, a method was proposed that may allow to study such weak binding in more detail. The method is based on the idea that the binding of LPMOs to PET may interfere with the binding of a PETase, resulting in slower degradation of PET. To test this hypothesis, 2 µM Cels2 or Cels2$_{TR}$ were first pre-incubated with 5 mg of PET for 30 minutes at 40 °C in sodium phosphate buffer, pH 6.0 prior to the addition of 0.2 µM LC_ICCG PETase. The result of the experiment shows that adding both CelS2 and CelS2$_{TR}$ to the reaction slows it down (**Fig. 4.9.3**), which may indicate the binding of LPMO to PET. Furthermore, these results point out the fact that the CBM is not involved in this interaction at all. An alternative explanation, that cannot be excluded is that LPMOs and PETase bind to each other.
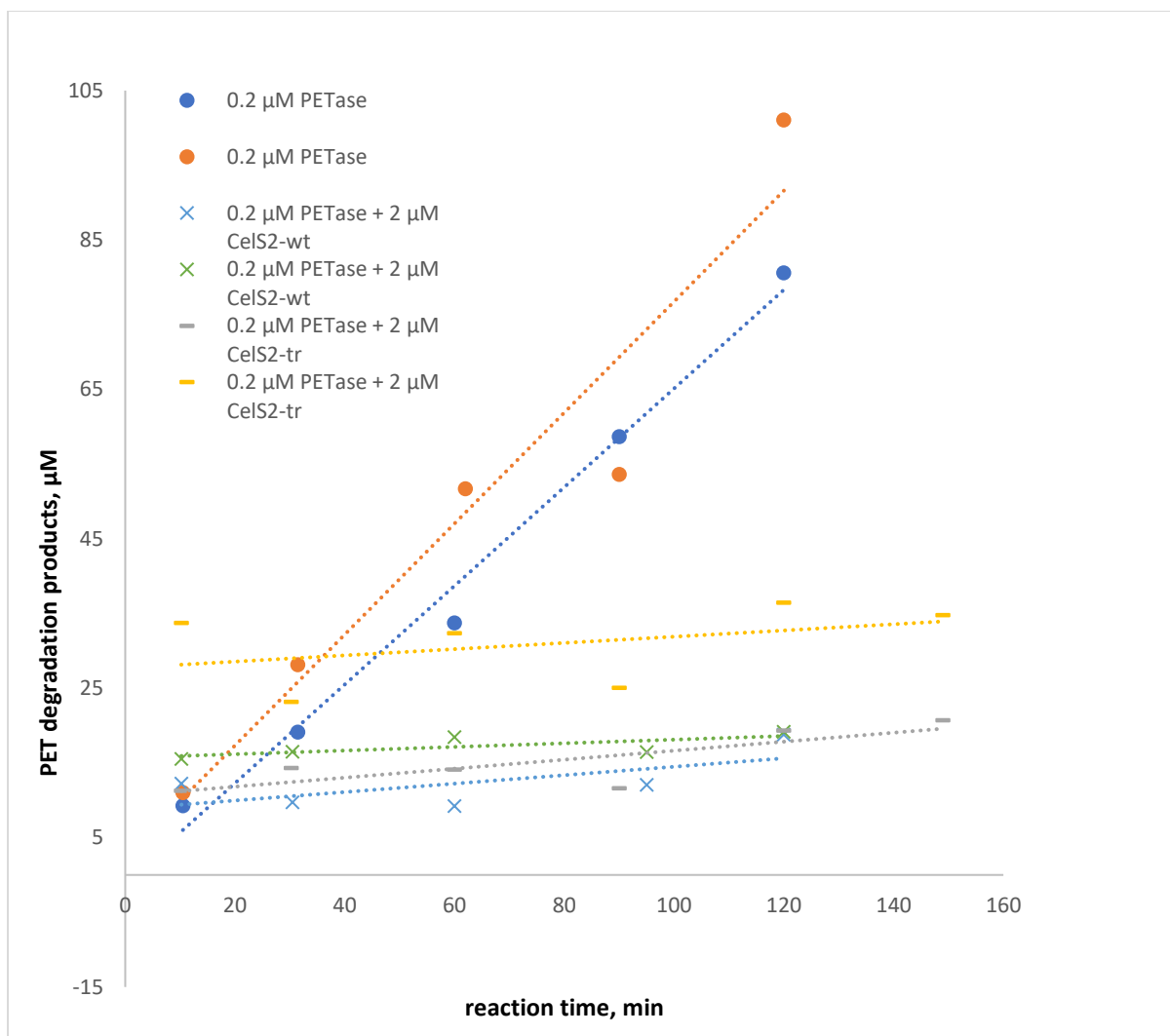
Fig 4.9.3. Degradation of PET by LCC_ICCG cutinase (PETase) in the presence of CelS2 or CelS2TR. The figure displays the release of hydrolyzed products in the PETase reaction (0.2 μM PETase in 50 μM sodium phosphate buffer, pH 6.0, 40°C) using 50 mg of PET, along with the presence or absence of 2 μM CelS2 or CelS2TR. It should be noted that the experiment involving PETase in the presence of CelS2 or CelS2TR resulted in a decreased activity of PETase towards PET.

5. Discussion

Taken together the data obtained for all LPMOs that were tested in this study reveals the difference in binding patterns to plastics (**Table 5.1**). CelS2 displayed noticeable binding to LDPE, HDPE, and PP. *Ao*LPMO13A was observed to bind to LDPE and HDPE as well, albeit to a lower extent compared to CelS2. CbpD was shown to bind PP, but not any other type of plastics. However, what was Interestingly, no LPMOs displayed significant binding. All in all, CelS2 was shown to have the strongest overall binding to most of the tested polymers.

Table 5.1. Binding of LPMOs to plastics according to UV spectroscopy

LPMO	Domain architecture	free protein, % PET ± SD	free protein, % LDPE ± SD	free protein, % HDPE ± SD	free protein, % PP ± SD
CelS2	AA10-CBM2	86.4 ± 4.7	65.3 ± 1.9	74.3 ± 4.7	74.6 ± 8.9
CelS2TR	AA10	No data	86.2 ± 14.8	No data	No data
CelS2-CBM1	AA10-CBM1	96.3 ± 7.0	97.5 ± 10.5	97.5 ± 10.5	101.5 ± 5.6
NcLPMO9C	AA9-CBM1	93.1 ± 9.34	90.2 ± 3.4	80.9 ± 7.8	93.1 ± 3.4
AoLPMO13A	AA13	87.5 ± 8.2	73.8 ± 2.7	80.95 ± 2.73	92.26 ± 12.9
CpbD	AA10-GbpA2-CBM73-His	91.9 ± 7.5	102.1 ± 7.0	95.07 ± 3.72	79.6 ± 4.0

CBM1/CBM2/CBM73, family 1/2/73 cellulose binding module; AA9/AA10/AA13, family 9/10/13 LPMO catalytic domain; GbpA2, domain of unknown function found in CbpD; His, hexahistidine purification tag.

Unfortunately, binding experiments performed with CelS2$_{TR}$ (lacking CBM) and LDPE resulted in very high standard deviations between replicates, therefore it was not clear whether the truncation of CBM resulted in much lower binding (**Fig 4.2.1**). However, comparing the binding data obtained for wild-type CelS2 (**Fig. 4.1.4**) and CelS2-CBM1 clearly revealed that the removal of the original family 2 CBM resulted in a very significant decrease in binding to LDPE, HDPE, and PP. In other words, this result indicates that it is the carbohydrate-binding module and not the catalytic domain that contributes the most to the binding of CelS2 to these types of plastics.

Importantly, previous reports indicated that CBM1 used to engineer CelS2-CBM1 in this study has a strong binding to PET films. (Rosie Graham 1 2 2022). This is very different from what was observed in the thesis. This discrepancy can be due to the differences in the degree of PET crystallinity, as powder was used in the current project instead of a film. The experiment with *Nc*LPMO9C possessing a family 1 carbohydrate-binding module further supported the idea that family 1 CBMs may have low plastic binding capacity (**Fig. 4.7.1 A**). This LPMO displayed a weak overall binding to all the types of plastics tested, which is comparable to the results obtained with CelS2-CBM1.   One contributing factor to the low plastic binding capacity of CBM1 could be the high conformational flexibility of this domain, which might impede effective binding when in contact with the plastic surface. Molecular dynamic simulations (MD) conducted by Weber et al. (Weber, et al. 2019) have demonstrated that family 1 CBMs may exhibit remarkable flexibility, making them susceptible to rapid changes in both secondary and tertiary structures. Consequently, the flexibility of family 1 CBMs may hinder its ability to form a robust and stable interactions with plastic substrate, compared to family 2 CBMs which were shown to possess less flexible folds (Weber, et al. 2019).   When it comes to the observed binding of CbpD to PP (**Fig. 4.7.2 A**), there is not enough data to speculate which of multiple LPMO domains contributed

to these results. The pronounced binding to PE observed with *Ao*LPMO13A was unexpected since this LPMO lacks any additional binding domains and is acting on starch which is less crystalline and less hydrophobic compared to cellulose. This result underpins the fact that binding is a complex process and that the affinity of LPMOs to plastics cannot be predicted using general information about the hydrophobicity of their natural substrates (one may expect more binding towards PE from a cellulose-active LPMO compared to starch-binding LPMO).

It is worth noting that the strongest degree of LPMO binding to plastics observed in this study (about 65% free protein detected after incubation of CelS2 with LDPE) should still be considered weak compared to the binding of LPMOs to their true substrates. E.g., no free protein was detected in the experiment involving CelS2 and Avicel (**Fig. 4.1.2**). This is not surprising, considering that LPMOs were not evolved to bind plastics.

On a side note, the contamination of Avicel and β-chitin with soluble compounds interfering with the protein concentration assay described in this study (**Fig. 4.1.3**) is an important observation, underpinning the importance of control experiments when looking at protein binding using UV-spectroscopy. There is not enough data to reveal the chemical nature of these contaminants. However, it is safe to say these compounds were not proteins, since no extra bands were observed on LDS-PAGE gel (**Fig. 4.1.2**).

Among three new CelS2 variants designed for this study (CelS2-CBM1, CelS2-PBM, and CelS2-DSI), only one variant was successfully produced in rather small amounts (approximately 1 mg per litre culture). CelS2-PBM was insoluble, which is likely a consequence of fusing a hydrophobic polyhydroxyalkanoate binding module to the LPMO. CelS2-DSI was not expressed at all, which may be explained by the fact that dermaseptin peptide added to the LPMO as a potential plastic-binding anchor is known to possess some anti-bacterial features and could be toxic for *E. coli* (Audrain, et al., 2013) (Jouennea, Mor, Bonato, & Junter, 1998) The experiments involving cellulose degradation by CelS2 in the presence of LDPE, performed in this study (**Fig. 4.9.2 A**) revealed that the suppression of the enzyme activity can indeed be used as an indicator of enzyme binding to plastics. However, this method turned out to be not very sensitive, as the competition experiment carried out with CelS2, cellulose and HDPE did not indicate any change in LPMO activity, despite that some degree of enzyme binding to this polymer was observed by UV-spectroscopy (**Fig. 4.1.4**). One possible explanation for this fact is that the lower binding of CelS2 to HDPE compared to LDPE may simply not be enough to effectively compete with cellulose that binds to this LPMO extremely well. Note that in contrast to HDPE, LDPE possesses an extensive branching (Couch and Binding 2000), potentially allowing this polymer to better "trap" and retain the LPMO, restricting its access to cellulose in the competition experiments. Despite the very

low binding of CelS2 to PET, it was observed that the addition of LPMO to the reaction containing PET and PET-degrading enzyme (LCC_ICCG) inhibit the PETase activity (**Fig. 4.9.3**). This result indicates that such an approach may be used as a sensitive tool to study LPMO binding to PET. However, it is worth noting that the collected data does not allow to exclude that the observed inhibition of LCC_ICCG activity was due to CelS2 binding the PETase and not the plastics.

6. Conclusion and future perspectives

All in all, the results obtained in this thesis indicate that some LPMOs indeed possess a noticeable degree of binding to LDPE, HDPE, and PP. This is particularly the case for CelS2, a model bacterial LPMO that was studied in detail by comparing the wild-type enzyme with two enzyme variants (CelS2$_{TR}$ and CelS2-CBM1). The data indicate that it is the CelS2 carbohydrate-binding module (family 2 CBM) and not the catalytic domain that contributes most to such binding. Interestingly, the ability of this family 2 CBM to guide the LPMO binding to plastics was shown to be much higher than that of family 1 CBM from *Tr*Cel7A, which was previously used to engineer a PETase with increased binding to PET **Invalid source specified.**. Therefore, the carbohydrate-binding module of wild-type CelS2 represents a potential target for future protein engineering campaigns aimed at creating proteins that can strongly bind to crystalline hydrophobic polymers, such as PE. Various techniques, such as directed evolution or machine learning-driven protein engineering, could be applied to improve the binding capabilities of this carbohydrate-binding module. It is important to note that any degree of LPMO affinity to plastics should not be taken as a sufficient condition for oxidative activity on these polymers, even in case the LPMO catalytic domain (and not just CBM) is capable of such binding. This work represents an attempt at quick screening of a collection of LPMOs towards the binding to industry-relevant types of plastics, and it has many limitations. The polymers involved in the study tend to build an electrostatic charge upon weighting, meaning that relatively high amounts of these substances (50 mg) and, consequently, relatively high reaction volumes (500 µl) had to be used to ensure consistency between replicates. As a result, the binding experiments required rather large quantities of LPMOs, limiting the number of replicates to just duplicates instead of triplicates in some cases, as indicated above. It is important to note that the particle sizes of plastics tested in this work varied between the materials (**Table 2.5.1**), meaning that the binding surface area was not the same across the experiments, which complicates the quantitative comparison of the data. Finally, the important question that was not addressed in this thesis and needs to be considered in future is how the observed LPMO binding to plastics is affected by the change of temperature or by the change in the crystallinity of the polymers of interest.

7. References

Andrady, Anthony L, and Mike A Neal. 2009. "Applications and societal benefits of plastics." *Philosophical Transactions of the Royal Society* 364 (1526): 1977–1984.

Askarian, Fatemeh, Satoshi Uchiyama, Helen Masson, Henrik Vinther Sørensen, Ole Golten, Anne Cathrine Bunæs, Sophanit Mekasha, et al. 2021. "The lytic polysaccharide monooxygenase CbpD promotes Pseudomonas aeruginosa virulence in systemic infection." *Nature communications* 12 (1): 1230. doi:10.1038/s41467-021-21473-0.

Austin, Harry P, Mark D Allen, Bryon S Donohoe, and Gregg T Beckham. 2018. "Characterization and engineering of a plastic-degrading aromatic polyesterase." *Biochemstry* 119 (19): 4350-4357.

Baker, Joel, Henk Bouwman, Sarah Gall, Valeria Hidalgo-Ruz, Angela Koehler, Kara Lavender, Sabine Pahl, et al. 2015. "Sources, fate and effects of microplastics in the marine environment." *Gesamp* 1-93.

Bennati-Granier, Chloé, Sona Garajova, Charlotte Champion, Sacha Grisel, Mireille Haon, Simeng Zhou, Mathieu Fanuel, et al. 2015. "Substrate specificity and regioselectivity of fungal AA9 lytic polysaccharide monooxygenases secreted by Podospora anserina." *Biotechnology for Biofuels* 8: 90.

Berselli, Alessandro, Maria J Ramos, and Maria Cristina Menziani. 2021. "NovelPet-DegradingEnzymes:Structure-FunctionfromaComputationalPerspective." *ChemBioChem* 22 (12): 2032-2050.

Besseling, Ellen, Bo Wang, Miquel Lürling, and Albert A. Koelmans. 2014. "Nanoplastic Affects Growth of S. obliquus and Reproduction of D. magna." *Environmental Science & Technology* 48 (20): 12336 - 12343.

Betts, Kellyn. 2008. "Why small plastic particles may pose a big problem in the oceans." *Environmental Science & Technology* (American Chemical Society) 42 (24): 8995-8995.

Bissaro, Bastien, Anikó Várnai, Åsmund K. Røhr, and Vincent G. H. Eijsink. 2018. "Oxidoreductases and Reactive Oxygen Species in Conversion of Lignocellulosic Biomass." *Microbiology and Molecular Biology Reviews.*

Bissaro, Bastien, Åsmund K Røhr, Gerdt Müller, Piotr Chylenski, Morten Skaugen, Zarah Forsberg, Svein J Horn, Gustav Vaaje-Kolstad, and Vincent G H Eijsink. 2017. "Oxidative cleavage of polysaccharides by monocopper enzymes depends on H2O2." *Nature Chemical Biology* 13: 1123–1128.

Borisova, Anna S., Trine Isaksen, Maria Dimarogona, Abhishek A. Kognole, Geir Mathiesen, Anikó Várnai, Åsmund K. Røhr, et al. 2015. "Structural and Functional Characterization of a Lytic Polysaccharide Monooxygenase with Broad Substrate Specificity." *Biological Chemistry* 290 (38): 22955–22969.

Borisova, Anna S., Trine Isaksen, Maria Dimarogona, Abhishek A. Kognole, Geir Mathiesen, Anikó Várnai, Åsmund K. Røhr, et al. 2015. "Structural and Functional Characterization of a Lytic

Polysaccharide Monooxygenase with Broad Substrate Specificity." *Enzymology* 290 (38): 22955–22969.

Brandon, Anja Malawi, and Craig S Criddle. 2019. "Can biotechnology turn the tide on plastics?" *Current Opinion in Biotechnology* 57: 160-166.

Brueckner, Tina, Anita Eberl, Sonja Heumann, Maike Rabe, and Georg Guebitz. 2008. "Enzymatic and chemical hydrolysis of poly(ethylene terephthalate) fabrics." *Polymer chemistry* 46 (19): 6435-6443.

Cauwenberghe, Lisbeth Van, and Colin R. Janssen. 2014. "Microplastics in bivalves cultured for human consumption." *Environmental Pollution* 193: 65-70.

Chang, Angela Y, Chau, Vivian WY, Landas, Julius A, Pang, Yvonne. 2017. "Preparation of calcium competent Escherichia coli and heat-shock transformation." 22-25. University of British Columbia: Jemi methods. https://ujemi.microbiology.ubc.ca/sites/default/files/Chang%20et%20al%20JEMI-methods%20Vol%201%20pg%2022-25.pdf.

Chen, Sheng, Lingqia Su, Jian Chen, and Jing Wu. 2013. "Cutinase: Characteristics, preparation, and application." *Biotechnology Advances* 1754-1767.

Cheremisinoff, Nicholas P. 1989. *Handbook of Polymer Science and Technology.* Edited by Nicholas Cheremisinoff. Vol. 2. New York: M. Dekker.

Ciano, Luisa, Gideon J. Davies, William B. Tolman, and Paul H. Walton. 2018. "Bracing copper for the catalytic oxidation of C–H bonds." *Nature catalysis* 1: 571–577.

Çobanoğlu, Hayal, Murat Belivermiş, Ercan Sıkdokur, Önder Kılıç, and Akın Çayır. 2021. "Genotoxic and cytotoxic effects of polyethylene microplastics on human peripheral blood lymphocytes." *Chemosphere* 272: 129805.

Couch, M.A, and D.M Binding. 2000. "High pressure capillary rheometry of polymeric fluids." *Polymer* 41 (16): 6323-6334.

Courtade, Gaston, Le Simone Balzer, Sætrom Gerd Inger, Trygve Brautaset, and Aachmann Finn L. 2017. "A novel expression system for lytic polysaccharide monooxygenases." *Carbohydrate Research* 212-219.

Courtade, Gaston, Zara Forsberg, Ellinor B.Heggset, Vincent G.H. Eijsink, and Finn L. Aachmann. 2018. "PROTEIN STRUCTURE AND FOLDING." *The carbohydrate-binding module and linker of a modular lytic polysaccharide monooxygenase promote localized cellulose oxidation.*

Courtade, Gaston, Zarah Forsberg, Ellinor B. Heggset, Vincent G. H. Eijsink, and and Finn L. Aachmann. 2018. "The carbohydrate-binding module and linker of a modular." *Protein structure and folding* 293 (34): 13006-13015.

Couturier, Marie, Simon Ladevèze, Gerlind Sulzenbacher, Luisa Ciano, Mathieu Fanuel, Céline Moreau, Ana Villares, et al. 2018. "Lytic xylan oxidases from wood-decay fungi unlock biomass degradation." *Nature Chemical Biology* 14: 306–310.

Dade, Christopher M., Badreddine Douzi, Christian Cambillau, and Genevieve. 2022. "The crystal structure of CbpD clarifies." *Structural biology* 2059-7983.

Dade, Christopher M., Badreddine Douzi, Christian Cambillau, and Genevieve. 2022. "The crystal structure of CbpD clarifies substrate-specificity motifs in chitin-active lytic." *Structural Biology* 78: 2059-7983.

Dick, John S. 2009. *Rubber Technology 2E: Compounding and Testing for Performance 2nd Edition.* Hanser Publications; 2nd edition.

Ding, Zundan, Guoshun Xu, Ruiju Miao, Ningfeng Wu, Wei Zhang, Bin Yao, Feifei Guan, Huoqing Huang, and Tian Jian. 2023. "Rational redesign of thermophilic PET hydrolase LCCICCG to enhance hydrolysis of high crystallinity polyethylene terephthalates." *Journal of Hazardous Materials* 453.

Donelli, Ilaria, Paola Taddei, Philippe F Smet, Dirk Poelman, Vincent A Nierstrasz, and Giuliano Freddi. 2009. "Enzymatic surface modification and functionalization of PET: A water contact angle, FTIR, and fluorescence spectroscopy study." *Biotechnology and Bioengineering* 103 (5): 845-856.

Doris Ribitsch, Antonio Orcal Yebra, Sabine Zitzenbacher, Jing Wu, Susanne Nowitsch,. 2013. "Fusion of Binding Domains to Thermobifida cellulosilytica Cutinase to." *Bio macromolecules* 1-8.

Dubendorf, John W., and F.William Studier. 1991. "Controlling basal expression in an inducible T7 expression system by blocking the target T7 promoter with lac repressor." *Journal of Molecular Biology* 45-59.

Dutta, Joystu, and Moharana Choudhury. 2018. "Plastic Pollution: A Global Problem from a Local Perspectiv." *Waste Management & Xenobiotics* 1 (1): 1-2.

Eijsink, H Vincent G., Petrovic Dejan, Forsberg Zarah, Mekasha Sophanit, Røhr Åsmund K., Várnai Anikó, Bissaro Bastien, and Vaaje-Kolstad Gustav. 2019. "On the functional characterization of lytic polysaccharide monooxygenases (LPMOs)." *Biotechnology for Biofuels and Bioproducts.*

Forsberg, Zarah, and Gaston Courtade. 2023. "On the impact of carbohydrate-binding modules (CBMs) in lytic polysaccharide monooxygenases (LPMOs)." *Essays in Biochemistry* 67 (3): 561–574.

Forsberg, Zarah, Anton A Stepnov, Guro Kruge Nærdal, Geir Klinkenberg, and Vincent G.H. Eijsink. 2020. "Chapter One - Engineering lytic polysaccharide monooxygenases (LPMOs)." *Methods in Enzymology* 644: 1-34.

Forsberg, Zarah, Åsmund Kjendseth Røhr, Sophanit Mekasha, K Kristoffer Andersson, Vincent G. H. Eijsink, Gustav Vaaje-Kolstad, and Morten Sørlie. 2014. "Comparative Study of Two Chitin-Active and Two Cellulose-Active AA10-Type Lytic Polysaccharide Monooxygenases." *Biochemistry* 53 (10): 1647–1656.

Forsberg, Zarah, Åsmund Kjendseth Røhr, Sophanit Mekasha, K. Kristoffer Andersson, Vincent G. H. Eijsink, Gustav Vaaje-Kolstad, and Morten Sørlie. 2014. "Comparative Study of Two Chitin-Active and Two Cellulose-Active AA10-Type Lytic Polysaccharide Monooxygenases." *Biochemistry* 53 (10): 1647–1656.

Forsberg, Zarah, Bastien Bissaro, Jonathan Gullesen, Bjørn Dalhus, Gustav Vaaje-Kolstad, and Vincent G. H. Eijsink. 2018. "Structural determinants of bacterial lytic polysaccharide." *Enzymology* 293 (4): 1397-1412.

Garcia, Jeannette M., and Megan L. Robertson. 2017. "The future of plastics recycling." *Chemical advances are increasing the proportion of polymer waste that can be recycled* 870-872.

Gasteiger E., Hoogland C., Gattiker A., Duvaud S., Wilkins M.R., Appel R.D., Bairoch A. 2005. *BioExpacy ProtParam.* https://web.expasy.org/protparam/.

Gaston Courtade, Zarah Forsberg, Ellinor B Heggset, Vincent G H Eijsink, Finn L Aachmann. 2018. "The carbohydrate-binding module and linker of a modular lytic polysaccharide monooxygenase promote localized cellulose oxidation." 13006-13015.

Geyer, Roland, Jenna R. Jamebeck, and Kara Lavender Law. 2017. "Production, use, and fate of all plastics ever made." *Science Advances* 3 (7): 1-5.

González-Pérez, J.A., N.T. Jiménez-Morillo, J.M. de la Rosa, G. Almendros, and F.J. González-Vila. 2015. "Pyrolysis-gas chromatography–isotope ratio mass spectrometry of polyethylene." *Journal of Chromatography A* 1388: 236-243.

Graham, Rosie, Erika Erickson, Richard K. Brizendine, Gregg T. Beckham, John E. McGeehan, and Andrew R. Pickford. 2022. "The role of binding modules in enzymatic poly(ethylene terephthalate) hydrolysis at high-solids loadings." *Chem Catalysis* 2 (10): 2644–2657.

Guebitz, Georg M, and Artur Cavaco-Paulo. 2008. "Enzymes go big: surface hydrolysis and functionalisation of synthetic polymers." *Trends in Biotechnology* 26 (1): 32-38.

Guillén, Daniel, Sergio Sánchez, and Romina Rodríguez-Sanoja. 2010. "Carbohydrate-binding domains: multiplicity of biological roles." *Applied Microbiology and Biotechnology* 85 (5): 1241–1249.

Han, Xu, Weidong Liu, Jian-Wen Huang, Jiantao Ma, Yingying Zheng, Tzu-Ping Ko, Limin Xu, Ya-Shan Cheng, Chun-Chi Chen, and Rey-Ting Guo. 2017. "Structural insight into catalytic mechanism of PET hydrolase." *Nature Communications* .

Han, Xu, Weidong Liu, Jian-Wen Huang, Jiantao Ma, Yingying Zheng, Tzu-Ping Ko, Limin Xu, Ya-Shan Cheng, Chun-Chi Chen, and Rey-Ting Guo. 2017. "Structural insight into catalytic mechanism of PET hydrolase." *Nature Communications* 8: 2106. doi:10.1038/s41467-017-02255-z.

Hemsworth, Glyn R., Esther M. Johnston, Gideon J. Davies, and Paul H. Walton. 2015. "Lytic Polysaccharide Monooxygenases in Biomass Conversion." *Trends in Biotechnology* 33 (12): 747-758.

Hirano, Kazuhisa, and Masakatsu Asami. 2013. "Phenolic resins—100 years of progress and their future." *Reactive and Functional Polymers* 73 (2): 256-269.

Icon, Freddie J. JenningsORCID, Myria W. Allen, and Thuy Le Vu Phuongb Department of Desi. 2019. "More Plastic than Fish: Partisan Responses to an Advocacy Video Opposing Single-Use Plastics." *Enviromental Communication* 218-234.

Ishigaki, Tomonori, Wataru Sugano, Akane Nakanishi, Masafumi Tateda, Michihiko Ike, and Masanori Fujita. 2004. "he degradability of biodegradable plastics in aerobic and anaerobic waste landfill model reactors." *Chemosphere* 54 (3): 225-233.

Jerves, Carola, Rui P. P. Neves, Maria J Ramos, Saulo da Silva, and Pedro A. Fernandes. 2021. "Reaction Mechanism of the PET Degrading Enzyme PETase Studied with DFT/MM Molecular Dynamics Simulations." *ACS Catalysis* 11 (18): 11626–11638.

Joho, Yvonne, Vanessa Vongsouthi, Matthew A. Spence, Jennifer Ton, Chloe Gomez, Li Lynn Tan, Joe A. Kaczmarski Alessandro T. Caputo, Santana Royan, Colin J. Jackson*, and and Albert Ardevol. 2023. "Ancestral Sequence Reconstruction Identifies Structural Changes Underlying the Evolution of Ideonella sakaiensis PETase and Variants with Improved Stability and Activity." *Biochemistry* 437–450.

Kim, Ragaert, Delva Laurens, and Geem Van Kevin. 2017. "Mechanical and chemical recycling of solid plastic waste." *Waste Management* 69: 24-58.

Knyazev, Vadim D. 2007. "Effects of Chain Length on the Rates of C−C Bond Dissociation in Linear Alkanes and Polyethylene." *Physical Chemistry* 111 (19): 3875–3883.

Lee, Toni M, Mary F Farrow, Frances H Arnold, and Stephen L Mayo. 2011. "A structural study of Hypocrea jecorina Cel5A." *Protein Science* 20 (11): 1935 - 1940.

Levasseur, Anthony, Elodie Drula, Vincent Lombard, Pedro M Coutinho, and Bernard Henrissat. 2013. "Expansion of the enzymatic repertoire of the CAZy database to integrate auxiliary redox enzymes." *Biotechnology for Biofuels.*

Liu, Bing, Lihui He, Liping Wang, Tao Li, Changcheng Li, Huayi Liu, Yunzi Luo, and Rui Bao. 2018. "Protein Crystallography and Site-Direct Mutagenesis Analysis of the Poly(ethylene terephthalate) Hydrolase PETase from Ideonella sakaiensis." *ChemBioChem* 19 (14): 1471-1475.

Loose, ennifer S. M., Magnus Ø. Arntzen, Bastien Bissaro, Roland Ludwig, Vincent G. H. Eijsink, and Gustav Vaaje-Kolstad. 2018. "Multipoint Precision Binding of Substrate Protects Lytic Polysaccharide Monooxygenases from Self-Destructive Off-Pathway Processes." *Biochemistry* 57 (28): 4114–4124.

Lu, Hongyuan, Daniel J. Diaz, Natalie J. Czarnecki, Congzhi Zhu, Wantae Kim, Raghav Shroff, \ Daniel J. Acosta, et al. 2022. "Machine learning-aided engineering of hydrolases for PET depolymerization." *Nature* 662–667.

Lu, Hongyuan, Natalie J. Czarnecki Daniel J. Diaz, Congzhi Zhu, Raghav Shroff Wantae Kim, Daniel J. Acosta, Bradley R. Alexander, Hannah O. Cole, et al. 2022. "Machine learning-aided engineering of hydrolases for PET depolymerization." *Nature* 604: 662–667.

Luo, Yu-Ran. 2007. *Comprehensive Handbook of Chemical Bond Energies.* Boca Raton: CRC Press.

Madara, Diana Starovoytova, Saul Sitati Namango, and Charles Wetaka. 2016. "Consumer-Perception on Polyethylene-Shopping-Bags." *Journal of Environment and Earth Science* 6 (11): 12-31.

Manavalan, Tamilvendan, Anton A. Stepnov, Olav A. Hegnar, and Vincent G.H. Eijsink. 2021. "Sugar oxidoreductases and LPMOs – two sides of the same polysaccharide degradation story?" *Carbohydrate Research.*

Mato, Yukie, Tomohiko Isobe, Hideshige Takada, Haruyuki Kanehiro, Chiyoko Ohtake, and Tsuguchika Kaminuma. 2001. "Plastic Resin Pellets as a Transport." *Environ. Sci. Technol.* 35 (2): 318-324.

Mayer, Alfred M., and Richard C. Staples. 2002. "Laccase: new functions for an old enzyme." *Phytochemistry* 60 (6): 551-565.

Meier, Katlyn K., Stephen M. Jones, Thijs Kaper, Henrik Hansson, Martijn J. Koetsier, Saeid Karkehabadi, Edward I. Solomon, Mats Sandgren, and Bradley Kelemen. 2018. "Oxygen

Activation by Cu LPMOs in Recalcitrant Carbohydrate Polysaccharide Conversion to Monomer Sugars." *Chemical Reviews* 118 (5): 2593-2635.

Millet, Herve, Patricia Vangheluwe, Christian Block, Arjen Sevenster, Leonor Garcia, and Romanos Antonopoulus. 2019. "The nature of plasticand their societal usage." *Plastics and the enviroment* 47.

Miskolczi, N, A Angyal, L Bartha, and I Valkai. 2009. "Fuels by pyrolysis of waste plastics from agricultural and packaging sectors in a pilot scale reactor." *Fuel Processing Technology* 90 (7-8): 1032-1040.

Nerland, Inger Lise, Claudia Halsband, Ian Allan, and Kevin V Thomas. 2014. *Microplastics in marine environments: Occurrence, distribution and .* Oslo: Norwegian Institute for Water Research.

Niclas Büscher, Giovanni V. Sayoga, Kristin Rübsam, Felix Jakob, Ulrich Schwaneberg,. 2019. "Biocatalyst Immobilization by Anchor Peptides on an Additively." 1852-1859.

Noar, Jesse D, and Daniel H Buckley. 2009. "Ideonella azotifigens sp. nov., an aerobic diazotroph of the Betaproteobacteria isolated from grass rhizosphere soil, and emended description of the genus Ideonella." *International Journal of Systematic and evolutionary microbiology* 59 (8): 1941–1946.

Pandey, Prashant, Manisha Dhiman, Ankur Kansal, and Sarada, Prasannan Subudhi. 2023. "Plastic waste management for sustainable environment: techniques and approaches." *Waste Disposal & Sustainable Energy* 205-222.

Patel, M, von Thienen, E Jochem, and E Worrell. 2000. "Recycling of plastics in Germany." *Resources Concervation and Recycling* 29 (1-2): 65-90.

Paul Daly a b, Feng Cai, Christian P. Kubicek, Siqi Jiang, Marica Grujic, Mohammad Javad Rahimi, Mohamed Salah Sheteiwy, Richard Giles, Asad Riaz, Ronald P. de Vries b, Günseli Bayram Akcapinar i, Lihui Wei a, Irina S. Druzhinina. 2021. "From lignocellulose to plastics: Knowledge transfer on the degradation approaches by fungi." *Biotechnology Advances.*

Paul Daly, Feng Cai, Christian P. Kubicek, Siqi Jiang, Marica Grujic, Mohammad Javad Rahimi, Mohamed Salah Sheteiwy, Richard Giles, Asad Riaz, Ronald P. de Vries, Günseli Bayram Akcapinari, Lihui Wei a, Irina S. Druzhinina. 2021. "From lignocellulose to plastics: Knowledge transfer on the degradation ." *Biotechnology Advances.*

Pell, Gavin, Michael P. Williamson, Christopher Walters, Haomao Du, Harry J. Gilbert, and David N. Bolam. 2003. "Importance of Hydrophobic and Polar Residues in Ligand Binding in the Family 15." *Biochemistry* 9316-9323.

Pirillo, Valentina, Loredano Pollegioni, and Gianluca Molla. 2021. "Analytical methods for the investigation of enzyme-catalyzed degradation of polyethylene terephthalate." *The Febs Journal* 4730–4745.

Quinlan, R. Jason, Matt D. Sweeney, Leila Lo Leggio, Harm Otten, Jens-Christian N. Poulsen, Katja Salomon Johansen, Kristian B. R. M. Krogh, et al. 2011. "Insights into the oxidative degradation of cellulose by a copper metalloenzyme that exploits biomass components." *Chemistry* 108 (37): 15079-15084.

Qureshi, Muhammad Saad, Anja Oasmaa, Hanna Pihkola, Ivan Deviatkin, Anna Tenhunen, Juha Mannila, Hannu Minkkinen, Maija Pohjakallio, and Jutta Laine-Ylijoki. 2020. "Pyrolysis of

plastic waste: Opportunities and challenges." *Journal of Analytical and Applied Pyrolysis* 152: 1-9.

Radzicka, Anna, and Richard Wolfenden. 1995. "A Proficient Enzyme." *Science* 267 (5194): 90-93.

Ribitsch, Doris, Antonio Orcal Yebra, Sabine Zitzenbacher, Jing Wu, Susanne Nowitsch, Georg Steinkellner, Katrin Greimel, et al. 2013. "Fusion of Binding Domains to Thermobifida cellulosilytica Cutinase to Tune Sorption Characteristics and Enhancing PET Hydrolysis." *Bio Macromolecules* 14 (6): 769-1776.

Rosie Graham 1 2, Erika Erickson 2 3, Richard K. Brizendine 2 3, Davinia Salvachúa 3, William E. Michener, Yaohao Li, Zhongping Tan, Gregg T. Beckham, John E. McGeehan, Andrew R. Pickford. 2022. "The role of binding modules in enzymatic poly(ethylene terephthalate) hydrolysis at high-solids loadings." *Chem Catalysis* 2644-2657.

Sabbadin, F., B. Henrissat, N.C. Bruce, and S.J. McQueen-Mason. 2021. "Lytic Polysaccharide Monooxygenases as Chitin-Specific Virulence Factors in Crayfish Plague." *Biomolecules* 11 (8): 1180.

Sabbadin, Federico, Glyn R. Hemsworth, Luisa Ciano, Bernard Henrissat, Paul Dupree, Theodora Tryfona, Rita D. S. Marques, et al. 2018. "An ancient family of lytic polysaccharide monooxygenases with roles in arthropod development and biomass digestion." *nature communication* 9: 756.

Sagong, Hye-Young, Hogyun Seo, Taeho Kim, Hyeoncheol Francis Son, Seongjoon Joo, Seul Hoo Lee, Seongmin Kim, Jae-Sung Woo, Sung Yeon Hwang, and and Kyung-Jin Kim. 2020. "Decomposition of the PET Film by MHETase Using Exo-PETase Function." *ACS catalysis* 10 (8): 4805–4812.

Santo, Miriam, Ronen Weitsman, and Alex Sivan. 2013. "The role of the copper-binding enzyme – laccase – in the biodegradation of polyethylene by the actinomycete Rhodococcus ruber." *International Biodeterioration & Biodegradation* 84: 204-210.

Serrano, D.P, J Aguado, J.M Escola, J.M Rodríguez, and G. San Miguel. 2005. "An investigation into the catalytic cracking of LDPE using Py–GC/MS." *Journal of Analytical and Applied Pyrolysis* 74 (1-2): 370-378.

Shi, Lixia, Liu Haifeng, Gao Songfeng, Weng Yunxuan, and Zhu Leilei. 2021. "Enhanced Extracellular Production of IsPETase in Escherichia coli via Engineering of the pelB Signal Peptide." *Agricultur and Food Chemistry* 69 (7): 2245–2252.

Sivaram, Swaminatham, Aditi Roy, and Swapam K. Ray. 2021. "The paradox of plastics in healthcare and health." In *Climate change and the health sector*, 215–223. Routledge .

Son, Hyeoncheol Francis, In Jin Cho, Seongjoon Joo, Hogyun Seo, Hye-Young Sagong, So Young Choi, Sang Yup Lee, and and Kyung-Jin Kim. 2019. "Rational protein engineering of thermo-stable PETase from Ideonella sakaiensis for highly efficient PET degradation." *ACS Catalysis* 9 (4): 3519–3526.

Son, Hyeoncheol Francis, Seongjoon Joo, Hogyun Seo, Hye-Young Sagong, Seul Hoo Lee, Hwaseok Hong, and Kyung-Jin Kim. 2020. "Structural bioinformatics-based protein engineering of thermo-stable PETase from Ideonella sakaiensis." *Enzyme and Microbial Technology* 141: 1-8.

Stepnov, Anton A., Vincent G. H. Eijsink, and Zarah Forsberg. 2022. "Enhanced in situ H2O2 production explains synergy between an LPMO with a cellulose-binding domain and a single-domain LPMO." *Scientific Reports* 12.

Stepnov, Anton A., Zarah Forsberg, Giang-Son Nguyen Morten Sørlie, Alexander Wentzel, and Åsmund K. Røhr & Vincent G. H. Eijsink. 2021. "Unraveling the roles of the reductant and free copper ions in LPMO kinetics." *Biotechnology for biofuels.*

Tamilvendan Manavalan, Anton A. Stepnov, Olav A. Hegnar, Vincent G.H. Eijsink. 2021. "Sugar oxidoreductases and LPMOs – two sides of the same polysaccharide degradation story?" *Carbohydrate Research* 505.

Tiller, Rachel, and Elizabeth Nyman. 2018. "Ocean plastics and the BBNJ treaty—is plastic frightening enough to insert itself into the BBNJ treaty, or do we need to wait for a treaty of its own?" *Journal of Environmental Studies and Sciences* 411-415.

Tokiwa, Yutaka, and Tomoo Suzuki. 1977. "Hydrolysis of polyesters by lipases." *Nature* 270: 76–78.

Tournier, V., C. M. Topham, A. Gilles, B. David, C Folgoas, and E. Moya-Leclair. 2020. "An engineered PET depolymerase to break down and recycle plastic bottles." *Nature research* 580: 216–219.

Tournier, V., C. M. Topham, B. David A. Gilles, C. Folgoas, E. Moya-Leclair, E. Kamionka, M.-L. Desrousseaux, et al. 2020. "An engineered PET depolymerase to break down and recycle plastic bottles." *Nature* 216–219.

Tournier, Vincent, Sophie Duquesne, Frédérique Guillamot, Henri Cramail, Daniel Taton, Alain Marty, and Isabelle André. 2023. "Enzymes' Power for Plastics Degradation." *Chemical Reviews* 123 (9): 5612-5701.

Vaaje-Kolstad, Gustav, Bjørge Westereng, Svein J Horn, Zhanliang Liu, and Vincent G. H. Eijsink. 2010. "An Oxidative Enzyme Boosting the Enzymatic Conversion of Recalcitrant Polysaccharides." *Science* 330 (6001): 219-222.

Vaaje-Kolstad, Gustav, Zarah Forsberg, Jennifer SM Loose, Bastien Bissaro, and Vincent GH Eijsink. 2017. "Structural diversity of lytic polysaccharide monooxygenases." *Current Opinion in Structural Biology* 44: 67-76.

Vaaje-Kolstad, Gustav, Zarah Forsberg, Jennifer SM Loose, Bastien Bissaro, and Vincent GH Eijsink. 2017. "Structural diversity of lytic polysaccharide monooxygenases." *Structural Biology* 44: 67-76.

Vertommen, M.A.M.E., V.A. Nierstrasz, M. van der Veer, and M.M.C.G. Warmoeskerken. 2005. "Enzymatic surface modification of poly(ethylene terephthalate)." *Journal of Biotechnology* 120 (4): 376-386.

Weber, Joanna, Dušan Petrović, Birgit Strodel, Sander H. J. Smits, Stephan Kolkenbrock, Christian Leggewie, and Karl-Erich Jaeger. 2019. "Interaction of carbohydrate-binding modules with poly(ethylene terephthalate)." *Applied Microbiology and Biotechnology* 4801–4812.

Wei, Ren, Gerlis von Haugwitz, Lara Pfaff, Jan Mican, Christoffel P. S. Badenhorst, Weidong Liu, Gert Weber, et al. 2022. "Mechanism-Based Design of Efficient PET Hydrolases." *ACS catalysis* 12 (6): 3382–3396.

Wu, Miao, Gregg T. Beckham, Anna M. Larsson, Seonah Kim, Christina M. Payne, Michael E. Himmel, Michael F. Crowley, et al. 2013. "Crystal Structure and Computational Characterization of the Lytic Polysaccharide Monooxygenase GH61D from the Basidiomycota Fungus Phanerochaete chrysosporium*." *Biological Chemistry* 288 (18): 12828 –12839.

Yoshida, Shosuke, Kazumi Hiraga, Toshihiko Takehana, Ikuo Taniguchi, Hironao Yamaji, Yasuhito Maeda, Kiyotsuna Toyohara, Kenji Miyamoto, Yoshiharu Kimura, and Kohei Oda. 2016. "A bacterium that degrades and assimilates poly(ethylene terephthalate)." *Science* 351 (6278): 1196-1199. doi:10.1126/science.aad6359.

Yoshida, Shosuke, Somboon Tanasupawat, Toshihiko Takehana, Kazumi Hiraga, and Kohei Oda. 2016. "Ideonella sakaiensis sp. nov., isolated from a microbial consortium that degrades poly(ethylene terephthalate)." *International Journal of Systematic and Evolutionary Microbiology* 66 (8): 2813–2818.

Yuting Xu 1, Deeptak Verma 2, Robert P Sheridan 2, Andy Liaw 1, Junshui Ma, Nicholas M Marshall, John McIntosh, Edward C Sherer, Vladimir Svetnik, and Jennifer M Johnston. 2020. "Deep Dive into Machine Learning Models for Protein Engineering." *Journal of chemical information and modeling* 2773-2790.

Zarah Forsberg 1, Gustav Vaaje-Kolstad, Bjørge Westereng, Anne C Bunæs, Yngve Stenstrøm, Alasdair MacKenzie, Morten Sørlie, Svein J Horn, Vincent G H Eijsink. 2011. "Cleavage of cellulose by a CBM33 protein." 1479-83.

Zhao, Jingchan, Zhian Guo, Xiaoyan Ma, Guozheng Liang, and Junlong Wang. 2004. "Novel surface modification of high-density polyethylene films by using enzymatic catalysis." *Applied Polymer* 91 (6): 3673 - 3678.

8. Appendixes

LPMO and predicted molecular weight (kDa)	gene sequences

CelS2-CBM1 (30 kDa)	CATATGAACAAGACCAGCCGTACCCTGCTGAGCCTGGGTCTGCTGAGCGCG GCGATGTTTGGTGTGAGCCAGCAAGCGAACGCGCACGGTGTTGCGATGAT GCCGGGCAGCCGTACCTACCTGTGCCAGCTGGACGCGAAAACCGGTACCG GCGCGCTGGATCCGACCAACCCGGCGTGCCAGGCGGCGCTGGACCAAAGC GGTGCGACCGCGCTGTACAACTGGTTTGCGGTGCTGGACAGCAACGCGGG TGGCCGTGGTGCGGGTTATGTTCCGGATGGTACCCTGTGCAGCGCGGGTGA CCGTAGCCCGTACGATTTTAGCGCGTATAACGCGGCGCGTAGCGATTGGCC GCGTACCCATCTGACCAGCGGTGCGACCATCCCGGTTGAGTACAGCAACTG GGCGGCGCACCCGGGCGATTTTCGTGTTTATCTGACCAAACCGGGTTGGAG CCCGACCAGCGAGCTGGGTTGGGATGATCTGGAACTGATTCAAACCGTGAC CAACCCGCCGCAGCAAGGTAGCCCGGGTACCGATGGTGGCCACTACTATTG GGATCTGGCGCTGCCGAGCGGTCGTAGCGGTGACGCGCTGATCTTCATGCA GTGGGTGCGTAGCGATAGCCAAGAGAACTTCTTTAGCTGCAGCGACGTGGT TTTTGATGGTGGCAACGGTGAAGTTACCGGTATTCGTGGTAGCGGTAGCAC CCCGGACCCGGATCCGACCCCGACCCCGACCGATCCGACCACCCCGCCGAC CCACACCCCGACCCAGAGCCACTACGGTCAATGCGGTGGCATCGGTTATAG CGGTCCGACCGTGTGCGCGAGCGGTACCACCTGCCAGGTTCTGAACCCGTA CTATAGCCAATGCCTGTAACTCGAG
Cels2-PBM (30 kDa)	CATATGAACAAGACCAGCCGTACCCTGCTGAGCCTGGGTCTGCTGAGCGCG GCGATGTTTGGTGTGAGCCAGCAAGCGAACGCGCACGGTGTTGCGATGAT GCCGGGCAGCCGTACCTACCTGTGCCAGCTGGACGCGAAAACCGGTACCG GCGCGCTGGATCCGACCAACCCGGCGTGCCAGGCGGCGCTGGACCAAAGC GGTGCGACCGCGCTGTACAACTGGTTTGCGGTGCTGGACAGCAACGCGGG TGGCCGTGGTGCGGGTTATGTTCCGGATGGTACCCTGTGCAGCGCGGGTGA CCGTAGCCCGTACGATTTTAGCGCGTATAACGCGGCGCGTAGCGATTGGCC GCGTACCCATCTGACCAGCGGTGCGACCATCCCGGTTGAGTACAGCAACTG GGCGGCGCACCCGGGCGATTTTCGTGTTTATCTGACCAAACCGGGTTGGAG CCCGACCAGCGAGCTGGGTTGGGATGATCTGGAACTGATTCAGACCGTGAC CAACCCGCCGCAGCAAGGTAGCCCGGGTACCGATGGTGGCCACTACTATTG GGATCTGGCGCTGCCGAGCGGTCGTAGCGGTGACGCGCTGATCTTCATGCA GTGGGTGCGTAGCGATAGCCAAGAGAACTTCTTTAGCTGCAGCGACGTGGT TTTTGATGGTGGCAACGGTGAAGTTACCGGTATTCGTGGTAGCGGTAGCAC CCCGGACCCGGATCCGACCCCGACCCCGACCGATCCGACCACCCCGCCGAC CCATACCGCGTTCACCTGCACCGCGACCACCGCGAGCAACTATGCGCATGTT CAGGCGGGTCGTGCGCATGACAGCGGTGGCATTGCGTACGCGAACGGTAG CAACCAGAGCATGGGCCTGGATAACCTGTTTTATACCAGCACCCTGGCGCA AACCGCGGCGGGTTACTATATTGTTGGCAACTGCCCGTAACTCGAG
Cels2-DSI (27 kDa)	CATATGAACAAAACCAGCCGTACCCTGCTGAGCCTGGGTCTGCTGAGCGCG GCGATGTTTGGTGTGAGCCAGCAAGCGAACGCGCACGGTGTTGCGATGAT GCCGGGCAGCCGTACCTACCTGTGCCAACTGGATGCGAAGACCGGTACCG GTGCGCTGGATCCGACCAACCCGGCGTGCCAGGCGGCGCTGGACCAAAGC GGTGCGACCGCGCTGTACAACTGGTTTGCGGTGCTGGACAGCAACGCGGG TGGCCGTGGTGCGGGTTATGTTCCGGATGGTACCCTGTGCAGCGCGGGTGA CCGTAGCCCGTACGATTTTAGCGCGTATAACGCGGCGCGTAGCGATTGGCC GCGTACCCATCTGACCAGCGGTGCGACCATCCCGGTTGAGTACAGCAATTG GGCGGCGCACCCGGGTGATTTTCGTGTTTATCTGACCAAACCGGGTTGGAG CCCGACCAGCGAGCTGGGTTGGGATGATCTGGAACTGATTCAAACCGTGAC

78	CAACCCGCCGCAGCAAGGTAGCCCGGGTACCGATGGTGGCCACTACTATTG GGATCTGGCGCTGCCGAGCGGTCGTAGCGGTGACGCGCTGATCTTCATGCA GTGGGTGCGTAGCGATAGCCAAGAGAACTTCTTTAGCTGCAGCGACGTGGT TTTTGATGGTGGCAACGGTGAAGTTACCGGTATTCGTGGTAGCGGTAGCAC CCCGGACCCGGATCCGACCCCGACCCCGACCGATCCGACCACCCCGCCGAC CCACACCGGTCTGTGGAGCACCATCAAGCAGAAAGGCAAGGAAGCGGCG ATTGCGGCGGCGAAGGCGGCGGGTCAAGCGGCGCTGGGCGCGCTGTAAC TCGAG